Aleksander Juell

Production Optimization of Remotely Operated Gas Wells

Thesis for the degree of Philosophiae Doctor

Trondheim, January 2011

Norwegian University of Science and Technology
Faculty of Engineering Science and Technology
Department of Petroleum Engineering
and Applied Geophysics

NTNU – Trondheim
Norwegian University of
Science and Technology

NTNU
Norwegian University of Science and Technology

Thesis for the degree of Philosophiae Doctor

Faculty of Engineering Science and Technology
Department of Petroleum Engineering and Applied Geophysics

ISBN 978-82-471-3320-0 (printed ver.)
ISBN 978-82-471-3321-7 (electronic ver.)
ISSN 1503-8181

Doctoral theses at NTNU, 2012:29

Printed by NTNU-trykk

Acknowledgments

I would like to thank my supervisor, professor Curtis H. Whitson, for all his guidance and patience while working on this thesis. Without his continued help, this work would not have been possible.

I would also like to thank professor Michael Golan. He has been of great help with all the field work that was a part of this thesis. His humor and wealth of knowledge is an inspiration to me, and everyone around him.

Doug Summers and Chip Long at Paleo Inc. have been a great help during the field work in Oklahoma related to the ROOKIE project. I would like to thank them for all their patience with me, and all their generosity.

I would also like to thank Sage Technologies for the donation of their Fluid Logger IV system. The fluid logger made it possible to measure liquid levels in the wells that were investigated.

Finally, I would like to thank the Data Retrieval Corporation for letting me borrow their SPIDR well test system. Much of the initial testing on the wells mentioned in Chapter 1 was performed with the SPIDR.

Units

This work uses a mixture of metric and field units. If not otherwise stated, the units used are always the ones listed in the nomenclature at the end of each chapter. The most used unit conversions are listed below.

Unit Conversions		
From	To	Multiply By
psi	bar	0.0689
mcf/d	m^3/d	28.317
lb	kg	0.4536
ft	m	0.3048
R	K	5/9

Contents

List of Figures

List of Tables

Chapter 1

Remote Operations

1.1 Introduction

The Remote Operations in Oklahoma Intended for Education (ROOKIE) project is a remote field laboratory constructed as a part of this research project. ROOKIE was initiated to provide data in research on production optimization of low productivity gas wells. In addition to this, ROOKIE is used as a teaching tool.

Much of the remote operations technology used in the ROOKIE project has been used by the industry for several decades. The first use of remote data acquisition in Oklahoma was in 1989, as described by Luppens [7]. Even though this, for the most part, is old technology, the ROOKIE project is the first remote operations project set up with research and teaching as the main focus.

This chapter will discuss the process of establishing the remote field laboratory and the data storage facilities. Results from the project will also be discussed.

All testing, instrumentation installation, and modifications to the wells discussed in this chapter was performed by the author. The communication system between the well and NTNU, and the storage database was installed and configured by the author.

1.2 Well Selection

A total of 13 candidate wells were made available from Paleo Inc., a small Oklahoma City operator, for the ROOKIE project. Only one of the wells could be instrumented in the first phase of the project. Many of the wells

had been shut in for long periods of time prior to the project startup, and the most viable well had to be selected. The well selection criteria included:

- Access to electrical power.
- Well integrity.
- Production potential.
- Production optimization potential.

1.2.1 Initial Screening

All the available wells were visited to investigate well integrity and the availability of electrical power. Three wells had both wellheads in good condition and were located close to the existing power grid:

- Boyd Cable #2
- Darrell Allen
- Noblin #2

These wells were then further studied by performing a well test to assess productivity.

1.2.2 Well Testing

To assess the production potential of the wells, a well test was performed on each well. The well tests were conducted with the SPIDR from the Data Retrieval Corporation [2] (DRC). The SPIDR records wellhead pressure and gas production rate form the well every 5 seconds. Fig 1.1 shows the SPIDR mounted on a well during a well test. The differential pressure (DP) cell connected to the SPIDR is shown in Fig. 1.2. The DP cell measures pressure drop over an orifice plate. This pressure drop is used to calculate the gas production rate of the well. The gas rate, q_g, is calculated from [1]:

$$q_g = C\sqrt{h_w p} \tag{1.1}$$

where, h_w is the pressure drop across the orifice plate, p is the upstream pressure, and C is a constant dependent on pipe diameter, orifice opening, temperature, and gas gravity.

Fig. 1.1 – The SPIDR unit mounted on a well during a well test. The center cable is used for communication with a laptop computer, the left cable connects to the DP cell, and the spiral tube to the right is used to measure tubinghead pressure.

The welltests consisted of an initial drawdown period, followed by a buildup period, then again followed by a drawdown period. Fig 1.3 presents the measured data from a well test performed on the Noblin #2.

In addition to the well test, the fluid level was measured on all the candidate wells. The fluid level was measured to evaluate the production optimization potential of the wells. If fluid is accumulating downhole, a significant increase in production may be achieved by continuously removing the liquid. The fluid level was measured with the Acoustic Fluid Logger IV (AFL) from Sage Technologies [5]. The AFL consist of two parts: A gun, and a control box. The gun is mounted to one of the annulus valves on the wellhead. Nitrogen gas pressurizes a holding chamber that is closed to the well by a fast actuating valve. The valve is opened by the control

Fig. 1.2 – The pressure differential cell connected to the SPIDR unit to measure gas production rate.

box, and the acoustic signal emanating from the well is recorded through a microphone located on the gun. The signal is processed by the control box, and transmitted to a laptop computer. Fig. 1.5 shows the AFL gun mounted on a well. The AFL control box is shown in Fig. 1.6, and an example of the acoustic signal recorded from the wells is shown in Fig. 1.4.

Based on the interpretation of the well tests and the fluid level measurements, the Noblin #2 showed the most potential, and was selected to be the first well in the ROOKIE project.

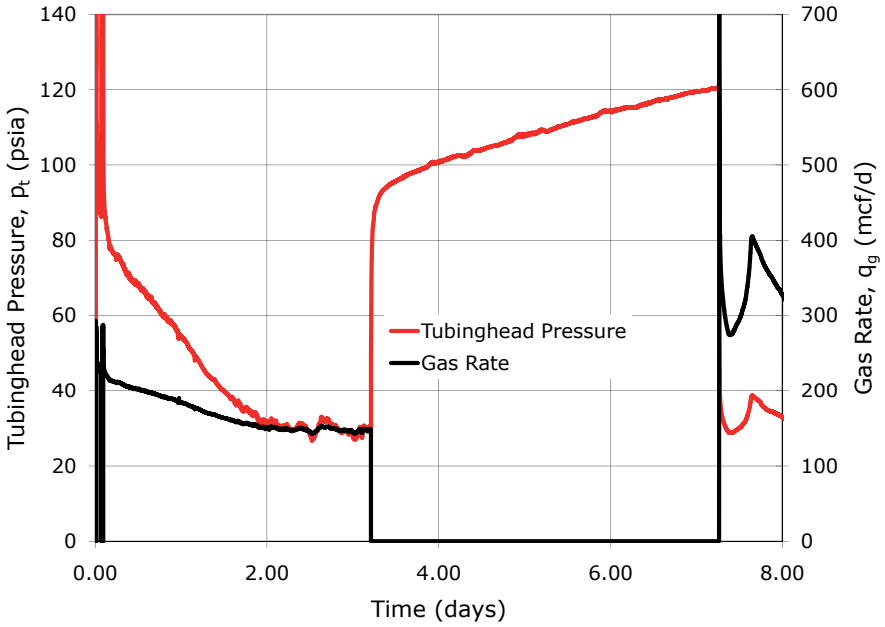

Fig. 1.3 – Measured tubinghead pressure and gas rate from a well test performed on the Noblin #2.

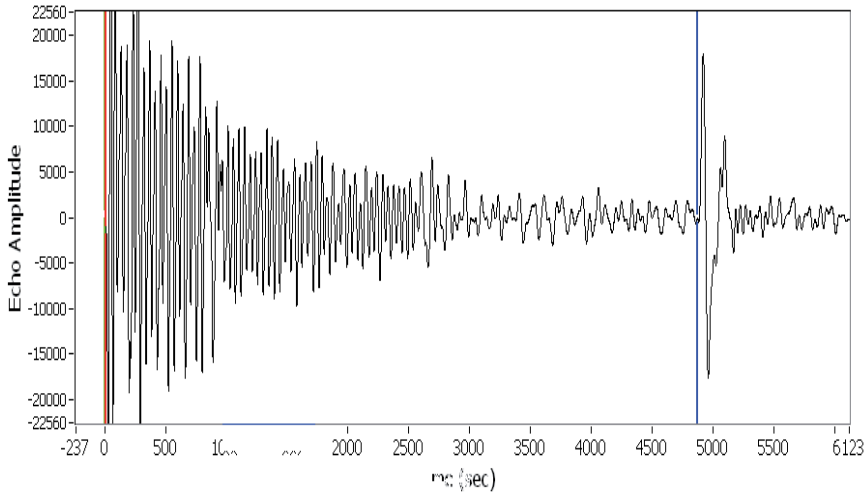

Fig. 1.4 – A fluid level recorded on the Noblin #2. A high magnitude signal where the blue marker is placed indicates the fluid level.

Fig. 1.5 – The Acoustic Fluid Logger IV gun mounted on a well. The nitrogen tank pressurizing the gun can be seen in the background.

Fig. 1.6 – The Acoustic Fluid Logger IV control box.

1.3 Description of the Noblin #2

1.3.1 Location

The Noblin #2 is located in Pittsburg county, Oklahoma, USA. The wellhead sits in the middle of a pasture, and the nearest farm is ∼150 meters away. A power line was stretched from the farm house to the wellhead, to provide power to the monitoring and communications equipment installed through the ROOKIE project. The wellsite of the Noblin #2 is shown in Fig. 1.7.

Fig. 1.7 – Noblin #2 wellsite. All major parts of the wellsite are marked on the figure.

1.3.2 Geology

The Noblin #2 is producing from the Atoka formation. The Atoka is a sandstone formation in the Akroma basin. Where the Noblin #2 is located, the Atoka is 9.8 meters thick, and the formation top is 1058 meters below the surface. A clear shale break can be seen from the log shown in Fig. 1.8. The shale break is located mid-formation. This might indicate a no-flow barrier.

The Atoka formation is a dry gas formation, with gas specific gravity of 0.59. The composition of the gas is given in Table 1.1.

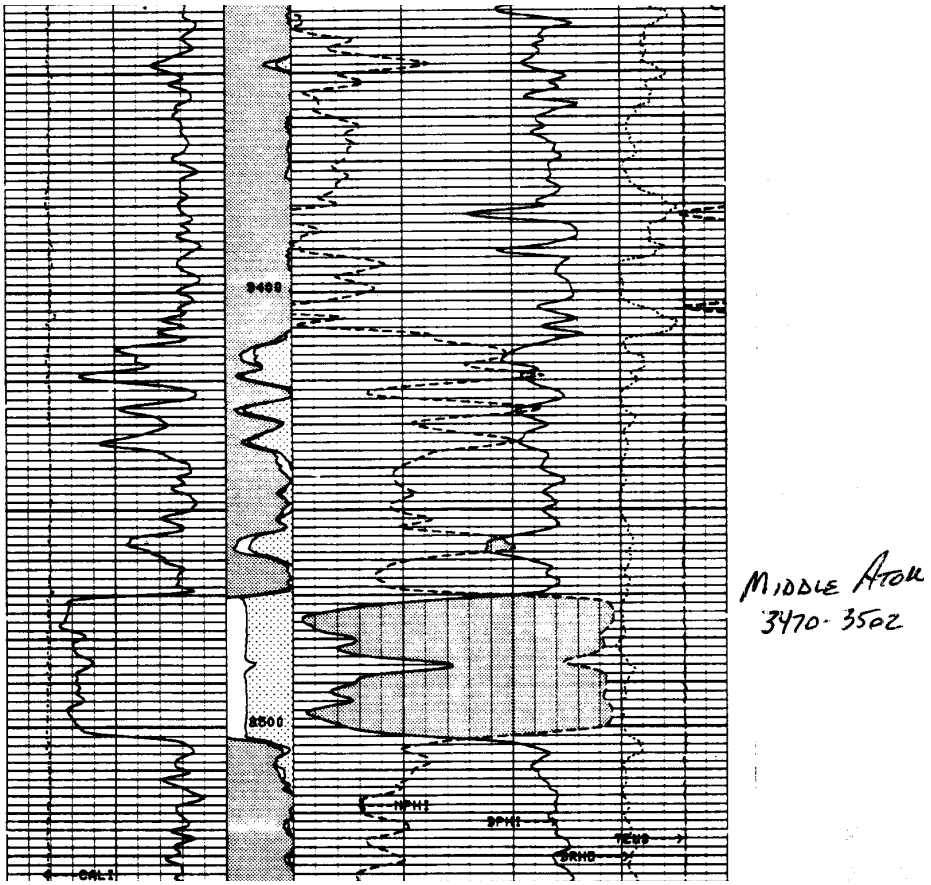

Fig. 1.8 – Noblin #2 gamma ray (GR) and neutron density logs. A clear shale break can be seen in the middle of the Atoka formation.

1.3.3 Wellhead Configuration

The wellhead of the Noblin #2 is shown in Fig. 1.9. Gas is produced through the annulus. No packer is installed downhole between the tubing and casing. Gas flows from the wellhead, through a two-phase separator, and further to a metering station. An orifice plate is installed in the flowline by the metering station, to measure gas rate.

A rod pump is installed in the tubing, and water is pumped up through the tubing, and is transported to a water holding tank located 10 meters from the wellhead.

TABLE 1.1 – Atoka formation gas composition. Measured from the produced gas from the Noblin #2.

Gas Composition	
Component	Amount $(mole - \%)$
CO_2	0.710
N_2	1.240
C_1	94.520
C_2	2.910
C_3	0.400
I-C_4	0.040
N-C_4	0.070
I-C_5	0.030
N-C_4	0.020
C_{6+}	0.050

Fig. 1.9 – Noblin #2 wellhead. Pipes transporting gas are painted yellow, and pipes transporting water are painted blue.

1.4 ROOKIE Well Instrumentation

A schematic of the instrumentation installed at the Noblin #2 wellsite, in relation to the ROOKIE project, is shown in Fig. 1.10. The different components of the instrumentation are discussed in detail in the following sections. The reason for, and importance of, each of the components are listed in Table 1.2.

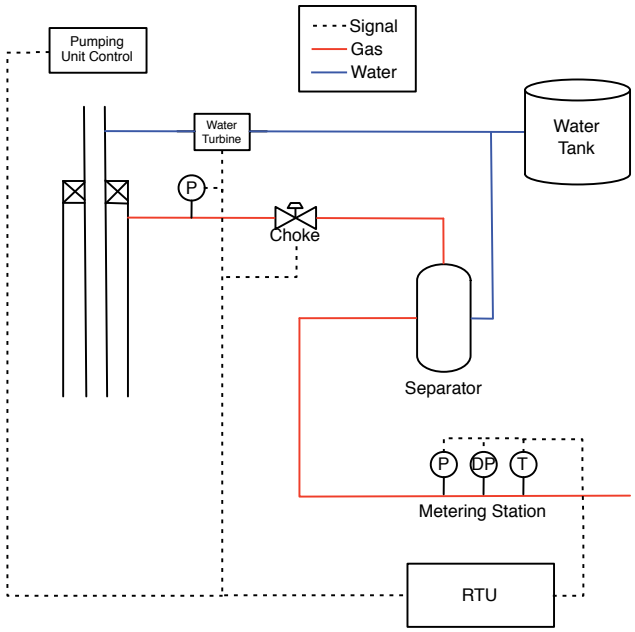

Fig. 1.10 – Well instrumentation on the Noblin #2.

1.4.1 Remote Telemetry Unit

A Remote Telemetry Unit (RTU) is installed at the wellsite. The RTU samples data from all connected sensors, and stores the data internally. It may be connected to both analog and digital sensors. Signals of the following types are compatible with the RTU:

- 4-20 mA (Analog)
- 0-10 V (Analog)
- Frequency (Analog)

TABLE 1.2 – List of equipment installed at the wellsite. Any item with high priority is essential for day to day operation of the well.

Wellsite Equipment		
	Priority	Note
RTU	High	Essential for communication, collecting data, and controlling the well.
Water turbine	High	Needed for controlling pumping cycles.
Pumping unit	High	Any low producing gas well will have problems with liquid accumulation downhole. A pumping unit is a practical way to dispose of the liquids.
Pressure gauge	Med	Needed for welltesting, but not for day to day operations.
Cameras	Low	In some cases it is good to have a live video stream from the well, e.g. to visually inspect problems with the pumping unit. However this is a luxury, not essential for day to day operations.
Choke	Low	Together with a pressure gauge at the wellhead, the choke may be used to perform well tests. This can give valuable information about the reservoir characteristics

- 0/22 V (Digital)

In addition to recording sensor input, the RTU may also control connected devices through analog and digital output signals of the following types:

- 4-20 mA (Analog)

- 0/22 V (Digital)

Communication with the RTU is facilitated through a local area network (LAN) connection. The RTU is connected to the local network at the well through a network router. The outside of the RTU installed on the Noblin #2 is shown in Fig. 1.11. The interior of the RTU is shown in Fig. 1.12.

Fig. 1.11 – The RTU installed at the Noblin #2.

Minimum Requirements

Any RTU to be used for remote operations, as in the ROOKIE project, must fulfill some minimum requirements. The RTU must be able to handle multiple sensor readings:

- Pressure drop across orifice plate; to calculate gas rate.
- Gas flowing temperature; to calculate gas rate.
- Pressure upstream orifice plate; to calculate gas rate.
- Water rate from pump; to detect when pump runs dry.

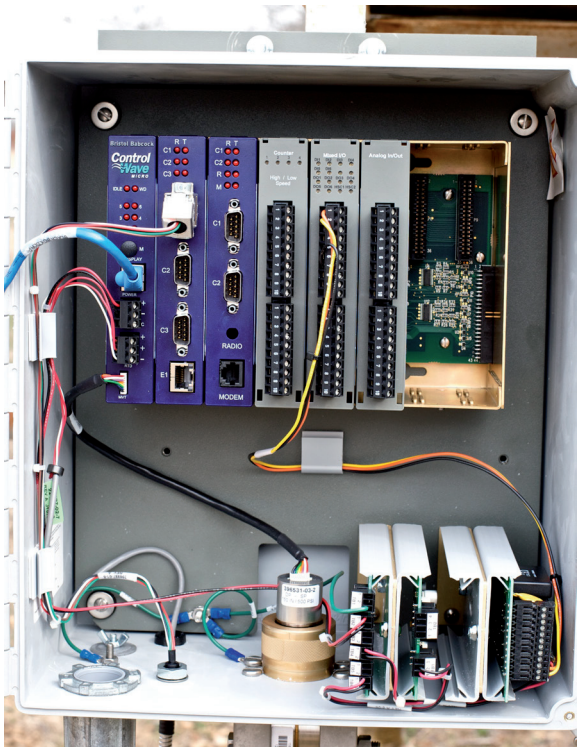

Fig. 1.12 – The inside of the RTU installed at the Noblin #2. The blue circuit boards contain the CPU and communication modules, while the grey circuit boards are used for input and control signals.

In addition to this, the RTU must also be able to turn on and off the pumping unit. A network interface is required for remote access.

These are the minimum requirements for an RTU to function in the context of remote operations. The RTU used in the ROOKIE project is connected to several other sensors, as discussed in the following sections.

1.4.2 Sensors

Several sensors are mounted on the well to monitor and optimize production performance. Each sensor is discussed in detail below.

Wellhead Pressure

A 0 – 250 psig pressure sensor is mounted after the annulus valve on the wellhead. The sensor transmits a 4 – 20 mA signal. The signal current is

linearly proportional to pressure. 4 mA corresponds to a pressure of 0 psig, and 20 mA corresponds to a pressure of 250 psig. The pressure gauge is shown mounted on the well in Fig. 1.13.

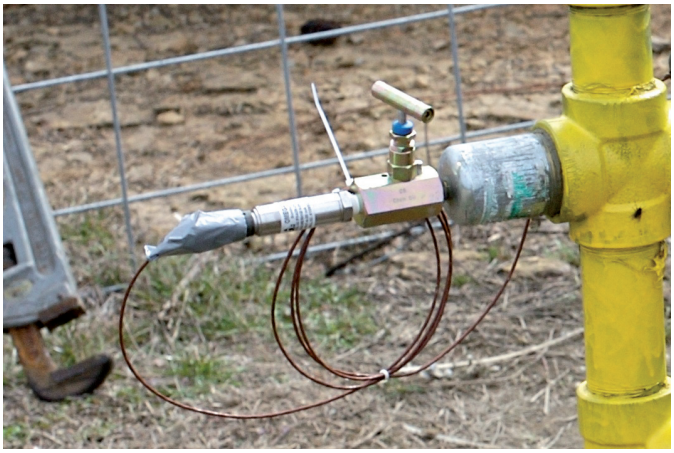

Fig. 1.13 – The wellhead pressure gauge installed on the Noblin #2. The brown signal wire is connected to the RTU, and transmits a current proportional to the measured pressure.

Water turbine

A 1 inch water turbine meter is mounted after the tubing valve on the wellhead. The turbine meter is shown in Fig. 1.14. Water pumped through the tubing by the pumping unit passes through the water turbine. It is possible to bypass the turbine meter if needed. The bypass loop is 2 inch, and is opened and closed with a manual valve.

The water turbine outputs a sinusoid signal with the frequency proportional to the water rate.

$$q_w = 18000f \tag{1.2}$$

where q_w is the water rate in gal/min, and f is the signal frequency in Hz. The frequency signal is picked up and processed by the RTU.

Multi Variable Tool

The multi variable tool (MVT) is an array of sensors located internally in the RTU. The MVT measures:

Fig. 1.14 – The water turbine meter installed on the Noblin #2.

- Pressure upstream of orifice plate.
- Pressure downstream of orifice plate.
- Temperature downstream of orifice plate.

These three measurements are used to calculate the instantaneous gas rate. This calculation is automatically performed by the RTU.

The MVT sensors are mounted by the wells metering station, as seen in Fig. 1.15. The pressure difference across the orifice plate is calculated from the difference in the two measured pressures.

1.4.3 Choke

A remotely operated choke is located after the wellhead pressure sensor on the gas flow line from the casing-tubing annulus. The choke is used to restrict the flow of gas from the well, or to shut in the well entirely. Because the choke is installed downstream of the wellhead pressure sensor, it is possible to perform build-up tests on the well. If the pressure sensor was installed on the other side of the choke, it would not be possible to record pressures from the well when shut-in. The choke is shown in Fig. 1.16.

Control

The choke is controlled through a 4 – 20 mA signal. The signal is transmitted from the RTU. 4 mA corresponds to completely closed, and 20 mA corresponds to completely open.

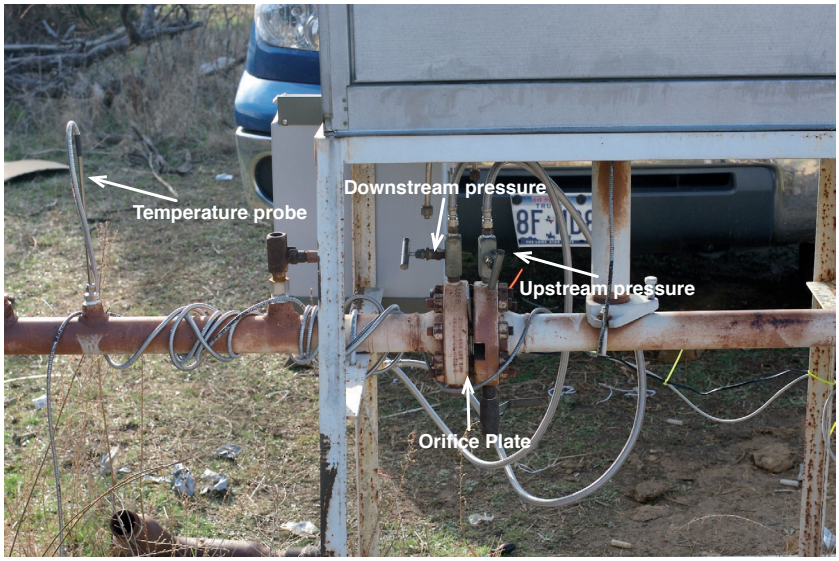

Fig. 1.15 – The multi variable tool sensors installed on the Noblin #2.

Fig. 1.16 – The remotely controlled choke installed on the Noblin #2. A motorized actuator (gray and blue box) is mounted on top of the choke. The actuator receives a control signal from the RTU to open or close.

Feedback

The choke sends a feedback signal to the RTU. This is also a 4 – 20 mA signal. The feedback signal is used to monitor that the choke functions properly. If there is any mismatch between the control signal set point and the feedback from the choke, this indicates that the choke might be stuck.

1.4.4 Pumping Unit

A rod pumping unit is mounted on the well. The pumping unit pumps water from the bottomhole through the tubing. The pumped water is fed through the water turbine meter, and to a water holding tank. The pumping unit is shown in Fig. 1.17.

Fig. 1.17 – The pumping unit installed on the Noblin #2.

Control

The pumping unit is remotely controlled through a 0/22 V digital signal. The signal is sent from the RTU to the pumping unit control box. When a voltage of 22 V is transmitted, the pumping unit is turned on; and when the voltage is turned to 0 V, the pumping unit is turned off. Fig 1.18 shows the pumping unit control box.

Fig. 1.18 – The pumping unit control box installed on the Noblin #2. The control box is connected to the RTU, and starts and stops the pumping unit.

1.4.5 Cameras

Network IP cameras are installed at the wellsite. The cameras use Power over Ethernet (PoE). Both data transfer and power supply is provided by a single ethernet cable. The cameras provide a live video feed from the well, and may be viewed through a normal web browser, or through the client application described in Section 1.7. Fig. 1.19 shows one of the two cameras installed on the Noblin #2.

1.5 Communication

The wellsite is equipped with a satellite internet connection. Many of the onshore well locations in the United States are remote, and far from any cable or phone lines. Internet via satellite is convenient in these cases, as it does not require any existing infrastructure. The satellite dish connecting the Noblin #2 wellsite to the internet is shown in Fig. 1.20.

A virtual private network (VPN) router connects the RTU to the satellite dish. The VPN connection servers two purposes:

- A secure connection between the data logging server and the wellsite.
- Remote access to the local network at the wellsite.

Fig. 1.19 – One of the two IP cameras installed on the Noblin #2. The cameras transmit live video feeds that can be viewed through the ROOKIE client application.

This makes it possible to connect securely to the RTU from any remote location.

Fig. 1.20 – The satellite dish installed on the Noblin #2.

A schematic of the data flow in the ROOKIE project, from sensors at the wellsite to the final user, is shown in Fig. 1.21. The data storage server and user application shown in this schematic are described in later sections.

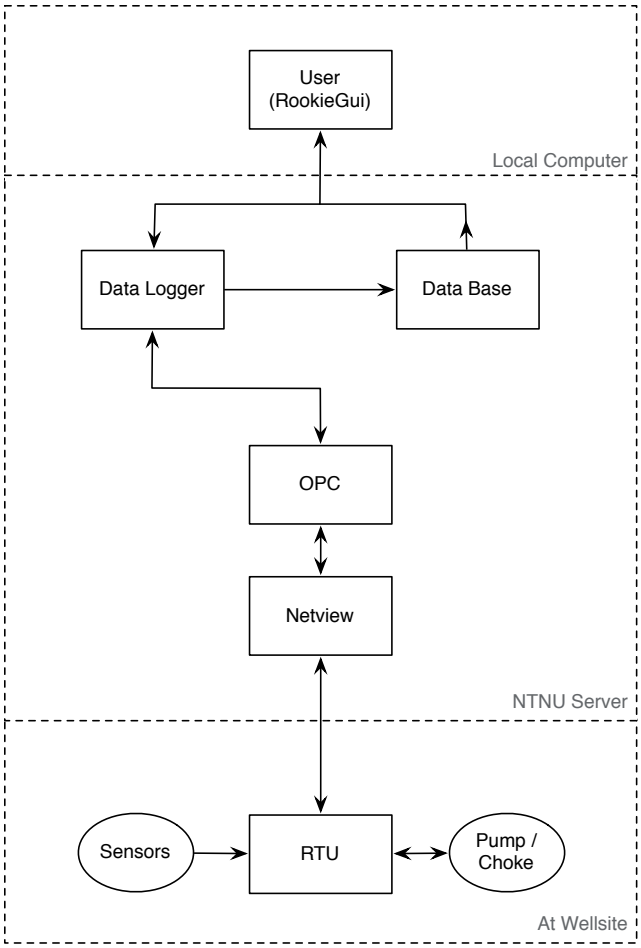

Fig. 1.21 – Data flow in the ROOKIE project. Arrows indicate direction of data flow.

1.5.1 Network Equipment Installed at the Well

All network equipment needed to facilitate communication between the well-site equipment and the satellite connection is located in a weather resistant box. The box contains:

- Satellite modem; to connect with the outside world.
- PoE switch; to supply cameras with power and network connection.
- VPN router; to connect all equipment to the local network.

- Cooling fan; to keep temperature lower that 40 ^{o}C during the summer.
- Enclosure heater; to keep enclosure temperature above freezing during the winter.
- Thermostats; to control heater and fan.
- Power outlets; to supply power to all the equipment above.

The network equipment box was custom built by the author for the ROOKIE project.

Fig. 1.22 shows the Noblin #2 metering station, where the network equipment box is located. The interior of the network equipment box is shown in Fig. 1.23.

Fig. 1.22 – The Noblin #2 metering station. From left: network equipment box, chart meter cabinet, and RTU. The chart meter is no longer used, because gas rates are now measured by the RTU.

1.6 Data Storage and Retrieval

The vendor of the RTU installed at the well, supplies software for remote communication with the RTU. This software is split into two applications: Netview and OPC Server. Netview communicates directly with the RTU,

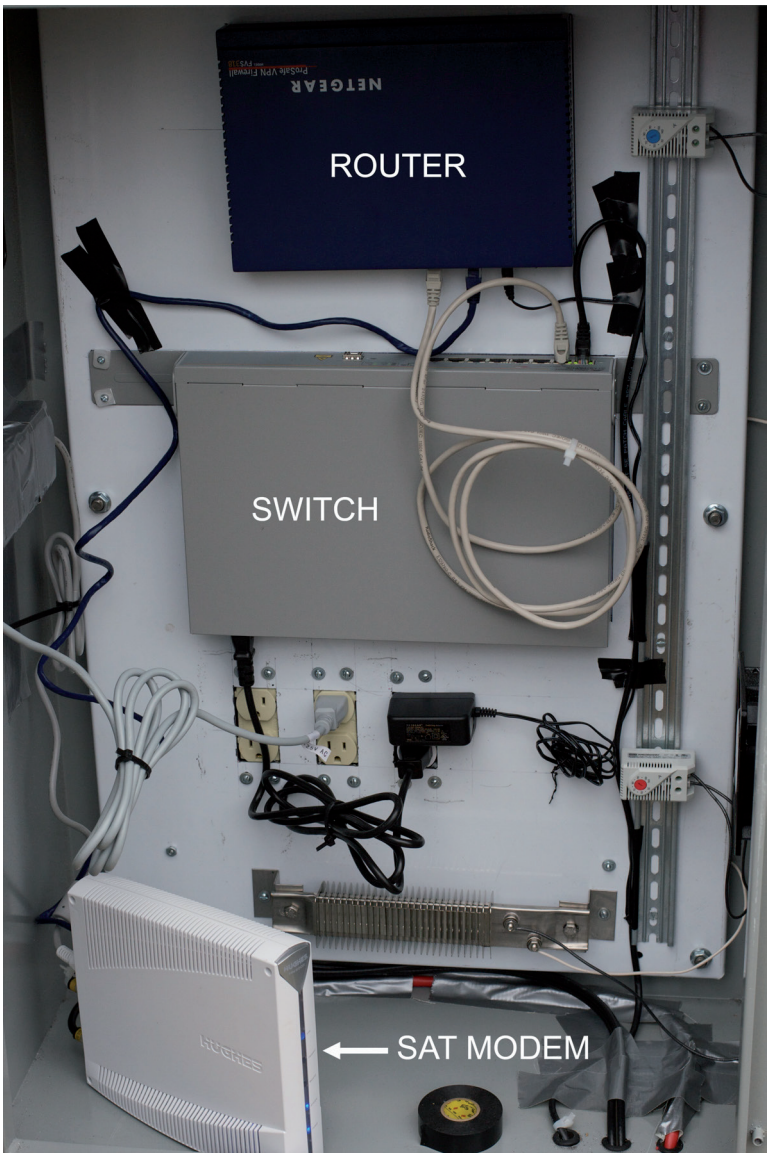

Fig. 1.23 – The interior of the network equipment box installed at the Noblin #2.

through the available VPN connection, and can access sensor values and instruct the RTU to start / stop the pump and control the choke. The OPC Server (OPC is short for OLE for Process Control) makes the RTU available for third-party applications through the Object Linking and Embedding

(OLE) interface. As noted by Mathieson et al. [8], OPC is one of the most widely used interfaces for process control.

A server application was developed to communicate with the RTU through the OPC Server. This server application, called the "data logger", makes it possible for users of the ROOKIE project to retrieve data from, and control the connected wells.

The data logger retrieves the current values for all sensors connected to the RTU. This data is stored in a MySql data base. The following data is stored:

- Sensor values; every 5 seconds.
- Pumping cycles; when pump is activated.
- Choke changes; when choke position is changed.

The structure of the database makes it easy to add new wells to the system. A schematic of the data base is shown in Fig. 1.24. A short description of each of the tables in the data base follows:

data All measured signal values are stored in this table. New values are retrieved every 5 seconds. The signals stored include: gas rate, wellhead pressure, temperature, and differential pressure.

signals A list of all the signals (measurement points), with a short description and associated units.

pump_cycles Every time the pumping unit is activated, a new entry is added to this table. Start and stop times are recorded together with the amount of water that was pumped, measured by the water turbine. The user responsible for controlling the pump is also stored.

choke_changes Stores all changes to the choke setting. The time, choke opening, and the user responsible for the change is stored.

wells A list of all the wells connected to the system. Currently, only one well is connected.

As a precaution, the database is automatically backed up to an external disk once every week.

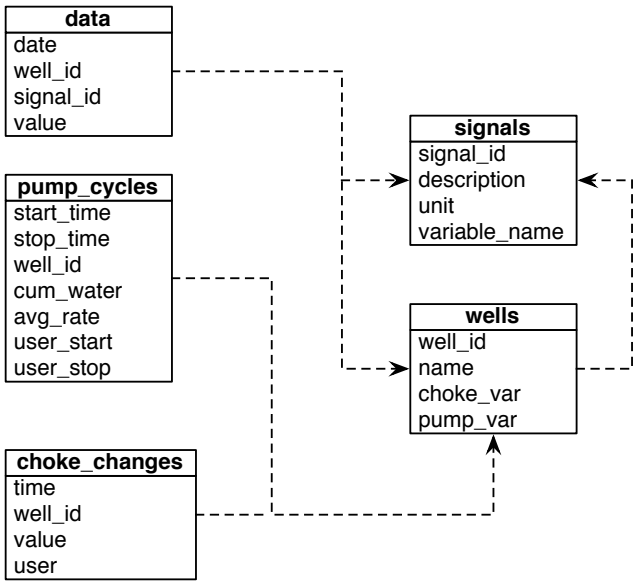

Fig. 1.24 – Structure of the production data base.

1.7 Client Application

A custom client application, RookieGUI, has been developed to facilitate monitoring and control of the wells connected to the ROOKIE system. The application lets the user:

- View real time data from the wells.
- Retrieve historical data.
- Adjust choke.
- Start / stop pumping unit.
- Set up automatic pump control.
- View live video feed from wellsite.

The user application connects to the data logger through an encrypted connection. All communication with the RTU from the user application goes through the data logger, as shown in Fig. 1.21. Multiple users may use the client application simultaneously. Viewing data is currently open to the

public. A login username and password is required to either change choke settings, or to start / stop the pumping unit.

A screen shot of the main window of the client application is shown in Fig. 1.25. In this screenshot gas rates and wellhead pressure for the last 10 hours is shown. Every 5 seconds, new data is automatically retrieved from the database, and displayed on screen. It is possible to display historical data stored in the database. The data can easily be exported to excel.

The client application is programed in LabView [6], a graphical programming language. This makes the transition to new programmers easy. The application was programmed by several students at NTNU.

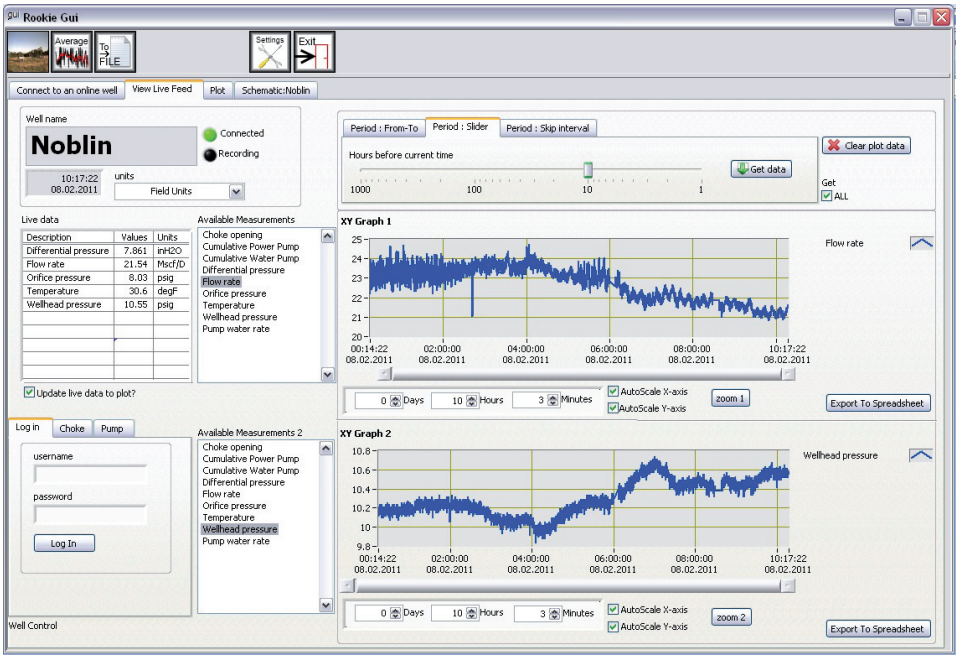

Fig. 1.25 – Main window of the client application. Plots of gas rate and wellhead pressure for the last 10 hours are shown.

1.8 Pumping Automation

Wells experiencing liquid loading must be unloaded on a regular basis to maximize the gas production. Once liquid accumulates above the perforations, the production will deteriorate. At the Noblin #2, a rod pumping unit was installed to unload the well. Manually controlling the pump every

time water has accumulated is time consuming. Logic to start and stop the pump automatically was implemented in the data logger.

Several strategies to automatically unload gas wells have been presented in the literature. Foo [3] looks at wells where there is communication between the tubing and annulus. The difference in annulus and tubing pressure is used to calculate the liquid level in the wellbore. This is not an option for the Noblin #2, because there is not communication between tubing and annulus. A more suitable automated pumping strategy is presented by Neely and Tolbert [9]. Their strategy requires a dynometer installed on the pumping unit to detect pumpoff. A dynometer measures the torque output by the pumping unit. The Noblin #2 does not have a dynometer, but the installed water turbine meter is a good way to detect pumpoff.

The pumping automation logic implemented on the Noblin #2 works as follows:

- The gas rate is continuously monitored to see if it falls below a user specified limit. This limit is specified through the client application, and indicates the onset of liquid loading.
- If a gas rate below the limit is detected, pumping should be initiated. The data logger waits until a user specified time of day to start pumping. This is done to prevent pumping during the middle of the night, which could disturb neighbors.
- The pump is started at the specified time, and continues to pump until either:
    1. The measured water rate from the water turbine falls below a user defined limit, i.e. the pump has run dry.
    2. The maximum pump time is reached. This limit is specified by the user, and acts as a safeguard to prevent damage to the pump due to excessive pumping.
- After the pumping cycle has ended, the monitoring of the gas rate starts over.

The user specified limit on the gas rates that triggers a new pumping cycle should reflect the gas rate of the well when water starts accumulating above the perforations. If nothing is done to the well at this point, more water will accumulate above the perforations, and the performance of the well will deteriorate rapidly. On the other hand, if the rat hole is pumped

free of water before liquid reaches the perforations, the productivity of the well does not deteriorate.

Fig. 1.26 shows the gas production rates for the Noblin #2. The red vertical line in this figure indicates when the pumping automation logic was initiated. Prior to this, the pump was controlled manually, and the well was pumped ∼once a week. After the pumping logic was initiated, the well was pumped on average once a day for 10 minutes, and the production rate stabilized at 20 mcf/d.

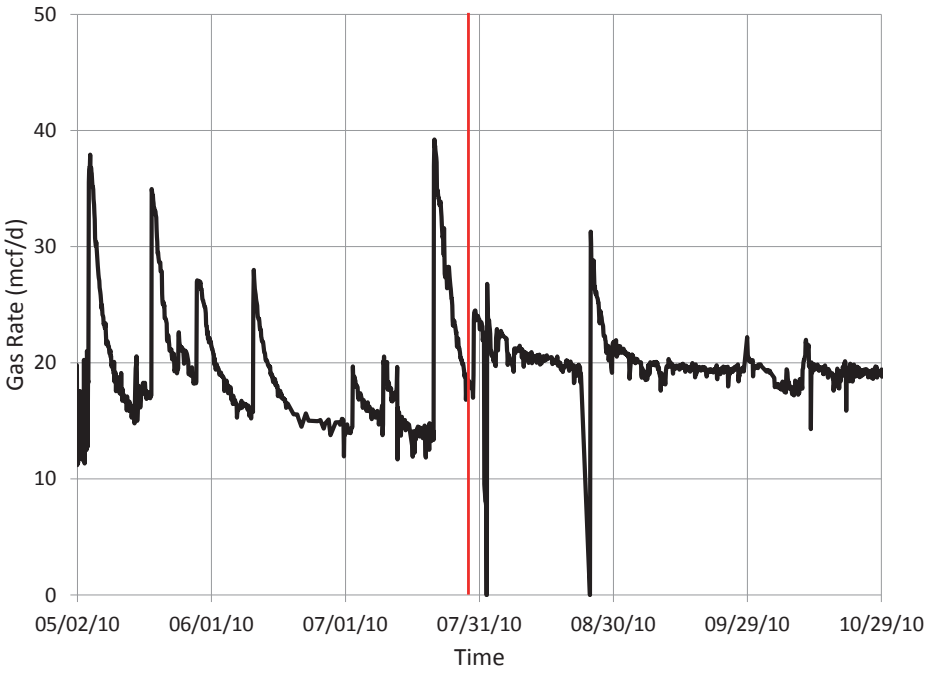

Fig. 1.26 – Production gas rates from the Noblin #2. The red vertical line indicates when the pumping automation logic was initiated.

Giangiacomo and Hill [4] look at using an AFL-gun to determine when to start and stop the pumping unit, by detecting changes in the liquid level acoustically.

The experience from the Noblin #2 is that acoustic signals shot while the well is flowing, are too dominated by noise to detect liquid levels accurately. In order to use acoustic signals from the Noblin #2, the well must be shut-in. The current pumping automation does not require the well to be shut in, so the use of acoustic signals on the Noblin #2 was abandoned.

1.9 Environmental Considerations

The climate in Oklahoma is hot and humid during the summer, with temperatures exceeding 40 ^{o}C. During the winter the climate is cold, with temperatures dipping below -10 ^{o}C. This puts high demands on both electronic equipment and hardware.

All communications equipment, e.g. router, switch, satellite modem, etc., is contained within a NEMA 3R weather proof enclosure. This enclosure is fitted with a thermostat controlled heater and fan, to keep the internal temperature of the enclosure between 5 and 35 ^{o}C. The enclosure is in addition insulated on the outside with a reflective foam coating.

During cold periods, the water discharge pipe connecting the tubing with the water disposal tank, may freeze. If the pumping unit is activated while the pipe is frozen, the pumping unit itself, or the water turbine meter, may be damaged. It is therefore important to restrict pumping to above freezing temperatures.

Many of the wells in Oklahoma are located in, or close to, cattle grazing grounds. Fences around all sensitive equipment is necessary to avoid cows from causing damage.

1.10 Local Maintenance

Even though the goal of the ROOKIE project is to shift operations from the field to a centralized location, some local maintenance is impossible to avoid.

A pumper is needed to regularly visit the wellsite. The pumpers duties varies with the seasons.

Summer:

- Empty separator; once a week.
- Check metering station; 1 – 2 times a week.

Winter:

- Empty separator; once a week.
- Check metering station; 1 – 2 times a week.
- Check surface piping for water slugs that may freeze; when cold.

The pumper is not trained to handle technical problems related to the monitoring and automation equipment. If any problem with this equipment occurs, other personnel must be contacted. The equipment installed at the Noblin #2 has been very reliable since some infancy problems were taken care of, but maintenance trips have been scheduled every six months to prevent problems from arising.

1.11 Lessons Learned

Several problems with the original design of the instrumentation at the wellsite, the communications equipment, and the data logger were revealed during the course of the work on the ROOKIE project. These problems are discussed below.

1.11.1 Pumping Automation

In the spring of 2011, an error occurred in the pumping automation logic. A pumping cycle was started as normal. When the water rate dropped below the specified limit, a signal was sent to the RTU to stop pumping. This signal was never received by the RTU, and pumping continued. There was no self-check in place in the pumping automation logic to ensure the pumping actually stopped, so the continued pumping went on undetected. The pump continued pumping dry for two days, until the error finally was detected manually, and the pump was shut off. By this time, the pump was stuck downhole, and had to be replaced.

Additional safety measures should have been implemented to avoid this situation.

1.11.2 Protection Against Cattle

When the Noblin #2 was first instrumented, the wellhead and metering station were not fenced in. As the well is situated in the middle of a pasture where cattle graze, the cattle had free access to the equipment at both locations. The control box for the AFL was damaged by the cattle, as well as a network cable connecting one of the cameras. Shortly after this was noticed, fences were installed. The fence around the wellhead serves an additional purpose of keeping children away, as children playing by the wellhead could get injured if the pumping unit starts running.

1.11.3 Hot Weather

The electronic equipment located in the network equipment box is sensitive to high temperatures. Most of the equipment is not designed to withstand temperatures exceeding 40 ^{0}C. Even though a fan was installed in the box for cooling purposes, the internal temperature of the box could get higher than this during hot summer days. This resulted in the router occasionally shutting down.

To lower the temperature, a reflective insulation foam was fitted on the outside of the box. The foam was installed in the spring of 2010, and no heat related problems with the equipment has been detected since.

1.12 Future Extensions

1.12.1 Bottomhole Pressure Measurements

To fully understand the behavior of any low productivity gas well that may undergo liquid loading, it is necessary to continuously monitor bottomhole pressures.

Automation of pumping cycles are made much more accurate when the bottomhole pressure is available. Instead of using a user defined minimum gas rate to initiate pumping, and the surface measurements of pumped water to stop the pumping cycles, the bottomhole pressure could be used. By looking at the pressured differential between tubinghead and bottomhole, the amount of liquid in the wellbore could at any time be calculate accurately.

The main obstacle against installing a bottomhole pressure gauge is the high associated cost. Currently, equipment and installation costs for a well like the Noblin #2 is in the range of $50,000. This equals the total revenue from the well for one and a half years. Vendors of bottomhole pressure measurement hardware have been contacted, but at the current time it has not been possible to get equipment donated for the project.

As the market for bottomhole pressure gauges in low productivity wells, like the Noblin #2, should be significant. One can expect that equipment cost will go down with time, making it a more viable option.

1.12.2 Adding New Wells

As of November 2011, the process of selecting a second well to be added to the ROOKIE project is underway.

Anglin #3

The Anglin #3 was evaluated in late 2010 as a candidate for the ROOKIE project. Anglin #3 is completed in the Heartshorne formation in Latimer County, Oklahoma, and has been shut-in since 2005 due to liquid loading. A bottom hole pressure survey was performed on the well. The shut-in pressure survey is shown in Fig. 1.27, and the flowing pressure survey is shown in Fig. 1.28. A solid water column extending almost to the top perforation was identified from the shut-in survey. When the well was flowing, this water column was dispersed over almost 1500 ft. The bottomhole pressure was recorded at 157 psia when shut-in, and 155 psia when flowing. After the well was blown down, the gas rate declined rapidly towards zero.

A rod pumping unit was installed on the well to asses the unloaded production potential. A total of 1240 bbl of water was pumped off the well over a period of several months. The well showed no increase in gas rate (constant at $\sim$ 3 mcf/d), and new water from the reservoir continuously maintained the liquid level in the wellbore. There is evidence of a 4 – 5 ft coal layer within the perforated section of the wellbore from logs. This might be the source of the water influx.

Because the Anglin #3 did not show any sign of drying up, the well was abandoned as a candidate for the ROOKIE project.

Stafford #1

The Stafford #1 is producing from the Osborn formation in McClain County, Oklahoma. This is a lean gas condensate reservoir. The well is currently on plunger lift. The operator of the well is currently being contacted to allow instrumentation for the ROOKIE project. If the operator agrees, this will be the second well added to the project.

Nomenclature

C	Orifice constant
f	Frequency (Hz)
h_w	Pressure differential (in. H_2O)
p	Pressure (bara)
q	Rate (std m^3/d)

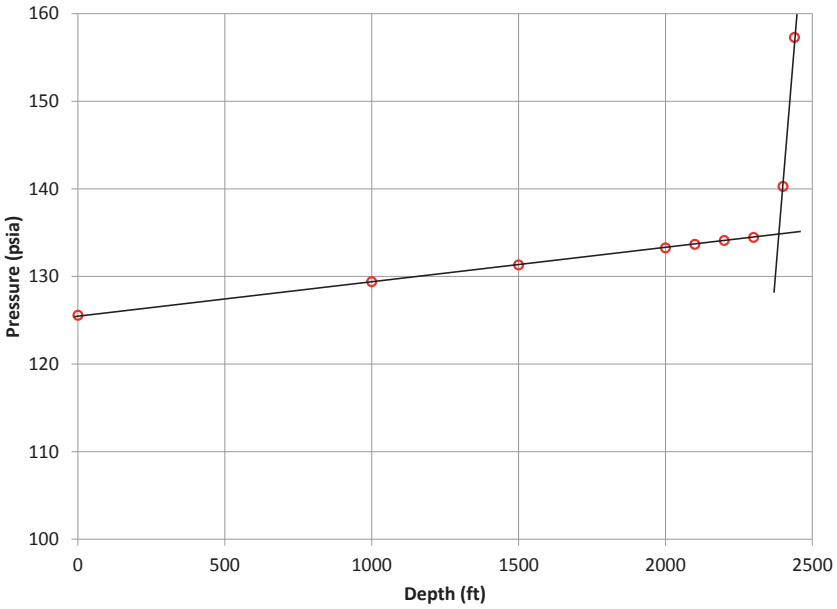

Fig. 1.27 – Shut-in bottomhole pressure survey on the Anglin #3. The fluid level is estimated at 2387 ft, and the perforations are from 2377 – 2431 ft.

Subscripts

g	Gas
w	Water

Abbreviations

AFL	Acoustic fluid level
DP	Differential pressure
MVT	Multi variable tool
NEMA	National electrical manufacturers association
NTNU	Norwegian university of science and technology
OLE	Object linking and embedding
OPC	OLE for process control

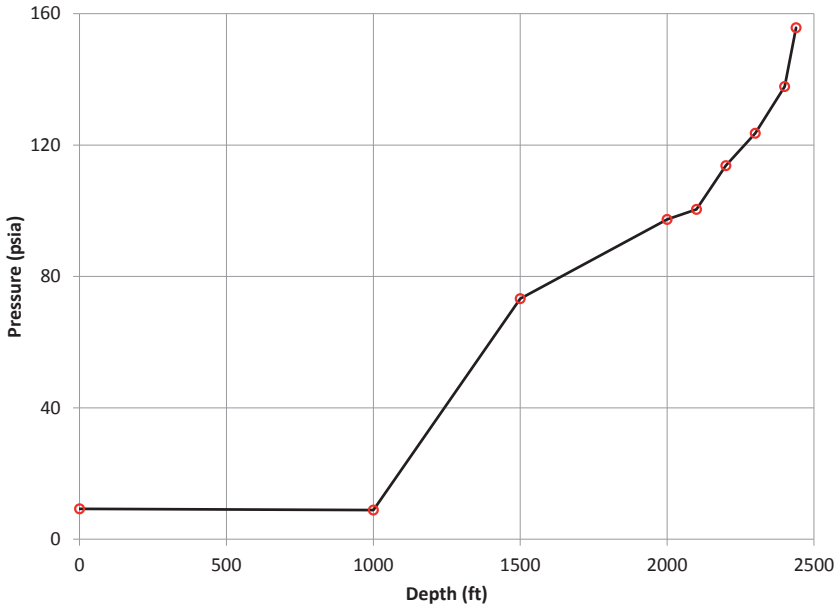

Fig. 1.28 – Flowing bottomhole pressure survey on the Anglin #3. The fluid column is dispersed over 1500 ft, and a solid water gradient is only seen in the bottom of the well.

PoE	Power over ethernet
RTU	Remote telemetry unit
ROOKIE	Remote operations in Oklahoma intended for education
VPN	Virtual private network

Bibliography

[1] Texas Rail Road Commision. Gas flow rate measurement. pages 1–61, Aug 1986.

[2] Data Retrieval Corporation. http://www.spidr.com.

[3] D.B Foo. Production optimization of gas wells by automated unloading: Case histories. In *SPE/CERI Gas Technology Symposium*, 2000.

[4] L.A Giangiacomo and D.R Hill. Optimizing pumping well efficiency with smart fluid-level controller technology. In *SPE Mid-Continent Operations Symposium*, 1999.

[5] Sage Technologies Inc. http://www.sageoiltools.com.

[6] National Instruments LabVIEW. http://www.ni.com/labview/.

[7] J.C Luppens. Practical automation for mature producing areas. *SPE Computer Applications*, 7(2):44–48, 1995.

[8] D Mathieson, C Giuliani, A Ajayi, and M Smithson. Intelligent well automation - design and practice. In *SPE Annual Technical Conference and Exhibition*, 2006.

[9] A.B Neely and H.O Tolbert. Experience with pumpoff control in the permian basin. *Journal of petroleum technology*, 40(5):645–649, 1988.

Chapter 2

Liquid-Loading

2.1 Introduction

Liquid-loading (LL) occurs in gas wells when the gas production rate falls below a critical limit, and the gas no longer is able to carry produced liquids up the wellbore. The production performance of a well experiencing liquid-loading may be drastically reduced compared to an unloaded well.

This chapter describes the theory of liquid-loading, and presents both numerical and analytical models to predict well performance for wells experiencing liquid-loading. Remediation strategies to mitigate liquid-loading are discussed towards the end of this chapter.

It is of interest to accurately model the liquid-loading phenomena. Most wells experiencing liquid-loading are completed in low pressure, low permeability reservoirs, where testing and intervention budgets are low. In these wells it is often not economically feasible to meter downhole data during a welltest. When surface test data is used to determine reservoir characteristics, liquid-loading effects must be accounted for to yield accurate results.

Data from the Noblin #2 well, accuired through the ROOKIE project, is used to validate the proposed liquid-loading models.

2.2 Background

2.2.1 Multiphase Flow in Gas Wells

It is important to understand how liquids and gas interact within the wellbore to understand liquid-loading. Multiphase flow in a vertical conduit can be represented by the five different flow regimes shown in Fig. 2.1. A flow regime is determined by the gas and liquid velocities, and the relative

amounts of gas and liquid present in the conduit (liquid holdup). Flow regimes may change with height within the wellbore.

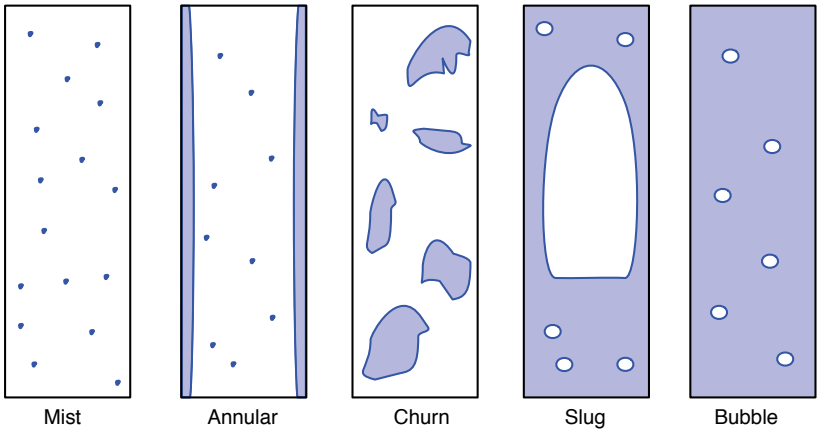

Fig. 2.1 – Flow regimes in a pipe with two phase flow. Liqiud holdup is monotonically increasing from left to right.

The different flow regimes can be summarized as follows:

Mist The gas phase is continuous, and the liquid is entrained in the gas as small droplets (mist). The pressure gradient is dominated by the gas flow.

Annular The gas phase is still continuos, but in addition to the liquid droplets within the gas, a liquid film forms along the pipe wall. The pressure gradient is still dominated by the gas flow.

Churn The flow changes from continuos liquid to continuos gas phase. Gas flow still dominates the pressure gradient, but liquid effects are becoming significant

Slug Gas bubbles expand as they rise and coalesce into larger bubbles. Liquid is now the continuos phase. Both gas and liquids significantly affect the pressure gradient.

Bubble The flow conduit is almost completely filled with liquids. Free gas rise as bubbles through the continuos liquid phase. The pressure gradient is dominated by liquids.

2.2.2 Liquid-Loading in Gas Wells

When gas flows through the wellbore, the gas carries liquids to the surface if the gas velocity is high enough. High gas velocity results in mist flow, where liquid drops are finely dispersed in the gas. In mist flow, the percentage of liquids in the wellstream by volume, referred to as liquid holdup, is low. This results in a low gravitational pressure drop in the wellbore.

As the gas velocity in the wellbore declines with time, the gas will no longer be able to carry liquids to the surface. The flow pattern in the bottom of the wellbore will gradually change from mist flow towards bubble flow.

As the liquid holdup increases, so does the gravitational pressured drop in the well. The presence of more liquids accumulating in the wellbore can either decrease production, or stop gas production altogether.

Few, if any, gas wells produce completely dry gas. Liquids can either be produced as free water or oil from the reservoir, or condense out on the way from bottomhole to surface as a result of pressure and temperature changes.

According to Waltrich and Falcone [23] and Zhang et al. [26], 90% of onshore gas wells in the United States are experiencing liquid-loading. Understanding liquid-loading is therefore important, and remediating liquid-loading may increase recoverable gas reserves.

2.3 Minimum Rate to Lift

The minimum rate to lift is the minimum gas rate required to bring *all* liquids co-produced with the gas to the surface. When the production rate falls below the minimum rate to lift, some fraction of the liquids will fall counter current to the gas, and start accumulating downhole.

Several correlations to predict the minimum rate to lift have been developed since the 1960's. The most used correlations are describe below.

2.3.1 Turner Equation

The Turner [21] equation was the first attempt, and current industry standard, to calculate the minimum rate to lift.

$$q_{min} = \frac{172.8\pi r^2}{B_g} \frac{(\sigma\Delta\rho)^{0.25}}{\sqrt{\rho_g}} \tag{2.1}$$

where the minimum rate to lift, q_{min}, is in mcf/d. Densities, ρ, are in lb/ft^3, and the radius of the flow conduit, r, is in ft.

This equation assumes a droplet model, where liquid is carried in the gas as perfect spheres. A force balance is applied to the droplet. The minimum rate to lift is the rate when gravitational and drag forces cancel each other out, as shown in Fig. 2.2.

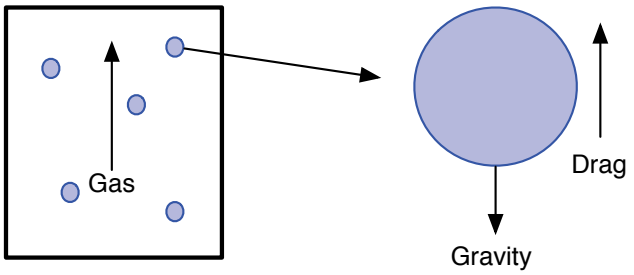

Fig. 2.2 – Force balance on a spherical liquid droplet in the Turner equation.

2.3.2 Coleman Equation

The Turner equation was later modified by Coleman et al. [3] to better describe low pressure gas wells.

$$q_{min} = \frac{9.61 \times 10^3 r^2 p v_{min}}{Tz} \tag{2.2}$$

where q_{min} is the minimum rate to lift in mcf/d, r is the flow conduit radius in ft, p is the pressure in psia, T is the temperature in ^{o}R, and v_{min} is defined as:

$$v_{min} = 1.912 \left(\frac{(\sigma \Delta\rho)^{0.25}}{\sqrt{\rho_g}} \right) \tag{2.3}$$

where the densities, ρ, are given in lb/ft^3.

The same assumptions as for the Turner equation are used in this minimum rate to lift equation.

2.3.3 Nosseir Equations

Nosseir et al. [18] developed a new correlation to predict the minimum rate to lift. This correlation still assumes the droplet model used by Turner, but takes into account different flowing regimes in the well. The first equation is applicable for low gas rates, where the Reynolds number, N_{Re}, is less than 1000.

$$v_{min} = 14.6\sigma^{0.35}\frac{(\Delta\rho)^{0.21}}{\mu_g^{0.134}}\rho_g^{0.426} \tag{2.4}$$

For highly turbulent flow ($N_{Re} > 1000$), the following equation applies:

$$v_{min} = 21.3\sigma^{0.25}\frac{(\Delta\rho)^{0.25}}{\rho_g^{0.5}} \tag{2.5}$$

where the densities, ρ, are given in lb/ft^3, the gas viscosity, μ_g, is given in lb s /ft^3 , and the minimum gas velocity, v_{min}, is in ft/s. Using the minimum gas velocity from these equations, the minimum rate to lift can be calculated from Eq. 2.2.

The Reynolds number for flow in pipe is defined as:

$$N_{Re} = \frac{2\rho v r}{\mu} \tag{2.6}$$

2.4 Flooding

Flooding refers to the condition where all liquid flows counter current to the gas. No liquid is carried upwards together with the gas, but accumulates downhole.

McQuillan et al. [15] give a correlation to calculate the flooding gas velocity, v_{gF}. This is the maximum gas velocity at which flooding occurs.

$$v_{gF} = \left(\frac{\pi}{4}\right)^{1/2}\left(\frac{gd\Delta\rho}{\rho_g}\right)^{1/2} \tag{2.7}$$

where d is the diameter of the flow conduit. If field units are used, Eq. 2.2 can be used to calculate the flooding rate, q_{gF}, substituting v_{gF} for v_{min}.

Between the flooding rate and the minimum rate to lift there is a transition where some fraction of the produced liquids are carried together with the gas to the surface.

The traditional equations predicting the onset of liquid-loading assumes that the flooding rate is equal to the minimum rate to lift. No transition is assumed from when the first liquid droplet starts flowing counter current to the gas, to when all liquid flows counter current.

2.5 Validity of Minimum Rate To Lift Equations

Both numerical models and a small scale laboratory experiment were carried out to test the assumptions and predictions of the minimum rate to lift equations discussed in the previous section.

2.5.1 Experimental Observations

A 10 m long vertical transparent tube was mounted in the laboratory at the Department of Petroleum Engineering and Applied Geophysics, NTNU. The tube has an inner diameter of 1.5 in. Water and air (as a substitute for natural gas) are injected at the bottom of the tube through separate valves. The air is injected with a backpressure of 2 bara. Water is collected at the top of the tube.

Since the tube is transparent, it is easy to observe the flowing conditions within the tube.

Observed Flow Regimes

1. Liquid-Unaffected Gas Flow Regime

   Liquid covers the pipe walls as a thin film. The liquid film travels upwards, driven by the gas. No liquid is accumulated in the pipe, and the liquid never travels counter current with respect to the gas.

   In this flow condition, the pressure drop in the pipe is essentially as expected for gas-only fully-turbulent flow, perhaps with an extra gravity term because of the liquid. Total pipeflow pressure drop is essentially unaffected by liquids.

2. Liquid-Affected Gas Flow Regime

   In this flow condition, after steady-state conditions are reached, all liquid flowing into an elemental volume of the pipe also flows out of that elemental volume. However, a clear liquid presence exists within the flow conduit.

   (a) At higher rates in this flow regime, the liquid is a swirling thin film on the pipe surface. The thickness of the swirl increases as gas rate decreases.

   (b) At lower rates in this flow regime, a hanging, pulsating liquid appears within the pipe. The pipe has a measurable liquid fraction. Most important, though, the liquid seems to have a steady-state upward mobility which guarantees that liquid in = liquid out of any

elemental volume along the pipe. Physically it seems the gas 'lifts' liquid upward some distance, then the liquid falls back down, but the next liquid movement is upwards. The net liquid movement is upwards. Another characteristic of this regime is that the bottom of the hanging liquid zone stabilizes some distance above the gas entry point.

(c) Once the bottom of the hanging liquid zone reaches the gas entry point, even lower gas rates do not see liquid flowing downward, countercurrent to gas flow.

In this flow regime the total pipeflow pressure drop is significantly affected by the presence of liquids, but all liquids are still being produced.

3. Liquid-Loaded Gas Flow Regime

The flooding gas rate (q_{gF}) marks the gas rate where the hanging liquid drops below the gas entry point, so that the liquid flows downward countercurrent to the gas flow.

2.5.2 Transient Wellbore Model

Studies were conducted by J. S. Plasencia and O. A. Al Saif, using a transient pipe flow simulator to investigate the behavior of a well experiencing liquid-loading. These results are not previously published. The model is shown in Fig. 2.3. It consists of 50 horizontal cells. The internal pipe diameter is 1.625 inches, and the total height of the well is 1032 m. The gas specific gravity, γ_g, is 0.6. Gas and water is injected in the bottom of the well, and the well is produced against a constant bottomhole pressure of 25 psia. Liquid accumulation in the wellbore is calculated.

Several combinations of gas and water rates were simulated to determine the minimum gas rate when liquid starts accumulating downhole. All the cases run are presented in Table 2.1. The liquid holdup throughout the wellbore for one of the cases is presented in Fig. 2.4.

The minimum rate to lift was calculated using the Turner, Coleman, and Nosseir equations to compare with the results from the transient wellbore simulator.

The interfacial tension, σ, needed for the minimum rate to lift calculatios, is calculated from Whitson [24].

$$\sigma = 15 + 0.91\Delta\rho_{wg} \tag{2.8}$$

where $\Delta\rho_{wg}$ is the density difference between water and gas in lb/ft^3.

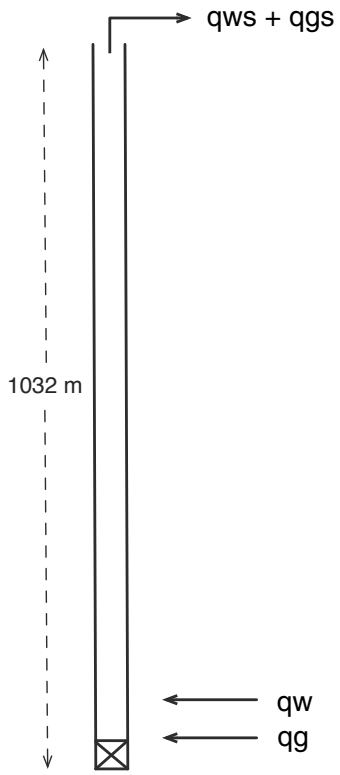

Fig. 2.3 – Visual representation of the transient pipe flow model. Water and gas is injected at the bottom of the well. The tubinghead pressure is kept constant at 25 psia, and resulting water accumulation in the wellbore, and production rates are calculated.

The calculated minimum rate to lift for the different correlations are 119.4, 114.1, and 42.5 mcf/d for the Turner, Coleman, and Nosseir equations, respectively.

The Turner and Coleman equations give very similar predictions for the minimum rate to lift, while the Nosseir equation predicts the minimum rate to lift to be less than half of what the other equations predict.

Some interesting conclusions can be drawn from these results:

1. Gas rates higher than or equal to 75 mcf/d will never result in liquid-loading for this well. This means that the Turner and Coleman equations are over predicting the minimum rate to lift by at least 40%.

TABLE 2.1 – Results from the transient wellbore model.

Results			
q_g mcf/d	q_w bbl/d	Max Holdup $-$	Liquid Column m
15	0.05	0.0007	–
15	0.15	0.0007	–
15	0.25	0.32	220
25	0.05	0.009	–
25	0.15	0.009	–
25	0.25	0.3	410
50	0.05	0.009	–
50	0.15	0.009	–
50	0.25	0.22	435
75	0.05	0.002	–
75	0.15	0.002	–
75	0.25	0.009	–
100	0.05	0.0045	–
100	0.15	0.0045	–
100	0.25	0.009	–

The Nosseir equation gives a reasonable value for the minimum rate to lift.

2. When liquid-loading occurs, a solid liquid column is *not* formed. The maximum liquid holdup encountered in all the simulated cases was 0.32. The liquid content is highest at the bottom of the liquid column, and decreases towards the top.

3. The onset of liquid-loading is dependent on the gas-liquid ratio (GLR). As seen for the cases with gas rate of 50 mcf/d in Table 2.1, liquid-loading only occurs for the low GLR case.

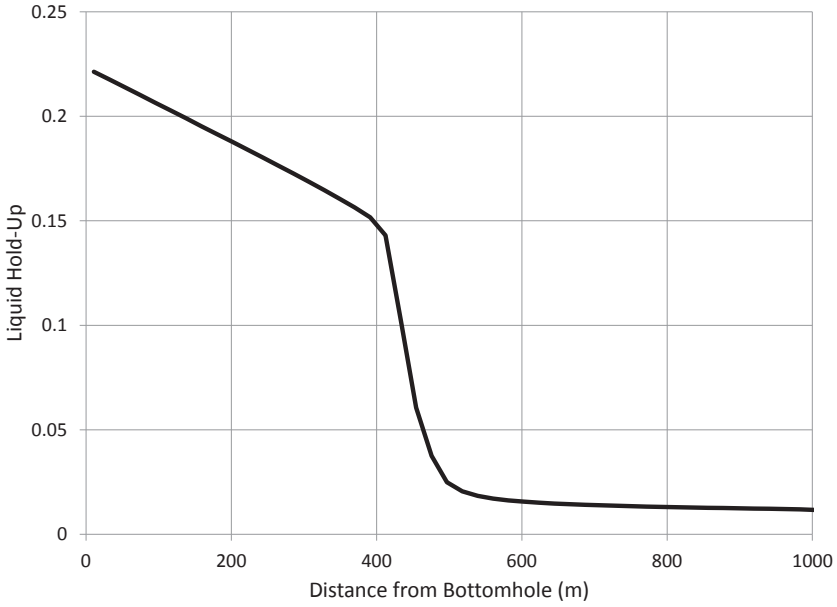

Fig. 2.4 – Liquid holdup calculated by the transient wellbore model. The gas rate is 50 mcf/d, and the water rate is 0.25 bbl/d.

2.6 Typical Liquid-Loading Well Performance

A normal gas well, not affected by liquid-loading, will have a near linear decline in gas production when plotted on semi-log scales, as seen in the classical paper by Arps [1]. This depletion performance will go on for the entire life of the well.

When a well starts to be affected by liquid-loading, a sharp drop in the productivity of the well is observed, i.e. faster decline. This drop in productivity is caused by the liquid column forming in the bottom of the wellbore. As the liquid accumulates, the backpressure on the reservoir increases. After some period of time the liquid column will stabilize. When the liquid column has stabilized, the decline in production will slow down. The production rate after the liquid column has stabilized is called the meta stable rate, a term coined by Dousi et al. [6]. The duration of the transition between unloaded (not affected by liquid-loading) and meta stable production, and at what rate the well stabilizes at, depends on well productivity, wellbore dimensions, and the amount of liquids co-produced with the gas.

Fig. 2.5 shows the production history of the McKee #1 well, producing from the Booch formation. As seen from the figure, this well started experiencing liquid-loading when the gas rate dropped below ∼50 mcf/d. Before the onset of liquid-loading, the well had a constant linear decline in production. When liquid-loading occurred, the decline became much steeper, before the well eventually stabilized at a meta stable rate of ∼3 mcf/d.

Another well experiencing liquid-loading is shown in Fig. 2.6. This is the Sarkey #1, producing from the Hartshorne formation. The production characteristic for the Sarkey #1 is much the same as for the McKee #1, but liquid-loading occurs at a gas rate of ∼100 mcf/d, and the well stabilizes at a meta stable rate of ∼20 mcf/d. The difference in onset of liquid-loading for the two wells could be caused by different tubing dimensions, produced gas-liquid ratio, etc.

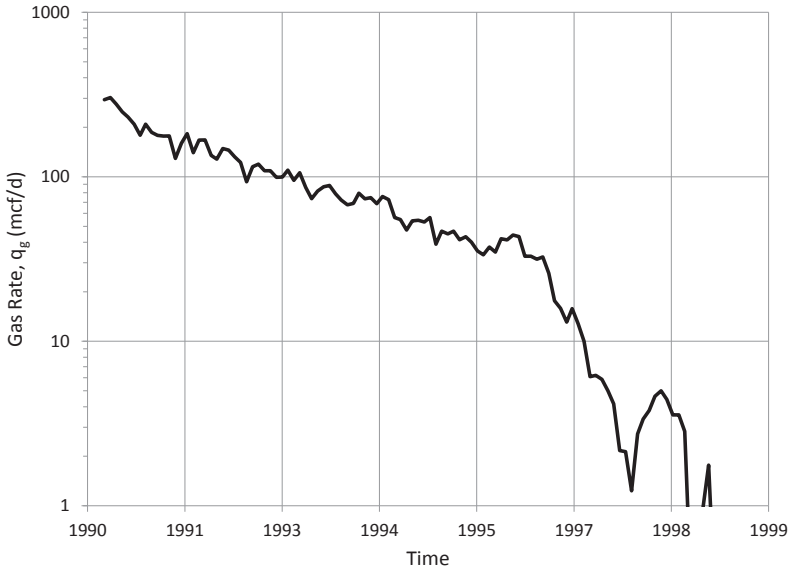

Fig. 2.5 – Historical gas production for McKee #1 producing from the Booch formation. A sharp decrease in productivity indicative of liquid-loading is seen when the well reaches a production rate of ∼50 mcf/d.

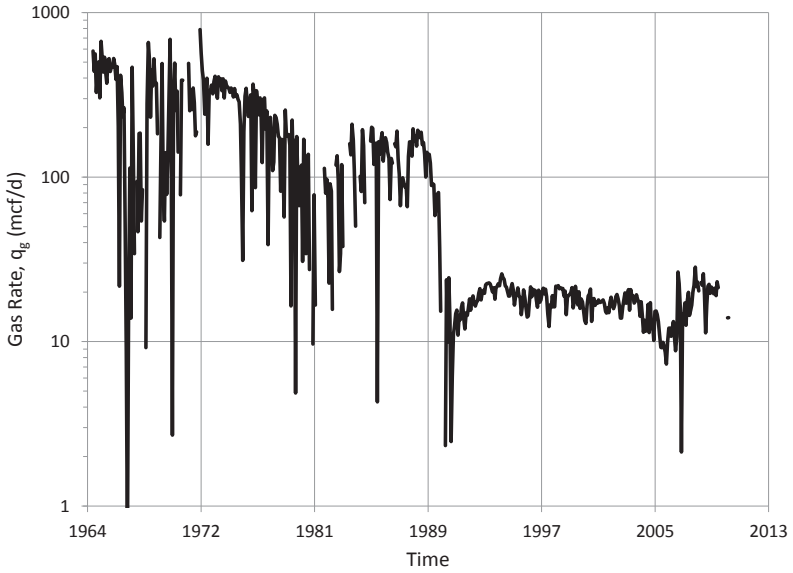

Fig. 2.6 – Historical gas production for Sarkey #1 producing from the Hartshorne formation. A sharp decrease in productivity indicative of liquid-loading is seen when the well reaches a production rate of ∼100 mcf/d.

2.7 Numerical Modeling

This section presents attempts to model liquid-loading numerically. A new numerical modeling strategy is presented, and the current numerical modeling strategies available to the industry are reviewed.

In numerical models, differential equations describing flow in reservoir, or wellbore, are discretized. The discretized versions of the equations are solved for a grid of cells representing the physical area of interest, i.e. the reservoir and/or wellbore. The most simple form of the differential equation governing flow in the reservoir, is for single phase one dimensional flow. This example is taken from Mattax and Dalton [14].

$$-\frac{d}{dx}\left(\frac{q_g}{B_g}\right) = A\frac{d}{dt}\left(\frac{\phi S_g}{B_g}\right) \tag{2.9}$$

where A is the flow area.

2.7.1 Previous Work

A number of attempts to model liquid-loading with numerical models have been made the last years. This section summarizes the major contributions to the literature.

Reservoir Only Models

Zhang et al. [26] studied the effect of the inflow performance relationship (IPR) of a well experiencing liquid-loading, using a near-well reservoir simulator with implicit pressure, explicit saturation (IMPES) formulation. The wellbore was not modeled in this work. A table of oscillating bottomhole pressures were used as input to the reservoir simulator, to mimic the transient behavior of liquid-loading in the wellbore. A U-shaped IPR is suggested to model wells undergoing liquid-loading. This U-shape is caused by a delay in pressure response from the liquid column in the wellbore extending out in the reservoir.

Coupled Models

Several attempts have been made to couple reservoir and dynamic wellbore models to model liquid-loading.

Hu et al. [9] was the first attempt to couple a numerical reservoir simulator with a transient well flow model. They coupled a transient pipe flow simulator implicitly with a near-well reservoir simulator. The pipe model

represents the wellbore. Sensitivities to the production rates with respect to wellbore pressure is passed from the reservoir simulator to the pipe model. Since only a near-well model represents the reservoir, this approach can not be used to model situations where depletion is important.

Chupin et al. [2] used this model to study liquid-loading behavior. The model was not tested against measured field data, but was found to reproduce the behavior of a well undergoing liquid-loading qualitatively.

2.7.2 Introduction to a New Numerical Modeling Approach

A radial single well model was built to model liquid-loading using a commercial numerical reservoir simulator. Production data from the Noblin #2 well was used to test the model. A single model is used to model both the reservoir and the wellbore.

2.7.3 Model Description

The model is a two dimensional radial single well model. Both the reservoir and the tubing/annulus are included in the grid. The layout of the grid is shown in Fig. 2.7. This model uses a fully implicit formulation to solve the flow equations.

An example simulator input file is given in Appendix B.

Completions

Gas is produced from the top cell of the casing-tubing annulus (cell [1,2]). A water production completion is located at the bottom of the rat hole, to simulate the pumping unit.

A water injection completion is also located at the bottom of the rathole. This completion is used to simulate liquids accumulating downhole.

Vertical Flow Performance

To simulate frictional pressure loss in the annulus, a high permeability value is given to the cells representing the wellbore.

The permeability in the annulus should be selected such that the pressure drop in the annulus in the model corresponds to a dry gas vertical flow performance equation. The following equation is taken from Fetkovich [7].

$$\Delta p_w = \left(\frac{q_g}{C_t}\right)^2 \tag{2.10}$$

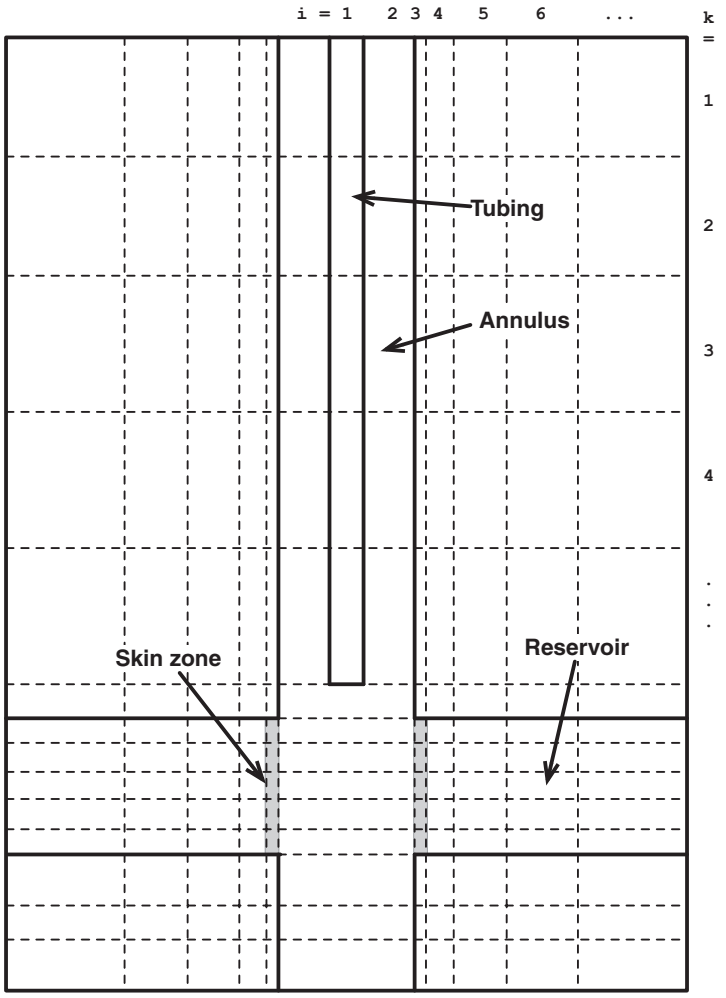

Fig. 2.7 – Numerical model grid cross section. Solid lines indicate no-flow boundaries. Dotted lines indicate cell boundaries.

where Δp_w is the frictional pressure drop in the tubing in psi.

$$C_t = \frac{13.0 \exp(S/2)}{\sqrt{e^S - 1} F_r \overline{T}\overline{z}} \tag{2.11}$$

$$S = \frac{0.0684 \gamma_g h}{\overline{T}\overline{z}} \tag{2.12}$$

and,

$$F_r = \frac{0.10797}{(d_c - d_t)^{2.612}} \tag{2.13}$$

where d_c is the inner casing diameter, and d_t is the outer tubing diameter, both in inches. h is the vertical depth of the well in ft, $\overline{T}$ is the average temperature in the wellbore in ^{o}R, and q_g is the gas rate in mcf/d.

Skin Zone

A zone near the wellbore with permeability, k_a, different from the reservoir permeability, k, is included in the model. This zone represents a skin factor, and can be calculated from Hawkins [10].

$$s = \left(\frac{k}{k_a} - 1\right) \ln \frac{r_a}{r_w} \tag{2.14}$$

If $k_a < k$, the skin factor is positive, and if $k_a > k$, the skin factor is negative.

In the numerical model representing Noblin #2, the damage zone radius, r_a, is 0.117 meters measured from the sandface.

Radial Gridding

The first column of cells in the radial direction ($i = 1$) represents the tubing, and the second column ($i = 2$) represents the casing-tubing annulus. No-flow boundaries are included between columns 1 and 2, and between columns 2 and 3 to represent the tubing and casing, respectively. These boundaries extend from the surface, and down to the top of the reservoir.

The radial grid outside the casing is geometrically spaced.

$$r_{i+1} = r_i \left(\frac{r_w}{r_e}\right)^{1/N} \tag{2.15}$$

where N is the number of cells in the radial direction within the reservoir.

Vertical Gridding

The tubing and annulus, from surface to the top of the reservoir, are represented by 99 grid rows of equal size in the vertical direction. Each row has a thickness of 10.68 m. The reservoir is represented by 8 grid rows, each 1.22 m thick, adding up to the total reservoir thickness of 9.76 m.

The rat hole is included in the grid, and is represented with 11 cell rows, each 1.22 m thick.

Water Handeling

Water is injected at the bottom of the wellbore to simulate the effect of liquid-loading. The water injection rate is calculated as a fraction of the gas production rate. This water fraction represents both free and solution water accumulating downhole.

To simulate the rod pump installed on the Noblin #2, water is produced intermittently from the bottom of the wellbore. The produced water amounts correspond to the recorded pumped water volumes.

At the start of the simulation, a 8 m^3 slug of water is injected in the well over a one day period, to simulate the acid treatment performed on the well when it was completed.

Relative Permeability

Corey [4] type relative permeability curves are used in the model. Separate curves are given to the following regions:

Annulus The relative permeability curves used in the annulus are straight line curves, with exponents, n, equal to one. This makes sure that capillary effects are disregarded in the wellbore.

Reservoir The relative permeability curves used for the reservoir are shown in Fig. 2.8. The exponents for both water and gas are 3.0. Endpoint saturations and relative permeabilities are all 1.0.

Skin zone The same relative permeability curve as for the rest of the reservoir is used for the skin zone, with one exception. The endpoint water relative permeability, $k_{rw}(S_{gc})$, is allowed to be lower. This mimics the effect of permeability damage due to fresh water backflow, as shown by Jurus [11].

Model Control

The numerical model is on rate control, constrained by a minimum tubing-head pressure of 1.03 bara (15 psia).

2.7.4 Noblin #2 Sweet Spot Model

A simulation model was built to match the entire production history of the Noblin #2, from startup in 1991, to June 2010.

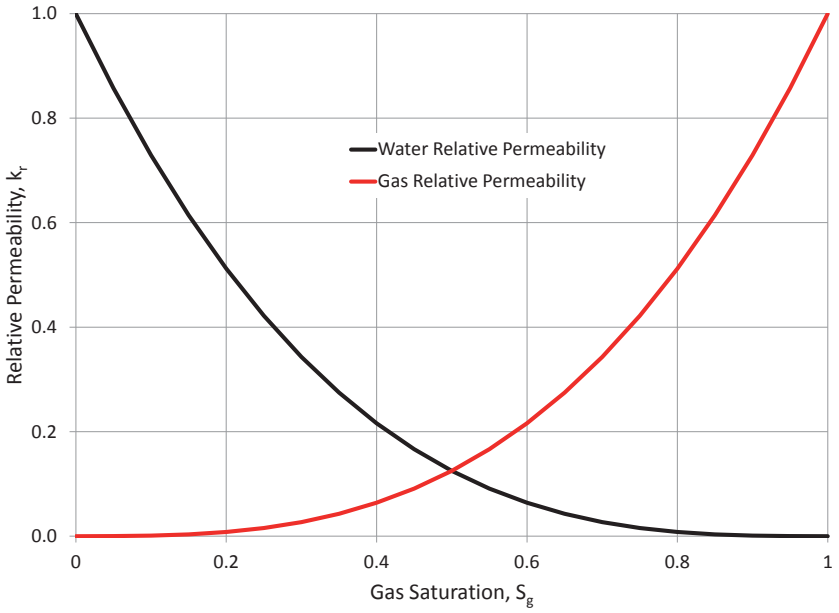

Fig. 2.8 – Relative permeability curves used for the reservoir section in the numerical model.

The model has uniform permeability in the reservoir, except for a small "sweet spot" near the wellbore. The sweet spot is a high permeability area, that might have been created by the initial acid treatment performed on the well. In the model, the sweet spot is located in the topmost layer of the reservoir. It is 1.22 m high, and extends 8.1 m into the reservoir from the wellbore.

Porosity is uniform throughout the reservoir, and is set to 10%. The drainage radius, r_e, in the model is 268 meters. This corresponds to a 55 acre well spacing.

The rat hole is included in the model, and water is unloaded from the well 12.2 m below the bottom of the reservoir. This reflects the current pump placement in the Noblin well. A schematic of the model is shown in Fig. 2.9.

Observed Data

Gas production rates are available throughout the life of the well. The rate data was collected from a number of sources, as given in Table 2.2.

Wellhead pressure data is only available after the wellhead pressure

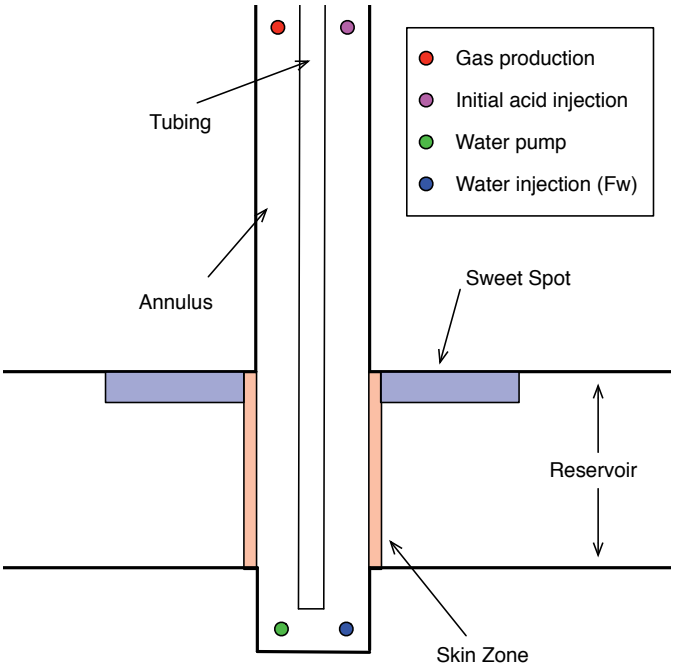

Fig. 2.9 – Sweet spot model used to history match the Noblin #2 production data.

TABLE 2.2 – Gas production data sources for the Noblin #2.

Data Sources			
From	To	Source	Interval
01.01.1991	01.10.2007	Public	monthly
01.10.2007	14.01.2008	Sales	daily
14.01.2008	22.01.2008	SPIDR Welltest	hourly
22.01.2008	03.09.2008	Sales	daily
03.09.2009	01.06.2010	Rookie DB	hourly

gauge was installed as a part of the ROOKIE project in December 2009, with the exception of a welltest performed on the well in 2008 using the SPIDR system. The pressure data sources are given in Table 2.3.

TABLE 2.3 – Wellhead pressure data sources for the Noblin #2.

Data Sources			
From	To	Source	Interval
14.01.2008	22.01.2008	SPIDR Welltest	hourly
04.12.2009	01.06.2010	Rookie DB	hourly

History Matching

The numerical model was history matched against the observed rate and pressure data. The following reservoir parameters were used as variables in the history matching process:

- Reservoir permeability (k)
- Sweet spot permeability (k_s)
- Skin zone permeability (k_a)
- Endpoint water relative permeability in skin zone $k_{rw}(S_{gc})$)
- Producing water cut (F_w)

The initial reservoir pressure, p_R, was not included as a variable in the history matching. It was set to 27.6 bara, based on the initial production test performed on the well. This information was taken from the well completion card.

The objective of the history matching process is to minimize the discrepancy between observed data and model predictions. This discrepancy is formalized with the sum of squares (SSQ), F_{SSQ}.

$$F_{SSQ,p} = \sum_{t=0}^{N} \left(\frac{p_{t,mod} - p_{t,obs}}{p_{ref}} \right)^2 \tag{2.16}$$

$$F_{SSQ,q} = \sum_{t=0}^{N} \left(\frac{q_{g,mod} - q_{g,obs}}{q_{ref}} \right)^2 \tag{2.17}$$

where $p_{t,mod}$ and $q_{g,mod}$ are tubinghead pressures and gas rates predicted by the simulator. $p_{t,obs}$ and $q_{g,obs}$ are observed tubinghead pressures and gas rates. The reference values, p_{ref} and q_{ref}, are representative values for the

tubinghead pressure and gas rate, respectively. These values are used to normalize the SSQ, and helps the optimization algorithm converge faster.

$$F_{SSQ} = F_{SSQ,p} + F_{SSQ,q} \tag{2.18}$$

where F_{SSQ} is the total SSQ, $F_{SSQ,p}$ is the tubinghead pressure SSQ, and $F_{SSQ,q}$ is the gas rate SSQ.

Even though the model is controlled on gas rates, there might be a mismatch between the model and observed rate data. This is the case when the minimum tubinghead pressure constraint is reached, and the model no longer is able produce the desired rate. For this reason, the gas rate mismatch, $F_{SSQ,q}$, is included in the SSQ.

An evolutionary strategy algorithm was used to history match the model. The algorithm is described in Appendix A.

Best-Fit Results

The best fit values for the variables in the history matching are presented in Table 2.4. A skin factor, s, of -0.48 is calculated from Eq. 2.14 for the best fit model.

TABLE 2.4 – Best fit reservoir parameters for the history matched sweet spot model on the Noblin#2 production data.

Noblin #2 Sweet Spot Model		
	Value	Unit
Reservoir permeability, k	9.34	md
Sweet spot permeability, k_s	161.8	md
Skin zone permeability, k_a	22.7	md
Water relative permeability, $k_{rw}(S_{gc})$	0.00704	–
Water cut, F_w	0.040	bbl/mcf

The gas production profile for the Noblin #2 used as input to the numerical model is shown in Fig. 2.10. Gas rate data is collected from the sources listed in Table 2.2. The history matched model is able to produce the observed gas rate for most of the well life.

Fig. 2.11 shows the tubinghead pressures for the history matched model, together with the available measured pressure data. As is seen from this

figure, pressure data is only available for two periods, as described in Table 2.3.

The first period where measured tubinghead pressures are available is from a welltest in 2008. The gas rates for this period, both measured and predicted by the model, are shown in Fig. 2.12. The tubinghead pressures for the same period are shown in Fig. 2.13. The pressure behavior during this period is matched well, especially the build-up period. Gas rates for the draw-down period prior to the build-up period are maintained by the model, but the draw-down period after the build-up is not matched properly.

The last period where measured tubinghead pressures are available is from after the ROOKIE project came online. The gas rates for this period are shown in Fig. 2.14, and the tubinghead pressures are shown in Fig. 2.15. During this period the well is being regularly unloaded by the pumping unit installed on the well. These pumping cycles are included in the model as described previously. From the figure showing the gas rates for this period, it is clear that the history matched model is able to maintain the observed rates with some minor exceptions. The tubinghead pressure performance is matched fairly well for most of the period, with one exception. The build-up pressure performance during the shut-in of the well starting at 7000 days is not predicted well by the model. The tubinghead pressure at the end of this shut-in is over predicted with almost 2.

Over all the history matched model is able to capture the performance of the Noblin #2 reasonably well.

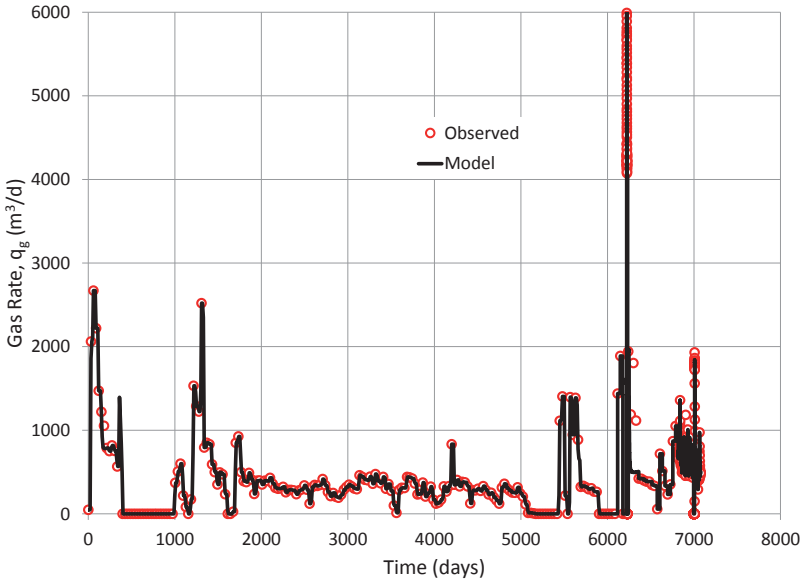

Fig. 2.10 – Gas rates used as input in the history matching of the sweet spot model.

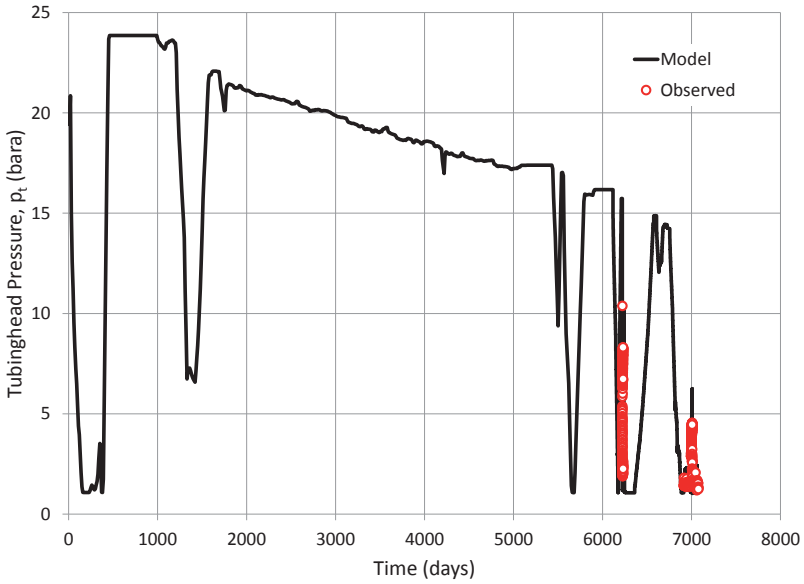

Fig. 2.11 – History matched tubinghead pressures for the sweet spot numerical model. Only two short periods of observed pressure data is available.

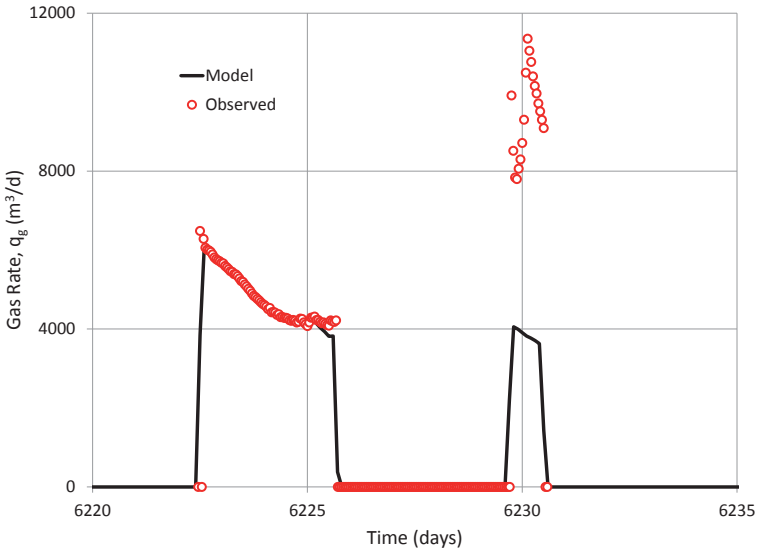

Fig. 2.12 – Gas rates for the history matched sweet spot model during a drawdown – buildup test.

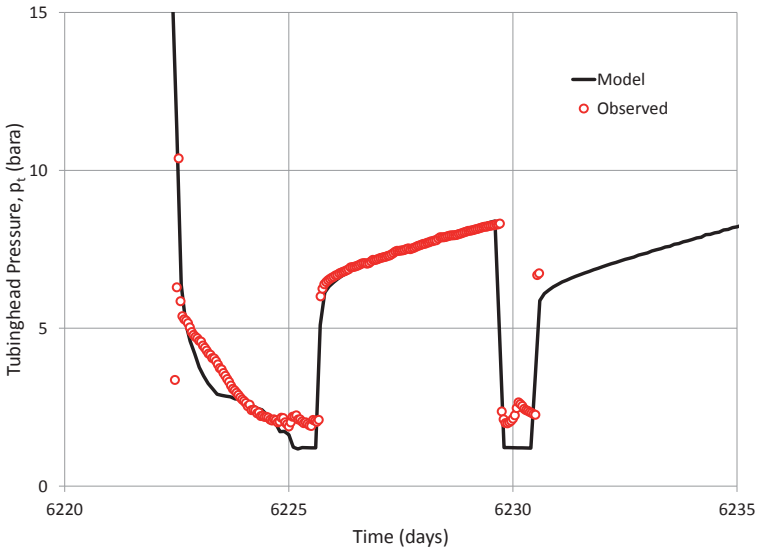

Fig. 2.13 – History matched tubinghead pressures of the sweet spot model during a drawdown – buildup test. This pressure data was recorded with the SPIDR system.

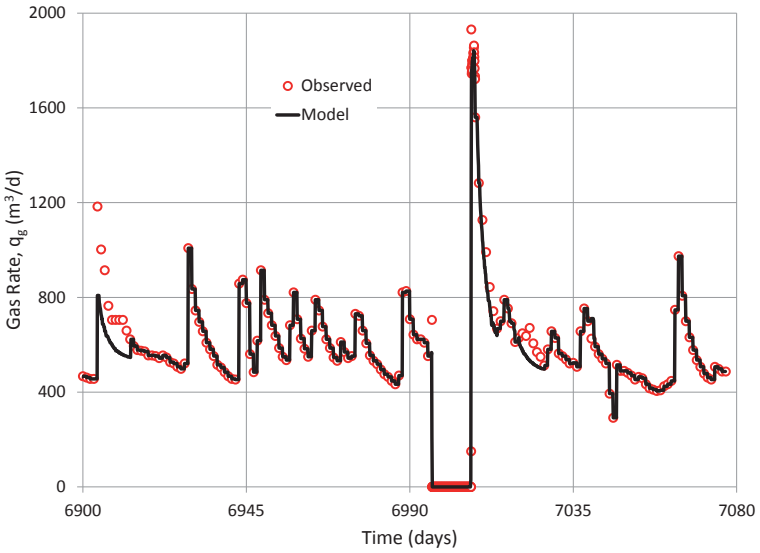

Fig. 2.14 – Gas rates for the history matched sweet spot model. This is the period when data is available from the ROOKIE project. During this time interval the well is regularly unloaded with the pumping unit.

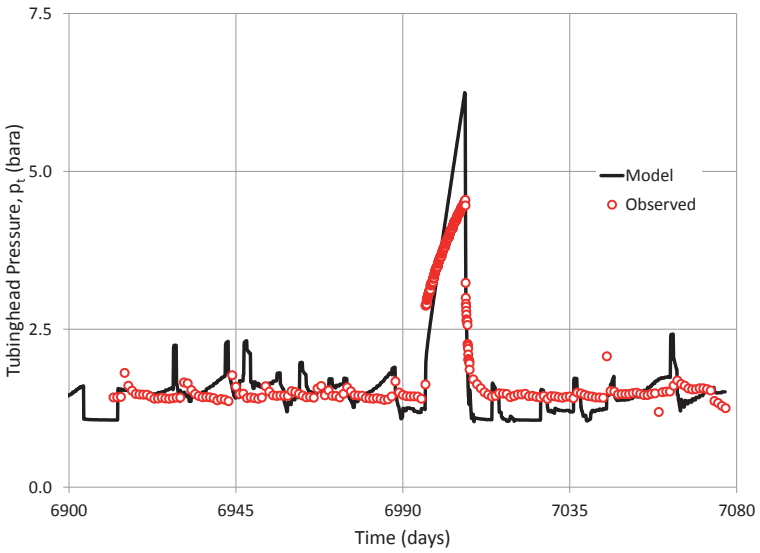

Fig. 2.15 – History matched tubinghead pressures of the sweet spot model for the period when data is available through ROOKIE. The build-up period starting at 7000 days is not captured very well.

2.7.5 Noblin #2 LNX Model

In addition to the sweet spot model, a layer-no-crossflow (LNX) model was built to match the observed data from the Noblin #2.

In this model, the reservoir is divided into two layers. The layers do not communicate within the reservoir, only through the wellbore. This model was selected since there is evidence of a shale barrier in the middle of the Atoka formation that the Noblin #2 is producing from. The shale barrier can be seen from the gamma ray log shown if Fig. 1.8. The log does not give any information on whether the shale break is permeable or not, but for this model it is considered a no-flow boundary.

Each reservoir layer, or unit, is modeled with 4 numerical layers. Both reservoir units are 4.88 m thick, adding up to the total reservoir thickness of 9.76 m. The skin zone extent, drainage radius, initial reservoir pressure, and reservoir porosity are the same for this model as for the sweet spot model. The model is shown in Fig. 2.16.

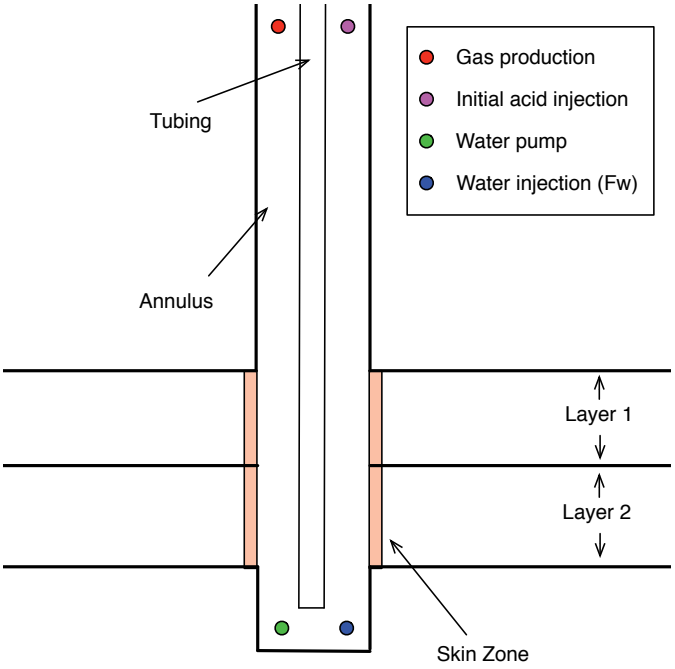

Fig. 2.16 – LNX model used to history match the Noblin #2 production data.

Observed Data

The same observed data as for the sweet spot model was used to history match the LNX model.

History Matching

The following reservoir parameters were used as variables in the history matching process:

- Layer 1 permeability (k_1)
- Layer 2 permeability (k_2)
- Skin zone permeability (k_a)
- Endpoint water relative permeability in skin zone ($k_{rw}(S_{gc})$)
- Producing water cut (F_w)

The same SSQ formulation as for the sweet spot model was used to asses the model fit to observed data. See Eq. 2.16 – 2.18. The evolutionary strategy algorithm used to minimize the SSQ for the sweet spot model was also used to history match this model.

Best-Fit Results

The best fit values for the variables in the history matching process are presented in Table 2.5. A skin factor, s, of -0.08 and -0.79 for layers 1 and 2, respectively, is calculated from Eq. 2.14 for the best fit model.

The gas production profile for the Noblin #2 used as input to the numerical model is shown in Fig. 2.17. Gas rate data is collected from the sources listed in Table 2.2. The history matched model is not able to produce the observed gas rate for certain periods of the simulation. The mismatch is significant between 1000 – 3500 days.

Fig. 2.18 shows the tubinghead pressures for the history matched model, together with the available measured pressure data. As is seen from this figure, pressure data is only available for two periods, as described in Table 2.3.

The gas rates, both measured and predicted by the model, for the well test from 2008 are shown in Fig. 2.19. The tubinghead pressures for the same period are shown in Fig. 2.20. The pressure build-up behavior is matched well for the well test, but the draw-down prior to the build-up period is not

TABLE 2.5 – Best fit reservoir parameters for the history matched LNX model on the Noblin#2 production data.

Noblin #2 LNX Model		
	Value	Unit
Layer 1 permeability, k_1	34.75	md
Layer 2 permeability, k_2	1.38	md
Skin zone permeability, k_a	38.61	md
Water relative permeability, $k_{rw}(S_{gc})$	0.00633	–
Water cut, F_w	0.041	bbl/mcf

matched well, and gas rates are not maintained at the observed values. The draw-down period after the shut-in is not matched well either.

The gas rates for the period where data is available through the ROOKIE project are shown in Fig. 2.21. The tubinghead pressures for the same period are shown in Fig. 2.22. The observed gas rates are met for much of this period, but not for the period between 6900 – 6940 days and the period between 7020 – 7060 days. The tubinghead pressure is matched reasonably well for the entire period, except for the extended shut-in starting at 7000 days. The shut-in pressures are highly over predicted by the model.

It was not possible to obtain a model match that satisfied both the periods when pressure data is available. A good match for the first period, leads to a poor match for the second period, and vice versa. Several starting points for the variables used in the history matching were tried, without improving the match.

2.7.6 Comparison of the History Matched Models

It is evident that the sweet spot model matches the observed data from the Noblin #2 better than the LNX model. This supports the view that the shale barrier seen from the logs is permeable, and does not act as a no-flow barrier.

A model with constant permeability throughout the reservoir was also tried matched to the observed data. The model did not contain a no-flow barrier within the reservoir. This model matched the data more poorly than the LNX model, and the results are not presented here. Because the uniform model was not able to match the observed data, the presence of a

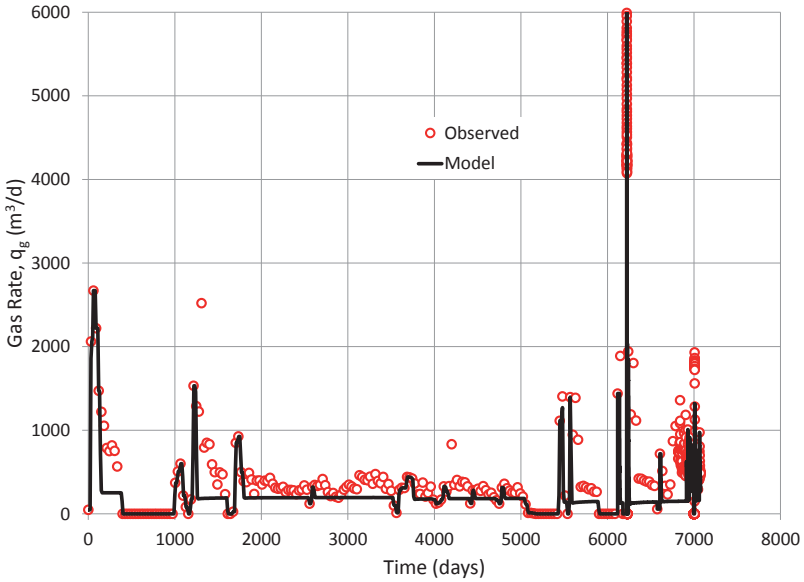

Fig. 2.17 – Gas rates used as input in the history matching of the LNX model.

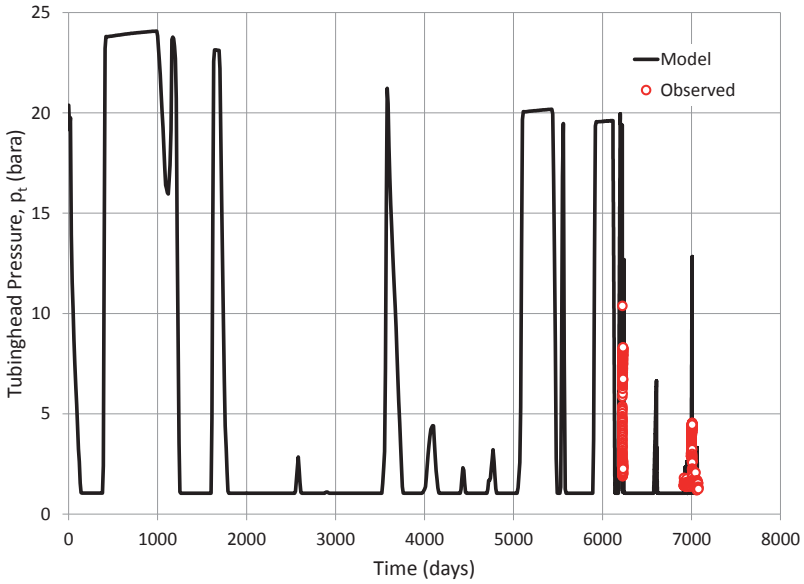

Fig. 2.18 – History matched tubinghead pressures for the LNX numerical model. Only two short periods of observed pressure data is available.

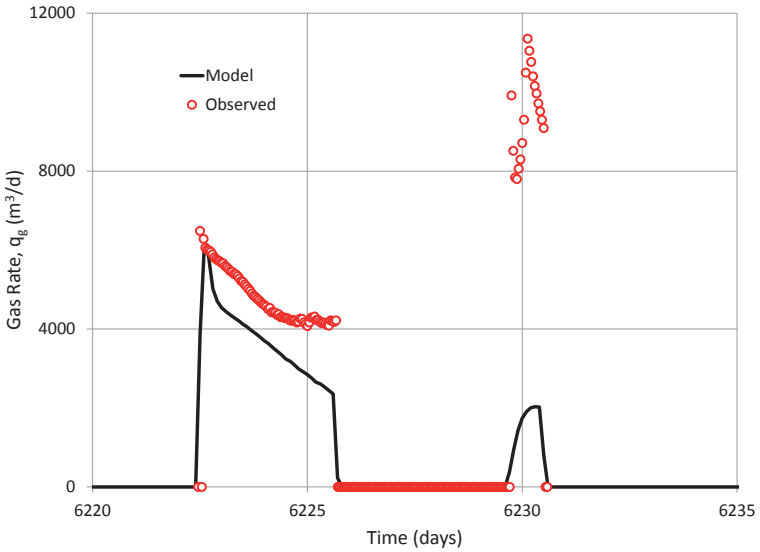

Fig. 2.19 – Gas rates for the history matched LNX model during a drawdown – buildup test.

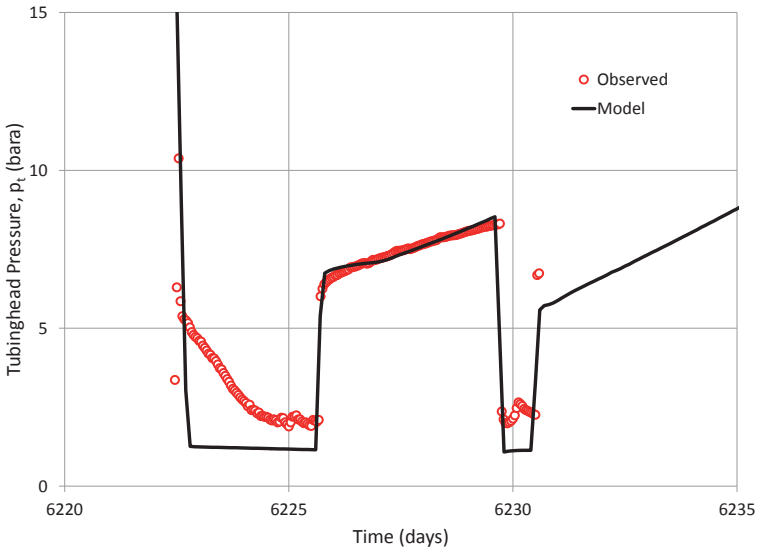

Fig. 2.20 – History matched tubinghead pressures of the LNX model during a drawdown – buildup test. This pressure data was recorded with the SPIDR system.

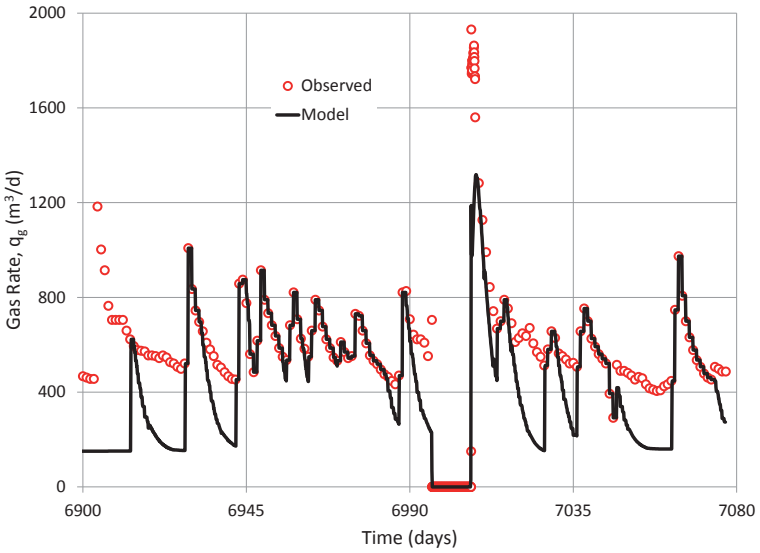

Fig. 2.21 – Gas rates for the history matched LNX model. This is the period when data is available from the ROOKIE project. During this time interval the well is regularly unloaded with the pumping unit.

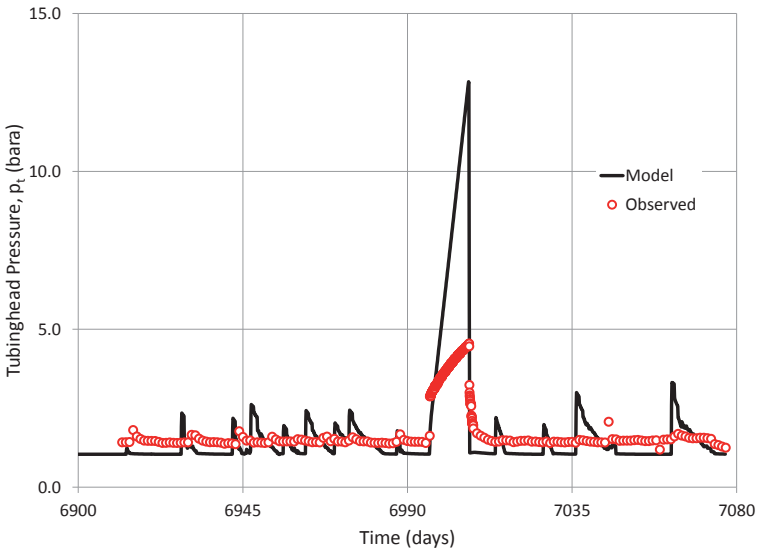

Fig. 2.22 – History matched tubinghead pressures of the LNX model for the period when data is available through ROOKIE. The build-up period starting at 7000 days is not captured very well.

high permeability sweet spot is likely. This sweet spot could be a natural heterogeneity in the reservoir, or induced by the acid treatment performed on the well.

2.7.7 Benefits of this Modeling Strategy

The proposed integrated wellbore-reservoir numerical model for liquid-loading wells uses one set of boundary conditions and governing equations. This differ from the coupled wellbore-reservoir models described in Section 2.7.1. Those models use two sets of boundary conditions and equations to solve the problem. This leads to an inefficient problem formulation, and run times for the coupled models are as a result significantly longer than for the integrated model presented here. The run time for the integrated model for the Noblin #2 history matching case is $\sim$1.5 minutes on a 2.8 GHz single core CPU with 1 GB of ram.

Many conventional reservoir simulators may be used to model liquid-loading with the modeling strategy presented here. The grid needs to be set up as shown in Fig. 2.7, and the correct production and injection points need to be defined. A conventional reservoir simulator is able to handle depletion within the reservoir correctly. All coupled wellbore-reservoir models described in the literature use a near-well simulator to model the reservoir. A near-well model will not predict long term depletion correctly, since only the part of the reservoir in close proximity to the wellbore is included in the model.

2.8 Semi-Analytical Model

This section discusses semi-analytical models to predict the behavior of liquid-loading gas wells. The models are called semi-analytical since they have separate analytical formulations for flow in the reservoir and wellbore. These formulations are connected together through an iterative procedure.

Usually a tubinghead pressure is input, and a gas rate is assumed. The tubinghed pressure and gas rate are then used to calculate a bottomhole pressure from the wellbore equations. Using the calculated bottomhole pressure, a gas rate is calculated from the reservoir equation. If there is a mismatch between the assumed and calculated gas rates, the calculation procedure is repeated with a new estimate for the gas rate. This is continued until convergence is reached.

2.8.1 Previous Work

Several semi-analytical models to predict liquid-loading behavior in gas wells have been proposed. A description of the most used models follows.

Dousi Model

The Dousi [6] liquid-loading model discretizes the reservoir into two points: a production point where gas is produced, and an injection point where the water co-produced with the gas is reinjected. See Fig. 2.23.

Tubinghead pressures, p_t, are input as a function of time. The bottomhole pressure, p_{fbh1}, at the reference point x_1 is calculated from the Cullender and Smith [5] well flow model:

$$p_{fbh1}^2 = Bp_t^2 + Cq_g^2 \tag{2.19}$$

Pressure losses due to friction are neglected below the reference point, x_1. The bottomhole pressure, p_{fbh2}, at the production point x_2, and the bottomhole pressure, p_{fbh3}, at the injection point x_3 are calculated from static pressure gradients.

$$p_{R,x_2}^2 - p_{fbh2}^2 = A_g q_g \tag{2.20}$$

$$p_{R,x_3} - p_{fbh3} = A_w q_{w,inj} \tag{2.21}$$

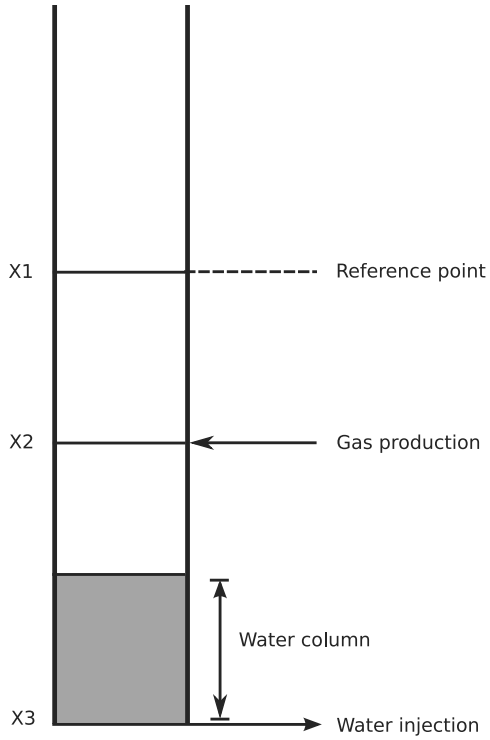

Fig. 2.23 – The Dousi well model

Gas production rate and water injection rate are calculated from Eq. 2.20 and Eq. 2.21, respectively. Eq. 2.20 assumes no non-Darcy flow in the reservoir. This is most likely a good assumption for gas wells experiencing liquid-loading, where production rates generally are low. Water production rate is calculated as a constant fraction of the gas production rate:

$$q_{w,prod} = q_g F_w \tag{2.22}$$

The minimum rate to lift is calculated from the simplified Turner [21] correlation:

$$q_{min} = C_{st}\sqrt{p_t} \tag{2.23}$$

If the gas rate falls below the minimum rate to lift, all co-produced water accumulates in the bottom of the well. Some of this water may be reinjected into the reservoir, in accordance with Eq. 2.21.

An iterative scheme is used to converge Eq. 2.20 and Eq. 2.19 for each time step, to yield gas production rate. An example of such an iterative scheme is given in Section 2.8.10.

Van Gool-Currie Model

The van Gool-Currie [22] model discretizes the reservoir into several layers, as shown in Fig. 2.24. A layer may either produce gas or inject water. If the bottomhole pressure at a specific layer depth exceeds the layer reservoir pressure, water is injected. If the layer reservoir pressure exceeds the bottomhole pressure, gas is produced. Apart from this, the van Gool-Currie model works on the same principles as the Dousi model.

A result of the water injection logic used in this model is that gas production completely stops from parts of the reservoir where there is water injection at the sandface. In reality this will not happen. Gas from the lower parts of the reservoir will crossflow upwards, and make its way to the sandface higher up.

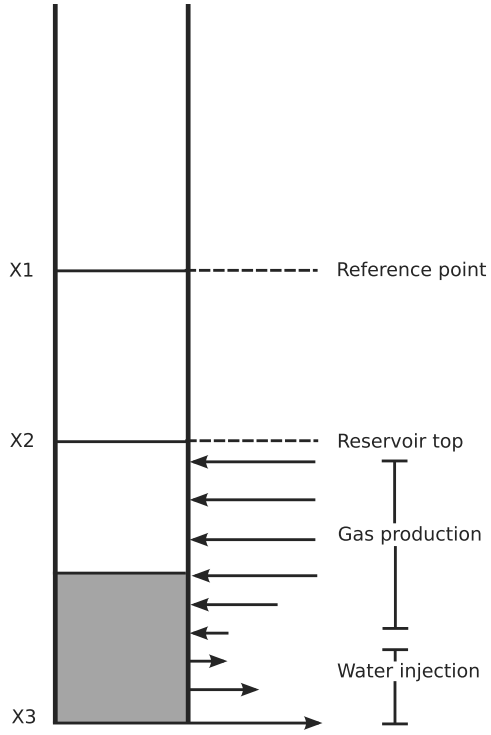

Fig. 2.24 – The van Gool-Currie well model

2.8.2 Introduction to a New Semi-Analytical Model

An improved semi-analytical liquid-loading model has been developed. The model works on the same basic principles as the Dousi and the van Gool-Currie models. The following sections gives a detailed description of the model.

2.8.3 Water Blockage Skin

When the bottomhole pressure in a liquid-loading gas well exceeds the reservoir pressure in an interval of the perforated reservoir, gas production will cease and water will start backflowing into the reservoir. Even though a reservoir interval has stopped producing gas at the sandface, gas will still flow from this interval into higher parts of the total gas interval away from the sandface. See Fig. 2.25.

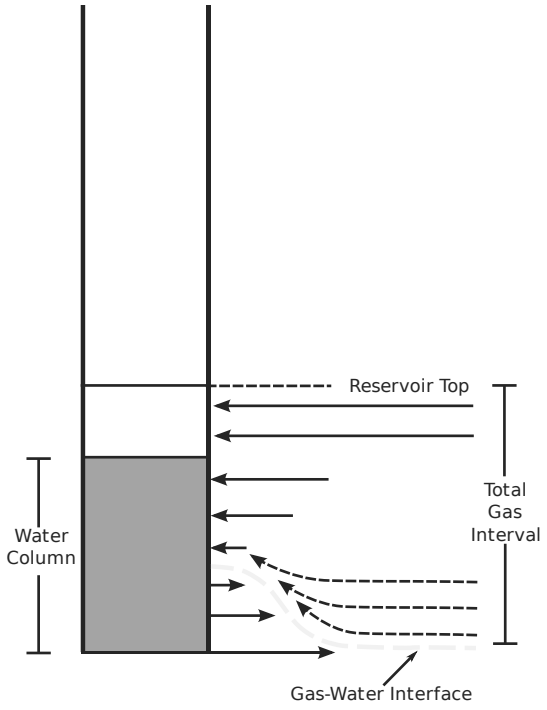

Fig. 2.25 – Even if parts of the sandface is not contributing to gas production, gas from lower parts of the reservoir will flow upwards through the higher parts of the reservoir.

Golan and Whitson [8] derive a partial penetration skin factor for wells

that are not fully penetrating the reservoir. This is based on the work of Muskat [16].

$$s_{wb} = (\frac{1}{b}[\ln h_D - G(b)]) \tag{2.24}$$

where,

$$G(b) = -\ln 4 + \frac{\ln C(b)}{2(1-b)}, \tag{2.25}$$

$$C(b) = \frac{\Gamma(0.875b)\Gamma(0.125b)}{\Gamma(1-0.0875b)\Gamma(1-0.125b)}, \tag{2.26}$$

and $\Gamma(x)$ is the gamma function of x.

In the proposed liquid-loading model, partial penetration is assumed to closely resemble the situation in a liquid-loaded gas well with gas production from only parts of the sandface. The water blockage skin affecting gas rate from the entire gas interval for a liquid-loaded gas well is calculated from Eq. 2.24, where b is the fraction of the total reservoir height currently producing gas at the sandface ($p_{R,k} > p_{wf}$), and h_D is the dimensionless reservoir thickness, h/r_w.

2.8.4 Wellbore Pressure Calculation

The pressure drop from bottomhole to wellhead is calculated in two steps:

1. Gravitational and frictional pressure drop is calculated for the liquid free part of the wellbore.

2. Below the liquid level, frictional effects are neglected, and pressure drop is only calculated based on gravitation.

$$\Delta p_f = \int_{h=0}^{D} \frac{\rho_g F_r}{r_w} \left(\frac{q_g B_g}{\pi r_w^2}\right)^2 \mathrm{d}h \tag{2.27}$$

$$\Delta p_g = \rho g \Delta h \tag{2.28}$$

where Δp_g is the static (gravitational) pressure drop, and Δp_f is the frictional pressure drop. Both are given in bar. The friction factor, F_r, can be calculated from Eq. 2.13.

$$p_{wf} = p_t + (\Delta p_{f,aboveLL} + \Delta p_{g,aboveLL} + \Delta p_{g,belowLL}) \tag{2.29}$$

The bottomhole pressure, p_{wf}, is calculated from Eq. 2.29.

2.8.5 Rate Calculation

Gas Rate

The gas production rate calculated by the van Gool-Currie model is too low. Gas production is completely lost from all layers where $p_{wf} \geq p_{R,k}$. As explained in Section 2.8.3, this is not the case for liquid-loaded wells.

$$q_g = \frac{p_R^2 - p_{wf}^2}{A_g} \tag{2.30}$$

where,

$$A_g = \frac{(\overline{\mu_g z})T}{2\pi kh}\left[\ln(\frac{0.47r_e}{r_w}) - \frac{3}{4} + s + s_{wb}\right] \tag{2.31}$$

Gas production rate in the proposed model is calculated from Eq. 2.30. The reservoir flow constant, A_g, is defined in Eq. 2.31, and includes the "water blockage" skin factor, s_{wb}. Except from the water blockage skin factor, this is the basic backpressure equation [7] for gas wells.

The gas viscosity, μ_g, is calculated from the Lee-Gonzalez [13] correlation.

$$\mu_g = A_1 \times 10^{-4} exp\left(A_2 \rho_g^{A_3}\right) \tag{2.32}$$

where,

$$A_1 = \frac{(9.379 + 0.01607M_g)\,T^{1.5}}{209.2 + 19.26M_g + T}, \tag{2.33}$$

$$A_2 = 3.448 + \frac{986.4}{T} + 0.01009M_g, \tag{2.34}$$

and,

$$A_3 = 2.447 - 0.2224A_2 \tag{2.35}$$

with T in $^\circ R$, and ρ_g in g/cm^3.

Water Rates

Water backflow into the formation in the proposed model is calculated in about the same way as in the van Gool-Currie model. The reservoir is divided into N layers. All layers, k, with bottomhole pressure exceeding the layer reservoir pressure are subject to water injection.

$$q_{w,k} = F_{ir} \frac{p_{wf,k} - p_{R,k}}{A_{w,k}} \tag{2.36}$$

where

$$A_{w,k} = \frac{\mu_w B_w}{2\pi k h_k} \left[\ln(\frac{0.47 r_e}{r_w}) - \frac{3}{4} + s \right] \tag{2.37}$$

The by-layer injection rate is calculated from Eq. 2.36. The only difference compared to the van Gool-Currie model is the inflow reduction factor, F_{ir}. This factor is a combination of water relative permeability reduction, and near-well permeability reduction due to water damage to the formation, as described by Jurus [11]. The value of the inflow reduction factor can be between 1 (no damage) and 0 (total damage), and should be determined by matching the model to field data.

$$q_{w,inj} = \sum_{k=1}^{N} q_{w,k} \tag{2.38}$$

The total water injection rate is the sum of the by-layer water injection rates, and is calculated from Eq. 2.38.

The free water produced from the reservoir, $q_{w,prod}$, is calculated after the gas production rate has been calculated. This water rate includes potential condensation of water from the gas in the wellbore.

$$q_{w,prod} = F_w q_g \tag{2.39}$$

where the water fraction, F_w, is in m^3 / m^3, and is user input.

2.8.6 Water Produced to Surface

The previous section describes water entering the wellbore from the fromation, and water backflowing from the wellbore to the formation. A description of water moving from bottomhole to surface follows.

Water Carried by Gas

The fraction of the produced water that is carried together with the gas to the surface is a function of the gas production rate, q_g. This water rate is here called the carried water rate, $q_{w,carried}$.

$$q_{w,carried} = \begin{cases} q_{w,prod} & \text{if } q_g > q_{min} \\ q_{w,prod}\left(\frac{q_g - q_{gF}}{q_{min} - q_{gF}}\right) & \text{if } q_{wF} < q_g < q_{min} \\ 0 & \text{if } q_g < q_{gF} \end{cases} \tag{2.40}$$

where the minimum rate to lift, q_{min}, is calculated from Eq. 2.1, and the flooding rate, q_{gF}, is calculated from Eq. 2.7. Other correlations could be used, if found more applicable.

This assumes that the amount of water carried with the gas is linear between the flooding rate and the minimum rate to lift. No water is carried to the surface if the gas rate is below the flooding rate, and all new water entering the wellbore is carried to the surface if the gas rate is above the minimum rate to lift.

Mechanical Unloading

It is possible to specify a water removal rate to simulate artificial lift. This water removal rate, $q_{w,pump}$, is lumped together with the water injection rate, $q_{w,inj}$, when the new liquid level in the wellbore is calculated, as described in the next section. The water removal rate is input by the user versus time, with a default value of zero.

2.8.7 Liquid Level Calculation

When the water production rate and water injection rate have been calculated, the new liquid level can be calculated.

$$h_{w,i} = h_{w,i-1} + \frac{(q_{w,prod} - [q_{w,inj} + q_{w,carried} + q_{w,pump}])}{\pi r^2}\Delta t \tag{2.41}$$

where $h_{w,i}$ is the liquid level during the current time step, and $h_{w,i-1}$ is the liquid level for the previous time step.

It is important to take into account that the flow conduit radius, r, changes where the tubing starts.

$$r^2 = \begin{cases} r_w^2 & \text{below end of tubing} \\ r_t^2 & \text{above end of tubing, if produced through tubing} \\ r_w^2 - r_t^2 & \text{above end of tubing, if produced through annulus} \end{cases} \tag{2.42}$$

2.8.8 Material Balance

A simple gas material balance is implemented in the model.

$$\frac{p_R}{z} = \frac{p_{Ri}}{z_i}\left(1 - \frac{G_p}{G}\right) \tag{2.43}$$

The reservoir pressure is updated after each time step with the gas production in the previous time step. This makes it possible to predict long term reservoir behavior, where depletion becomes an issue.

Water reinjected into the reservoir is not included in the material balance.

2.8.9 Multiple Reservoir Units

The model allows multiple reservoir units. Units do not communicate within the reservoir, only through the wellbore, i.e. layer-no-crossflow (LNX). Backflow between the formations through the wellbore is handled by the model.

2.8.10 Iteration Procedure

Tubinghead pressures vs. time are input to the model. The following pseudo-code explains how the model calculates gas rates and liquid-levels:

```
WHILE(not converged)
  calculate BHP from input THP;
  calculate gas rate;

  calculate THP from BHP and new gas rate;
  compare calculated THP with input THP;
END WHILE

calculate water production;
calculate water injection;
calculate new liquid-level;

goto next timestep
```

If the liquid-level changes too much from one time step to the next, the size of the time step is automatically cut in half, to ensure stability of the solution. The default maximum allowed water level change per time step is 2%.

2.8.11 Model Performance

The semi-analytical model was used to simulate the gas production from a well with properties summarized in Table 2.6. The model was controlled with a constant tubinghead pressure of 2 bara. The resulting rate profile is shown in Fig. 2.26. The rate profile shows that the well has a normal unloaded depletion performance the first 2300 days of production. At this point, the production rate falls below the minimum rate to lift, and liquids start accumulating in the wellbore. The calculated liquid level for the well is shown in Fig. 2.27.

The production performance of this synthetic well is very similar to the performance of the wells shown in Section 2.6. All showing the characteristic drop towards the meta stable rate after the minimum rate to lift is reached.

TABLE 2.6 – Model parameters used for the semi-analytical model to simulate the liquid-loading performance of a gas well.

Model Properties		
	Value	Unit
Initial pressure, p_R	15	$bara$
Permeability, k	10	md
Reservoir thickness, h	20	m
Drainage radius, r_e	1000	m
Porosity, ϕ	0.1	–
Water cut, F_w	2E-7	m^3/m^3
Reservoir depth, h_R	1000	m
Tubing radius, r_t	0.0275	m

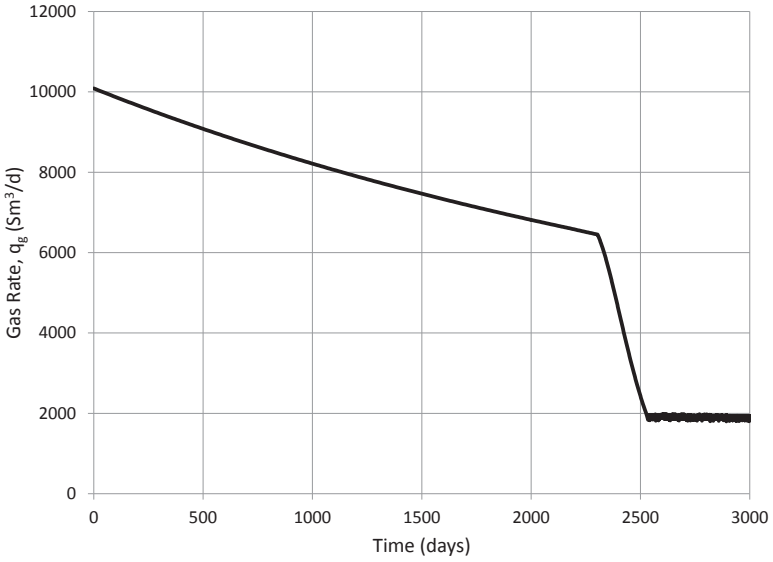

Fig. 2.26 – Calculated gas rates from the semi-analytical model for the entire life of a gas well. Liquid-loading occurs after ∼2300 days of production. After a transition period of 300 days, the well stabilizes at the meta stable rate.

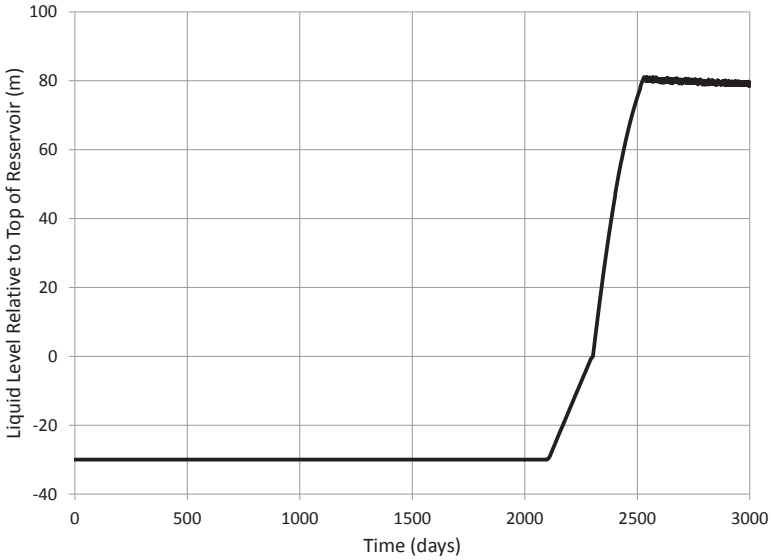

Fig. 2.27 – Liquid level in the wellbore calculated by the semi-analytical model. The reservoir is 20 m thick, and the well has a 10 m rat hole below the bottom of the reservoir.

2.8.12 History Matching

The semi-analytical liquid-loading model was tested against observed data from the Noblin #2 well. An 80 day time period, including a number of pumping cycles, was used. Tubinghead pressures together with measured pumped water rates were used as input to the model. Gas rates and liquid levels were calculated. The tubinghead pressures used as input are shown in Fig. 2.28. The pumped water rates input to the model are presented in Table 2.7. For conveniency, the pumped water rates when input to the model were converted to a constant rate from the pumped volume.

$$q_{w,pump} = \frac{Q_{w,measured}}{\Delta t} \tag{2.44}$$

where $\Delta t = 1$ hour, $Q_{w,measured}$ is the cumulative measured water for a pumping cycle in m^3, and $q_{w,pump}$ is the pump rate input to the model for the current pumping cycle.

TABLE 2.7 – Noblin #2 pumped water rates used as input in the history matching of the semi-analytical model.

Pumped Water Volumes		
From ($days$)	To ($days$)	Rate (m^3/d)
16.88	16.92	3.510
32.00	32.04	3.840
41.08	41.12	3.360
48.08	48.12	2.496
55.08	55.12	2.400
62.12	62.16	2.500
75.20	75.24	2.410

A two layer model is assumed, with no communication between the layers within the reservoir (LNX). The thickness of each layer is taken from the gamma ray log of the well (see Fig. 1.8), where the clear shale break in the middle of the perforated formation is assumed to be a no-flow barrier. The following parameters were used as variables in the history matching

- Layer reservoir pressures

- Layer permeabilities
- Layer skin factors
- Producing water cut

The SSQ defined in Eq. 2.17 is minimized to fit the model to the observed data. Only the rate part of the SSQ was included, since pressures are used as input to the model, and are honored at all times.

The history matching was performed with both the evolutionary strategy algorithm described in Appendix A, and a version of the Nelder-Mead simplex method [17].

2.8.13 Best Fit Results

Fig. 2.29 shows the best fit production rates from the history matching. The best fit values for the reservoir parameters are given in Table 2.8.

It is evident from the measured data that transients significantly impact the gas production rates shortly after the well has been pumped off. The semi-analytical model is not able to capture these effects, since it assumes pseudo-steady state. Even though the transients are not captured, the general behavior of the well is matched reasonably by the model.

The calculated liquid levels are presented in Fig. 2.30. During each pumping cycle, the well was pumped until the measured surface water rate reached close to zero. It is assumed that the liquid level in the wellbore after the pumping cycle ended, was at the pump intake depth. Fig. 2.30 shows that the model predict close to this behavior for all the pumping cycles. The pumped water rates input to the model, $q_{w,pump}$, are determined by the measured pump rates, so this gives confidence that the model is predicting liquid levels in the wellbore accurately.

2.8.14 Benefits of This Modeling Strategy

Semi-analytical model are fast compared to numerical models. The runtime for the proposed model is $\sim 1/100^{th}$ of the runtime for the numerical liquid-loading model. The semi-analytical model does not handle transient behavior in the reservoir. If transient significantly affect reservoir behavior, it is better to use a numerical model.

The proposed semi-analytical model has several improvements compared to already published semi-analytical models:

- Reservoir depletion is handled with a gas material balance. This makes it possible to use the model for long term production forecasting.

TABLE 2.8 – Best fit values for the history matching of the Noblin #2 pumping cycles. Values in parenthesis are not used as regression variables.

Noblin #2 Reservoir Properties			
	Layer 1	Layer 2	Unit
Reservoir pressure, p_R	6.9	8.1	$bara$
Permeability, k	15.0	10.6	md
Skin factor, s	3.6	1.0	–
Water cut, F_w	1.28E-5	1.28E-5	m^3/m^3
Thickness, h	(5.0)	(5.0)	m
Porosity, ϕ	(0.1)	(0.1)	–
Drainage radius, r_e	(740)	(740)	m

- Gas flow to the wellbore is handled more correctly with the use of the water blockage skin factor, s_{wb}.
- The amount of liquids carried together with the produced gas is handled more correctly since the flooding gas rate, q_{gF}, is accounted for.

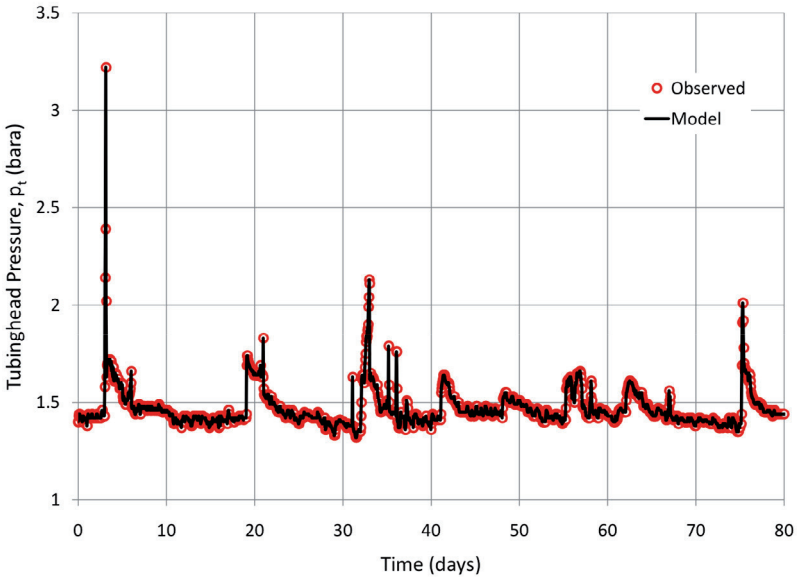

Fig. 2.28 – Input tubinghead pressures to the history matching of the Noblin #2 pumping cycles.

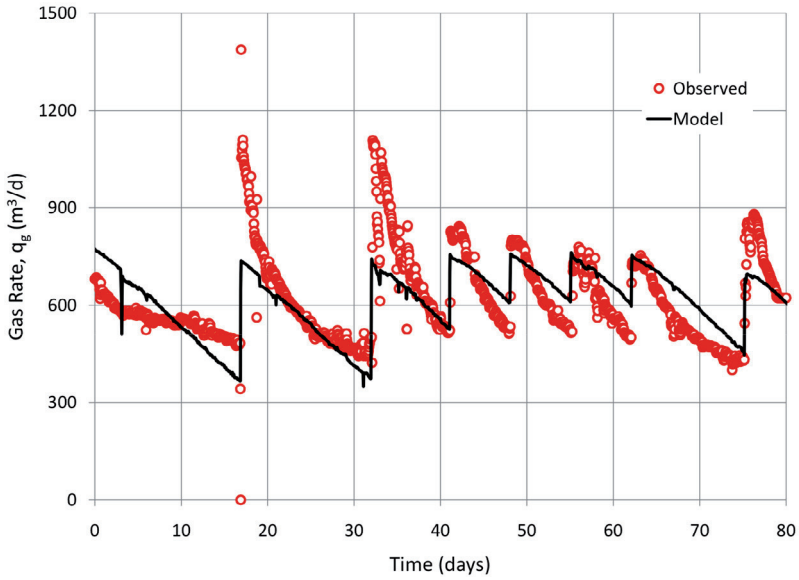

Fig. 2.29 – The semi-analytical model history matched against data from the Noblin #2. A number of pumping cycles span the 80 days of production that is history matched.

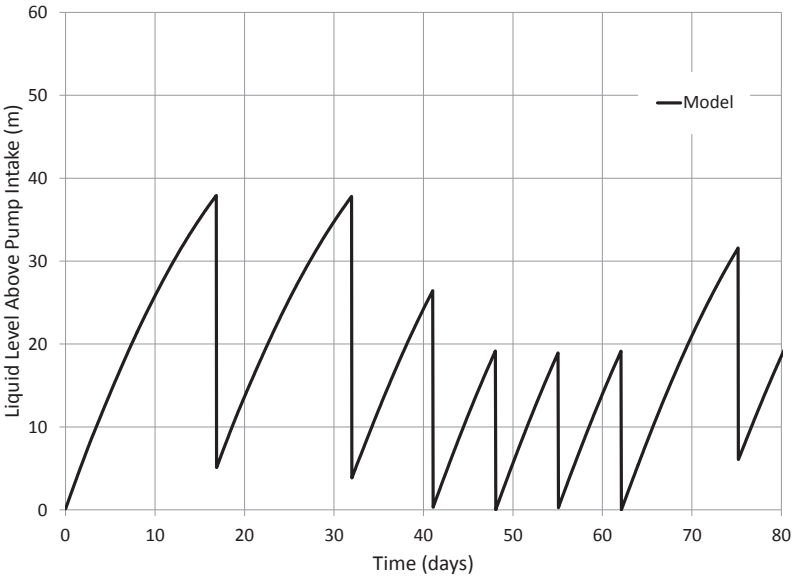

Fig. 2.30 – Liquid levels calculated by the semi-analytical model history matched to the Noblin #2 pumping cycles.

2.9 Remediation

A large number of remediation methods are available to unload liquids in wells undergoing liquid-loading. Each method may not be applicable for any well. This section will briefly describe the most promising methods to remediate liquid-loading.

2.9.1 Plunger Lift

Plunger lift is the most used method to remediate a liquid-loading well. Compared to other remediation methods, plunger lift is fairly inexpensive to install.

Plunger lift uses gas stored in the casing-tubing annulus, and inflow from the reservoir, to move a metal plunger up the tubing. Liquids are carried in front of the plunger to the surface. The plunger is kept at the surface while the well blows down. Then the plunger is released, and travels downhole. The well is usually shut-in after the plunger reaches the bottom of the well, to recharge the annulus for a new cycle.

One drawback of using a plunger lift is that the well must be intermittently shut-in to generate enough pressure to bring the plunger back to the surface. This could reduce the average production rate of the well. There is also a limit to the liquid-gas ratio (LGR) that can be handled by a plunger lift system. This is dependent on the depth of the well. An estimate of the required gas-liquid ratio (GLR) is given by Lea et al. [12].

$$GLR_{required} = 400 \left[\frac{scf}{bbl}\right] \frac{h}{1000} \tag{2.45}$$

where h is the depth of the well in ft, and $GLR_{required}$ is the minimum required GLR in scf/bbl.

2.9.2 Rod Pumping

Rod pumping units are widely used in gas-condensate and oil wells in depths up to 10,000 ft, but are seldom used in gas wells to unload co-produced water.

The rod pump is usually installed in the tubing, and a string of metal rods connect to a piston pump at the bottom of the well. At the wellhead the rods connect to a pump jack. The pump jack converts rotary motion into reciprocating motion to drive the pump. Water from the bottom of the well is pumped up through the tubing. A standing valve prevents water from flowing back into the annulus. Gas is produced through the annulus.

Normally, an electrical motor powers the pumping unit. The power requirement for the motor may be high for deep wells, and electricity from the grid is usually needed. The power requirement for the motor can be calculated from Lea et al. [12].

$$P = \frac{5.42 \times 10^{-6} q_w h}{\eta} \tag{2.46}$$

where P is the required electrical power in kW, q_w is the pump water rate in bbl/d, h is the height the water must be pumped to reach the surface in ft, and η is the electrical efficiency of the pumping unit.

Installing a rod pump is the best way to make sure that the wellbore is kept unloaded at all times. The well does not need to be shut-in during pumping, as shown through the work on the ROOKIE project. Gas will not lock up the pump if it enters the pump assembly at the bottom of the tubing.

Remote Well Locations

Poythress and Rowland [20] discuss the use of a solar powered rod pumping system to pump low volumes of liquid from a wellbore. Using solar power to drive the pumping unit mitigates the need to be close to the electrical grid. The solar powered motor running the pump is not strong enough to lift conventional metal rods, so glass fiber rods were used instead. Stretch is the main problem with glass fiber rods compared to conventional rods. The large stretch in the glass fiber rods will significantly decrease the stroke length of the pump, rendering it ineffective.

A better solution is to use a gas powered pumping unit. This type of pumping unit uses natural gas from the well to run, and generates enough power to use conventional metal rods. This type of pumping unit was used on the Anglin #3 (see Section 1.12.2), when it was evaluated for the ROOKIE project. The gas driven motor proved very reliable, and only consumed ∼2 mcf/d of gas when running continuously. The gas driven pumping unit is shown in Fig.2.31.

2.9.3 Heating the Wellbore

Pigott et al. [19] discuss the use of electrical cables to heat the wellbore to avoid condensation of liquids. This is only a viable unloading strategy if no free liquids are produced from the reservoir.

In areas with large seasonal changes in temperature, i.e. cold winters, significant cooling of the wellbore could occur. The top of the well might

Fig. 2.31 – The pumping unit installed on the Anglin #3. Gas from the annulus is fed through a pressure regulator to the pumping unit motor.

get cold enough to condense out liquids from the produced gas. If the well is producing below the minimum rate to lift, some of these liquids will start falling towards the bottom of the well and accumulate.

Whitson and Brulé [25] give a correlation to calculate the amount of water in solution in natural gas.

$$y_w = y_w^0 A_g A_s \tag{2.47}$$

$$\ln y_w^0 = \frac{0.05227p + 142.3 \ln p - 9625}{T + 460} - 1.117 \ln p + 16.44 \tag{2.48}$$

$$A_g = 1 + \frac{\gamma_g - 0.55}{1.55 \times 10^4 \gamma_g T^{-1.446} - 1.83 \times 10^4 T^{-1.288}} \tag{2.49}$$

$$A_s = 1 - 3.92 \times 10^{-9} C_s^{1.44} \tag{2.50}$$

where y_w is the mole fraction of water in solution in the gas, T is in ^oF, p is in psia, and C_s is the salinity of the water in ppm.

This equation can be used to calculate the amount of liquids that will condense out from the gas on the way from bottomhole to surface, by calculating the difference in solubility from bottomhole to surface conditions.

To investigate the seasonal temperature variations in the wellbore, a series of temperature probes were installed in the tubing of the Boyd Cable #2. One of the temperature probes is shown in Fig. 2.32. Five probes were installed in the wellbore, spaced 6 meters apart, with the top probe installed one meter below the surface. Another probe was located at the surface, on the outside of the wellhead, to record ambient temperature.

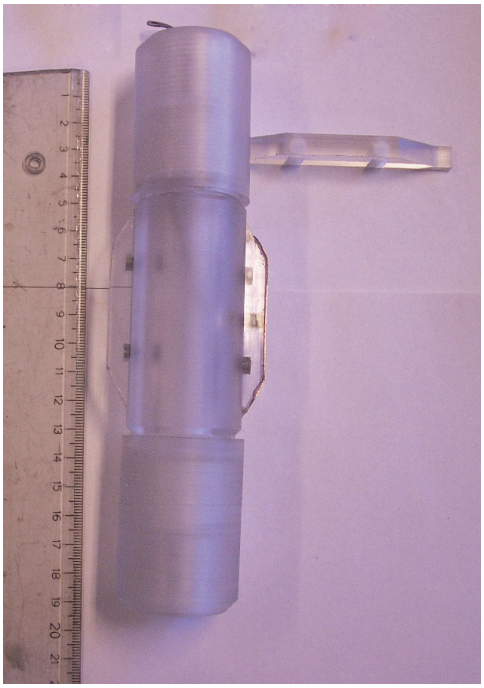

Fig. 2.32 – Downhole temperature probe installed in the Boyd Cable #2. The temperature is measured against the inner wall of the tubing. Five of these probes were installed in the wellbore, spaced 6 meters apart.

Signal wires from the temperature probes exit the wellhead through the swab valve. The wellhead of the Boyd Cable #2 after the installation was completed is shown in Fig. 2.33. The signal wires connect to a temperature logger located in a box by the wellhead. This box is shown in Fig. 2.34. The logger records the temperature for all the probes once every hour, and has storage capacity for over a year of continuous measurements. A 12 V car battery supplies the temperature logger with power. The battery is charged

by a solar panel installed on the wellhead.

Fig. 2.33 – The wellhead of the Boyd Cable #2. Wires from the temperature probes exit the well through the swab valve. A solar panel is mounted on the well, to power the temperature logger.

Fig. 2.35 shows the downhole temperatures recored on the Boyd Cable #2 from January 2008 – March 2009. The temperature recorded one meter below the surface follows the seasonal changes in ambient temperature closely, and is clearly affected by changing surface conditions. The next probe, located 7 meters below the surface, records a constant temperature throughout the year. The surface temperature does not affect the wellbore temperature at this depth. The same constant temperature behavior is seen for the probes further down in the well. Seasonal changes in temperature does not affect the temperature in the wellbore deeper than 7 meters below the surface.

The well was shut in during the entire experiment. This means that produced gas did not contribute to heating the wellbore. The results shown in Fig. 2.35 are therefore believed to be the worst case scenario in terms of wellbore cooling, at least for this particular well. This implies that in many

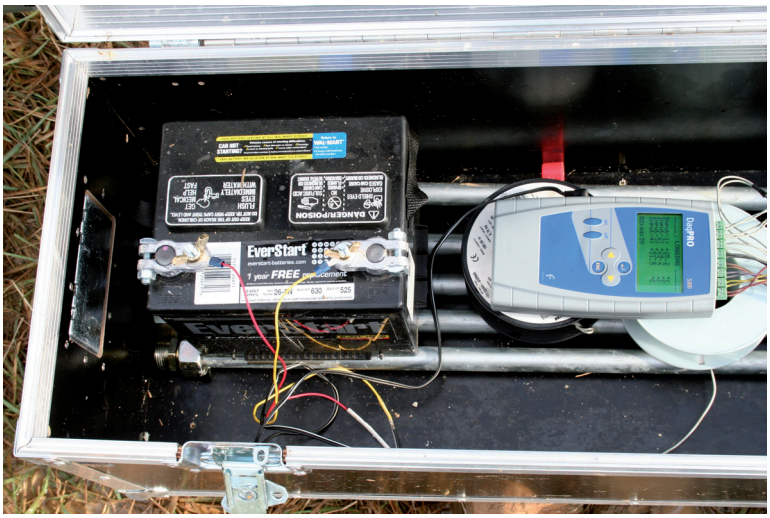

Fig. 2.34 – The equipment box at the Boyd Cable #2. The temperature logger is connected to a 12 V battery. The battery is charged by the solar panel mounted on the wellhead.

cases it would only be necessary to heat the very top of the well to avoid condensation of liquids in the wellbore.

2.9.4 Perforating Low Pressure Formation

Another method of remediating liquid-loading is by perforating a low pressure formation beneath the productive formation. Water dropping down the wellbore will then backflow into the low pressure zone, and water will not accumulate downhole. This concept is shown in Fig. 2.36.

Care should be taken when selecting candidate wells for this remediation tactic. If the pressure in the lower zone is less than the flowing bottomhole pressure of the well, gas will start backflowing, and production is lost. The pressure of the water disposal formation, $p_{R,w}$, should be such that:

$$p_{wf} \leq p_{R,w} \leq p_{wf} + \rho_w g \Delta h \tag{2.51}$$

where $p_{R,w}$ is the layer pressure of the water disposal formation, and Δh is the depth difference between the water disposal formation and the productive formation.

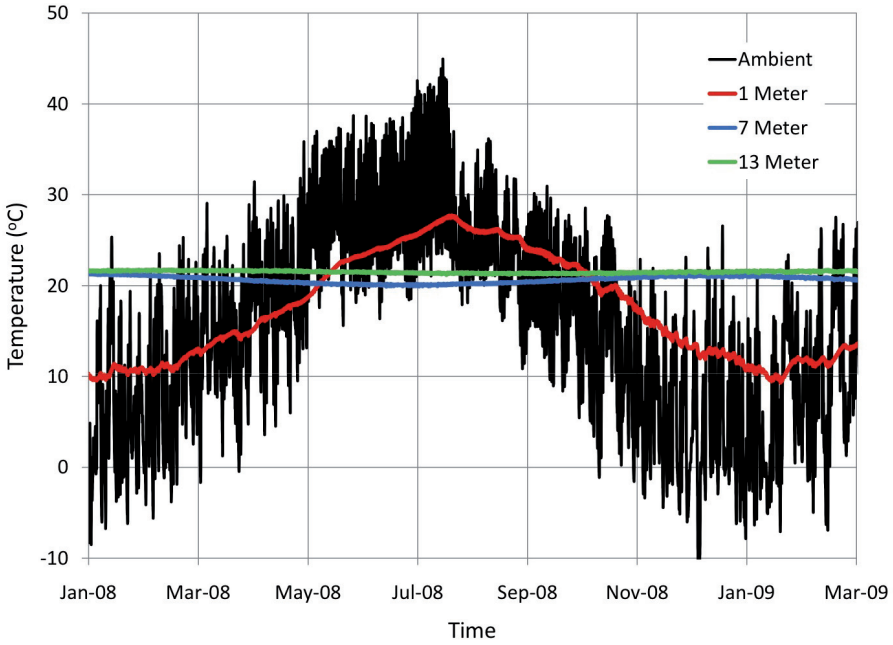

Fig. 2.35 – Downhole temperature measurements from the Boyd Cable #2 well. The temperature is stabile below 1 meter under the surface. Only values for the three topmost probes are shown, to increase clarity. Temperatures for the two remaining probes are equal to the temperature of the probe installed at 13 meters.

Nomenclature

A	Reservoir backpressure constant
B	Cullender and Smith gravitational constant
b	Fraction of reservoir producing gas at sandface
B_g	Gas formation volume factor, (m^3/Sm^3)
C	Cullender and Smith friction constant
C_s	Water salinity, (ppm)
C_{st}	Simplified Turner constant

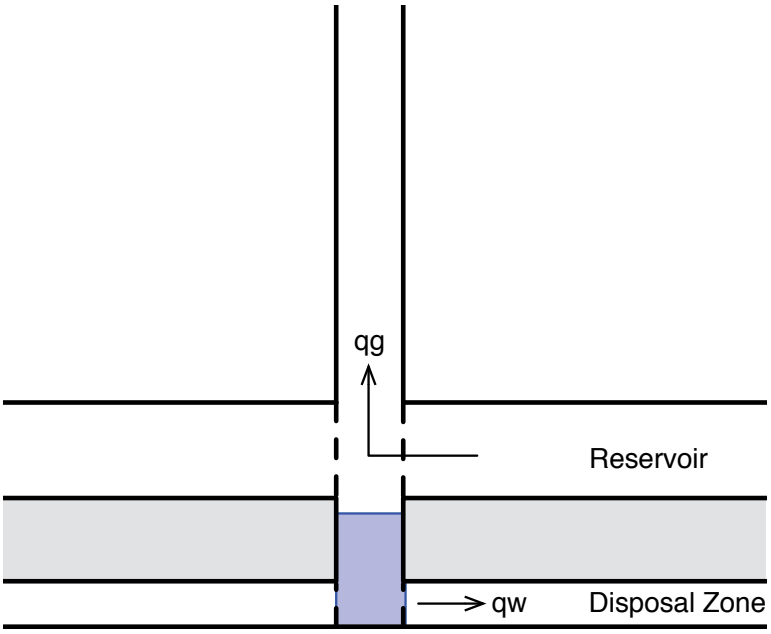

Fig. 2.36 – Liquids produced from the reservoir, and liquids coming out of solution with the gas, is pushed into the water disposal zone perforated below the reservoir. This may prevent a liquid column forming in the wellbore above the reservoir perforations.

d	Diameter, (m)
F_ir	Water inflow reduction factor
F_r	Friction factor
F_{SSQ}	Sum of squares
F_w	Water fraction
G	Initial gas in place, (m^3)
g	Gravitational constant, $(9.81\ m/s^2)$
G_p	Cumulative gas produced, (m^3)
G_w	Cumulative water produced, (m^3)
h	Height, (m)

h_D	Dimensionless reservoir thickness, h_r/r_w, (m/m)
k	Permeability, (md)
M	Molecular weight
N_{Re}	Reynolds number
P	Electrical power, (kW)
p	Pressure, $(bara)$
q	Flow rate, (m^3/d)
r	Radius, (m)
r_w	Wellbore radius, (m)
r_e	Drainage radius, (m)
S	Gravitational exponent
s	Skin factor
S_g	Gas saturation
S_{gc}	Critical gas saturation
T	Temperature, (K)
t	Time, $(days)$
v	Velocity, (m/s)
z	Z-factor
y_w	Mole fraction of water in solution in gas

Greek Symbols

Δ	Difference
η	Electrical efficiency
Γ	Gamma distribution
γ	Specific gravity, $(kg - m^3/kg - m^3)$

μ	Viscosity, (cp)
ϕ	Porosity
ρ	Density, (kg/m^3)
σ	Interfacial tension, $(dynes/cm)$

Subscripts

a	Damage zone
c	Casing
F	Flooding
f	Friction
$fbh1$	Bottomhole at reference point x_1 in the Dousi model
$fbh2$	Bottomhole at reference point x_2 in the Dousi model
i	Cell number in radial direction
inj	Injection
k	Layer number
g	Gas
min	Minimum to lift
mod	Model
obs	Observed
$prod$	Production
R	Reservoir
r	Relative
ref	Reference value used for SSQ normalization
t	Tubinghead
w	Water

wb	Water blockage
wf	Flowing bottomhole
$x1$	Reference point in Dousi model
$x2$	Production point in Dousi model
$x3$	Injection point in Dousi model

Abbreviations

GB	Giga byte
GLR	Gas-liquid ratio
IMPES	Implicit pressure, explicit saturation
IPR	Inflow performance relationship
LL	Liquid-loading
LGR	Liquid-gas ratio
LNX	Layered-no-crossflow
NTNU	Norwegian university of science and technology
ROOKIE	Remote operations in Oklahoma intended for education
SSQ	Sum of squares

Bibliography

[1] J.J Asps. Analysis of decline curves. *Transactions of the American Institute of Mining, Metallurgical and Petroleum Engineers*, 160:228, 1945.

[2] G Chupin, B Hu, T Haugset, J Sagen, and M Claudel. Integrated wellbore/reservoir model predicts flow transients in liquid-loaded gas wells. In *SPE Annual Technical Conference and Exhibition, 11-14 November 2007, Anaheim, California, U.S.A.*, 2007.

[3] S Coleman, H Clay, D McCurdy, and L Norris III. A new look at predicting gas-well load-up. *Journal of Petroleum Technology*, 43(3):329–333, 1991.

[4] A.T Corey. The interrelation between gas and oil relative permeabilities. *Producers Monthly*, 19(1):38–41, 1954.

[5] M.H Cullender and R.V Smith. Practical solution of gas-flow equations for wells and pipelines with large temperature gradients. *Trans. AIME*, 207:281–287, 1956.

[6] N Dousi, C.A.M Veeken, and P.K Currie. Numerical and analytical modelling of the gas well liquid loading process. *SPE Production and Operations*, 21(4):475–482, November 2006.

[7] M.J Fetkovich. Multipoint testing of gas wells. Presented at the SPE Mid-Continent Section, Continuing Education Course in Tulsa, Oklahoma, March 1975.

[8] M Golan and C.H Whitson. *Well Performance*, volume 2. Tapir Akademiske Forlag, Trondheim, Norway, 2003.

[9] B Hu, J Sagen, G Chupin, T Haugset, A Ek, and T Sommersel. Integrated wellbore-reservoir dynamic simulation. In *Asia Pacific Oil and Gas Conference and Exhibition*, 2007.

[10] M Hawkins Jr. A note on the skin effect. *Journal of Petroleum Technology*, 8(12):65–66, 1956.

[11] W Jurus. Permeability reduction and restoration in water sensitive sandstones. Master's thesis, Norwegian University of Science and Technology, September 2005.

[12] J Lea, H.V Nickens, and M Wells. *Gas Well Deliquification.* Gulf Professional Publishing, 2003.

[13] A.L Lee, L Gonzalez, H Mario, and E Bertram. The viscosity of natural gases. *Journal of Petroleum Technology*, 18(8):997–1000, August 1966.

[14] C.C Mattax and R.L Dalton. Reservoir simulation. spe monograph, henry l. doherty series, 1990.

[15] K.W McQuillan, P.B Whalley, and G.F Hewitt. Flooding in vertical two-phase flow. *International journal of multiphase flow*, 11(6):741–760, 1985.

[16] M Muskat. Partially penetrating wells in isotropic formations; potential distribution. *Physics*, 2:329, 1932.

[17] J.A Nelder and R Mead. A simplex method for function minimization. *The computer journal*, 7(4):308, 1965.

[18] M.A Nosseir, T.A Darwich, and M.H Sayyouh. A new approach for accurate prediction of loading in gas wells under different flowing conditions. *SPE Production Operations Symposium*, 1997.

[19] M.J Pigott, M.H Parker, D.C Mazzanti, L.V Dalrymple, D.C Cox, and R.A Coyle. Wellbore heating to prevent liquid loading. In *SPE Annual Technical Conference and Exhibition, 29 September-2 October 2002, San Antonio, Texas.*

[20] M Poythress and L Rowlan. Low-volume pumping systems: Moving gallons to produce thousands. In *CIPC/SPE Gas Technology Symposium 2008 Joint Conference, 16-19 June 2008, Calgary, Alberta, Canada*, 2008.

[21] R.G Turner, M.G Hubbard, and A.E Dukler. Analysis and prediction of minimum flow rate for the continuous removal of liquids from gas wells. *Journal of Petroleum Technology*, 21(11):1475–1482, November 1969.

[22] F van Gool and P.K Currie. An improved model for the liquid-loading process in gas wells. In *Production and Operations Symposium, 31 March-3 April 2007, Oklahoma City, Oklahoma, U.S.A.*, 2007.

[23] P.J Waltrich and G Falcone. Performance of vertical transient two-phase flow models applied to liquid loading in gas wells. In *Annual Technical Conference and Exhibition, Denver, Colorado, USA*, 2011.

[24] C.H Whitson. Minimum lift calculations for gas wells. NTNU, Nov 1990.

[25] C.H Whitson and M.R Brule. Phase behavior, monograph vol. 20 spe henry l. *Doherty Series, Richardson, Texas*, 2000.

[26] H Zhang, G Falcone, P Valko, and C Teodoriu. Numerical modeling of fully-transient flow in the near-wellbore region during liquid loading in gas wells. In *Latin American and Caribbean Petroleum Engineering Conference*, 2009.

Chapter 3

Layered Reservoirs

3.1 Contributions

The author performed all major work completing this paper [7]. C.H. Whitson had the original idea for the work presented in the paper, and contributed with developing the backpressure equation for layered gas reservoirs.

3.2 Backpressure Equation for Layered Gas Reservoirs

The following section is a reprint of Juell and Whitson [7]

3.2.1 Abstract

This paper presents a backpressure equation (BPE) for wells producing from layered gas reservoirs with or without communication. The proposed BPE handles backflow between the layers through the wellbore for non-communicating layered systems, and accurately describes performance of wells experiencing differential depletion.

The proposed multi-layer BPE has the same form as the familiar backpressure equation for single-layer gas reservoirs, where the correct averages are defined for reservoir pressure and backpressure constants.

The BPE is validated against numerical simulation models, as well as field data which include decades of historical production performance and annual shut-in pressures. All numerical models and field data used to validate the BPE are publicly available. This paper gives guidelines on welltest

design to quantify reservoir parameters in layered systems, based on systematic studies with numerical simulation models.

3.2.2 Background

Layered reservoirs without communication, also referred to as layered no-crossflow reservoirs, consist of separate layers without communication within the reservoir; layers only communicate through the wellbore.

One of the first attempts to study the transient performance of layered reservoirs was Lefkovits et al. [9]. They show individual layer gas rates as a function of each layer kh product, but do not consider production performance solutions for boundary-dominated (pseudosteady state, PSS) conditions.

Fetkovich et al. [3] studied and identified all key performance characteristics of layered no-crossflow systems producing under boundary-dominated conditions. One of their many important observations is Curve 6 in their Fig. 12, showing that the backpressure relation for a differentially depleting system is, in fact, a straight line with exponent n 1. We show, in this paper, that this is an expected and general observation for any layered system, and that the layered no-crossflow backpressure equation is the same as for a single-layer system with equal total kh, but using the layer PI-averaged shut-in pressure.

El-Banbi and Wattenbarger [1] developed a model to match production data from a layered no-crossflow system during boundary-dominated conditions, using individual-layer coupling of material balance and PSS rate equations. This model is used to estimate individual layer properties, for the assumption of constant bottomhole flowing pressure. Another attempt to estimate layer properties and gas in place for layered no-crossflow reservoirs was Kuppe et al. [8]. This work allows changes in bottomhole flowing pressure, but does not handle extended shut-ins resulting in backflow through the wellbore.

This paper will primarily consider layered no-crossflow reservoirs, but some results are shown to be applicable to reservoirs with partially- or fully-communicating layers. The backpressure equation presented is valid for all layered reservoirs, but the coupled material balance approach is only valid for non-communicating layer systems.

3.2.3 Standard Backpressure Equation

The standard backpressure equation for a well producing from a single layer reservoir is given by Fetkovich [2].

$$q_g = C_R \left(p_c^2 - p_w^2\right) \tag{3.1}$$

The back-pressure constant, C_R, is defined as:

$$C_R = \frac{4.18khe^S}{T_R \left(\ln \frac{r_e}{r_w} - \frac{3}{4} + s\right) \mu_g z} \tag{3.2}$$

with q_g in std m^3/d, p in bar, k in md, h in m, T_R in K, and μ_q in cp. The gravity term, S, is defined as:

$$S = \frac{0.0684\gamma_g D}{\overline{T}\overline{z}} \tag{3.3}$$

This S must not be confused with the skin factor, s.

The surface datum pressures, p_c and p_w, are converted to bottomhole pressures through the gravity term. The different pressure datums are shown in Fig. 3.1.

$$p_R = e^{S/2} p_c, \quad p_{wf} = e^{S/2} p_w \tag{3.4}$$

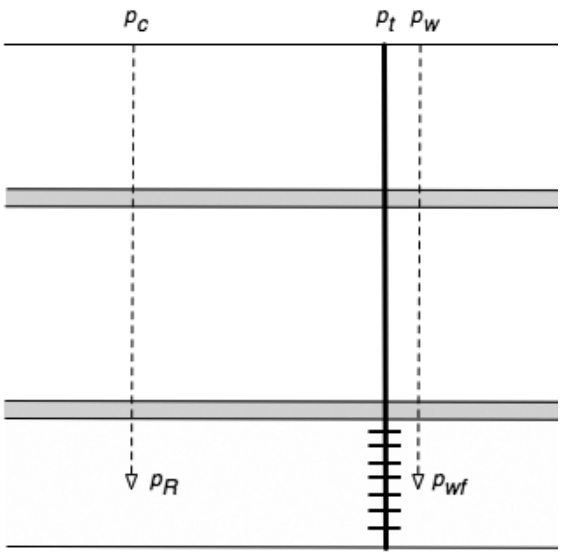

Fig. 3.1 – Pressure datums for the backpressure equation. The gravity term, S, is used to convert from surface to bottomhole pressures for static gas columns.

3.2.4 Multi-Layer Backpressure Equation

For a well producing from a layered no-crossflow reservoir, we have:

$$q_g = \sum_{l=1}^{N} q_{gl} = \sum_{l=1}^{N} C_{Rl} \left(p_{cl}^2 - p_w^2 \right) \tag{3.5}$$

where p_w is common for all layers, assuming no pressure drop in the wellbore throughout the perforated interval.

Eq. 3.5 can be rewritten as:

$$\frac{q_g}{\sum_{l=1}^{N} C_{Rl}} = \frac{\sum_{l=1}^{N} C_{Rl} p_{cl}^2}{\sum_{l=1}^{N} C_{Rl}} - p_w^2 \tag{3.6}$$

where we define the total productivity index (PI) as the sum of layer PIs:

$$C_R = \sum_{l=1}^{N} C_{Rl} \tag{3.7}$$

and,

$$\overline{p}_c^2 = \frac{\sum_{l=1}^{N} \left(C_{Rl} p_{cl}^2 \right)}{C_R} \tag{3.8}$$

The average wellhead shut-in pressure, $\overline{p}_c$, represents the PI-averaged reservoir pressure of all the layers at surface datum. Shut-in pressure $\overline{p}_c$ can be shown to represent the pressure recorded at the wellhead, as Eq. 3.5 is satisfied for $q_g = 0$ when $p_w = \overline{p}_c$.

Now, Eq. 3.6 can be written in the familiar backpressure form:

$$q_g = C_R \left(\overline{p}_c^2 - p_w^2 \right) \tag{3.9}$$

3.2.5 Numerical Model

A 2D numerical radial single well simulation model was constructed to validate the multi-layer backpressure equation. The simulation model is based on a model presented by Fetkovich et al. [3]. The reservoir properties are given in Table 3.1.

Both reservoir layers have a drainage radius of 908 m. The wellbore radius is 0.091 m. The model consists of 50 cells in the radial direction, and one horizontal cell-layer per reservoir layer. The reservoir gas has a specific gravity of 0.7.

The numerical model was produced for 10 years against a constant bottomhole pressure of 2.95 bara, and then shut in for one year. It was subsequently produced for three years, and shut in for another year. This was continued until the simulation time reached 20 years. The production profile of the model is shown in Fig. 3.2.

In addition to the BPE, a material balance is used to calculate the depletion performance of the numerically simulated well.

$$\left(\frac{p_c}{z}\right)_l = \left(\frac{p_{ci}}{z_i}\right)_l \left(1 - \frac{G_p}{G}\right)_l \tag{3.10}$$

TABLE 3.1 – Numerical model parameters.

Numerical Model Parameters			
	Layer 1	Layer 2	Unit
k	100	1	md
h	0.61	6.7	m
	2	22	ft
ϕ	0.15	0.15	–
p_i	29.5	29.5	bara
	428	428	psia
s	0	0	–
S_{wi}	0.514	0.514	–
C_R	17.79	1.96	std $m^3/d/bar^2$
	2.99E-3	3.29E-4	$scf/d/psi^2$

The production profile, together with the reservoir parameters given in Table 3.1, was used as input to the backpressure equation presented in this paper. Bottomhole pressures, individual layer pressures, and layer gas rates were calculated, and compared with the output from the numerical simulator. The bottomhole pressures are presented in Fig. 3.3, layer pressures are presented in Fig. 3.4, and individual layer gas rates are presented in Fig. 3.5.

As is seen from the comparison of the BPE calculations and the output from the numerical simulator, the BPE gives an accurate description of the layered reservoir.

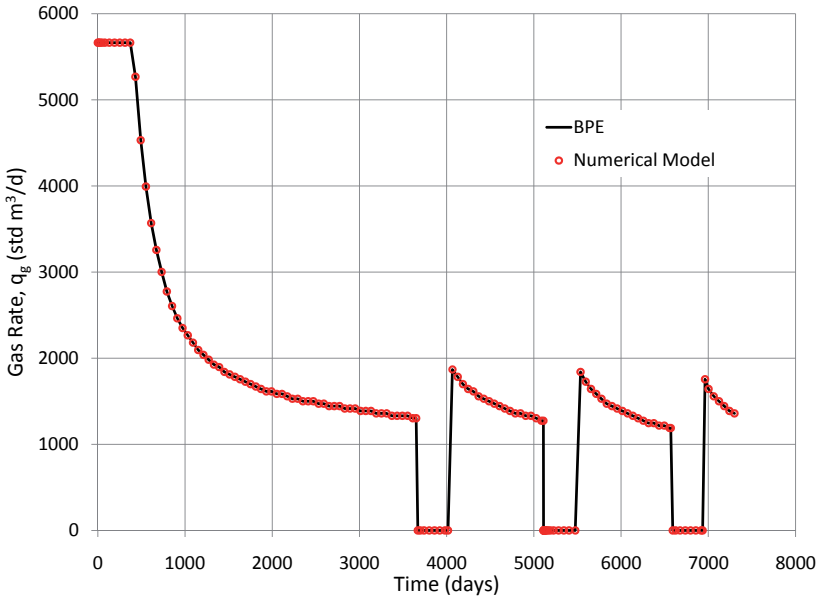

Fig. 3.2 – Production profile for the numerical two-layer model based on Fetkovich et al. [3].

3.2.6 Field Data

Production data from the Buf #3 well (API #3513900778), producing from the Guymon-Hugoton field in Oklahoma, USA was used to test the BPE against actual field data. This reservoir consists of three non-communicating productive layers. The well was completed in 1946. Production data from 1967 – 2009 was publicly available. Only the cumulative production in the beginning of 1967 was available to estimate the gas production rates prior to 1967. For simplicity, a constant gas rate was assumed between 1946 and 1967 (amounting to the known cumulative production in 1967). Annual wellhead shut-in pressure data was available for the period 1967 – 2000. This pressure data was used to validate the BPE.

The wellhead shut-in pressures were collected during annual 72-hour (96-hour since 1975) shut-ins. These shut-in periods were incorporated in the gas rate table used as input to the BPE, and the calculated tubinghead pressure at the end of the shut-ins was compared with the reported test pressures.

Reservoir parameters for the field are taken from Fetkovich et al. [4], and are presented in Table 3.2.

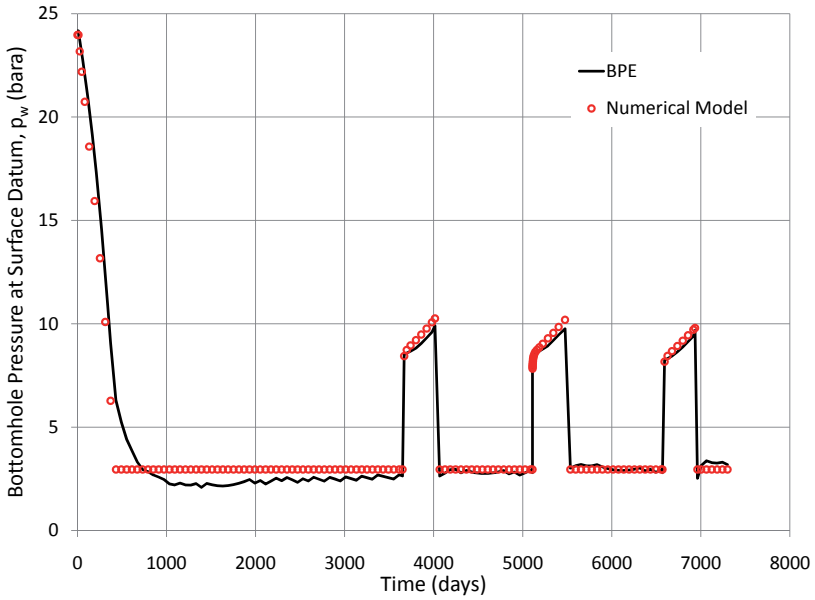

Fig. 3.3 – Bottomhole pressures predicted by the BPE vs. the numerical two-layer model based on Fetkovich et al. [3].

The specific gravity of the reservoir gas is 0.73, the depth to the top of the reservoir is 853.5 m, and the tubing outer diameter is 2-3/8 inches.

The available pressure data is all measured at the wellhead. It is therefore necessary to calculate tubinghead pressures, p_t, from the bottomhole pressures calculated by the BPE.

$$q_g = C_t \left(p_w^2 - p_t^2\right)^{0.5} \tag{3.11}$$

where the tubing constant, C_t, is:

$$C_t = \frac{13.0 \exp\left(S/2\right)}{\sqrt{e^S - 1} F_r \overline{T} \overline{z}} \tag{3.12}$$

Eq. 3.11 is used to convert the bottomhole pressures, p_w, from the BPE to tubinghead pressures, p_t. A friction factor, F_r, of 0.00612 was assumed. These tubinghead pressures are compared with the recorded pressure tests performed on the well.

The only unknowns remaining in the model are the drainage radii, r_{el}, for the individual layers. These drainage radii are used as regression variables to fit the tubinghead pressures calculated by the BPE to the test pressures recorded at the well.

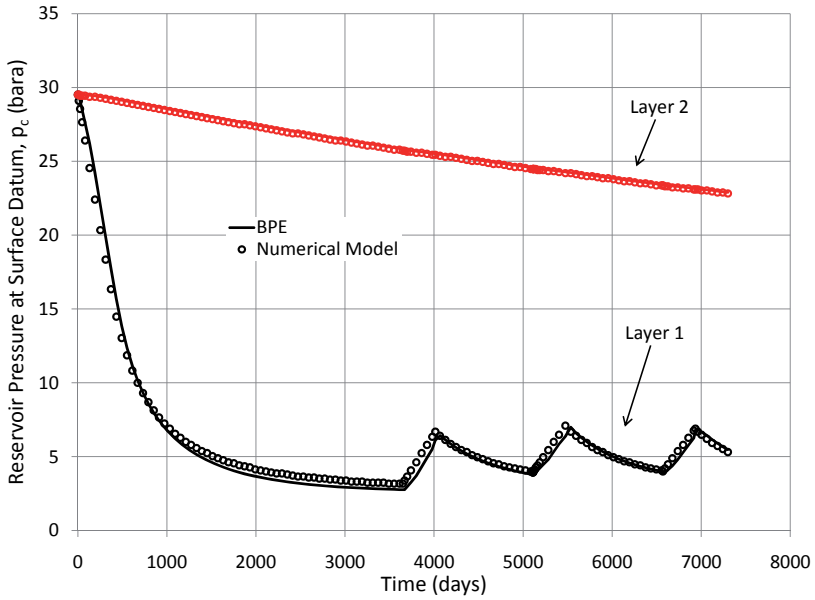

Fig. 3.4 – Layer pressures predicted by the BPE vs. layer pressures from the numerical two-layer model based on Fetkovich et al. [3].

$$F_{SSQ} = \sum_{t=0}^{T} \left(\frac{p_t^{BPE} - p_t^{obs}}{p_{ref}} \right)^2 \tag{3.13}$$

The accuracy of the BPE is evaluated from the sum of squares (SSQ), F_{SSQ}, and is calculated from Eq. 3.13. The drainage radii are fit to minimize the SSQ. These layer radii, r_{el}, represent layer gas in place, G_l, and realistically over such a long period of time their value could change because of infill drilling.

In addition to the tubinghead shut-in pressures, a bottomhole pressure test was conducted for the individual reservoir layers in the beginning of 1989. This gives an extra independent verification of the BPE, but is not included in the fitting of the drainage radii.

The production profile for the well is presented in Fig. 3.6. As seen from this figure, the gas rate is set constant prior to the start of the publicly available production data.

The resulting best-fit values for the drainage radii are 832 m, 1119 m, and 1041 m, for layers 1 – 3 respectively (908 m represents spacing of 640 acres). The tubinghead pressures for the best-fit model are presented in Fig. 3.7,

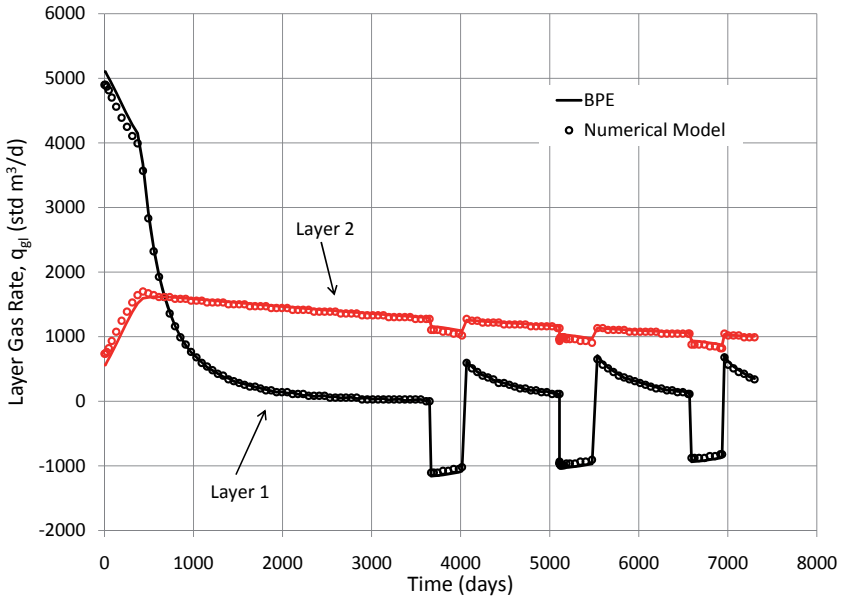

Fig. 3.5 – Layer gas rates from the BPE vs. layer rates from the numerical two-layer model based on Fetkovich et al. [3].

and the layer pressures are presented in Fig. 3.8. The individual layer gas rates are shown in Fig. 3.9. The BPE accurately predicts the performance of the well, and the differential depletion is represented correctly by the model, as seen from Fig. 3.8.

Fig. 3.7 shows some of the measured tubinghead pressures between 11500 and 14500 days (May 1978 – August 1986) are under predicted by the BPE. A possible cause could be longer shut-ins of the well than the required 96 hours. The BPE is also under predicting the two measured pressures between 7180 and 7550 days (June 1966 – June 1967), just at the start of publicly available rate data. Because the rate profile is not known prior to this, the under prediction could be caused by a long shut in of the well.

3.2.7 Numerical Model Based on Field Example

It is evident that the BPE fits the measured pressure data from the Buf #3 well reasonably. To illustrate how well the BPE would fit a gas well where all pressure data and individual layer rates were available; a numerical simulation model was built. The model is constructed based on the best-fit parameters from the field case. The model consists of 100 cells in the radial

TABLE 3.2 – Reservoir parameters for the Guymon-Hugoton field.

Reservoir Parameters for the Guymon-Hugoton field				
	Layer 1 Herrington	Layer 2 Krider	Layer 3 Winfield	Unit
k	0.1	9.0	3.3	md
h	17.7	15.2	12.2	m
	58	50	40	ft
ϕ	0.06	0.08	0.08	–
p_i	33.8	33.8	33.8	bara
	490	490	490	psia
s	-5.44	-5.44	-5.44	–
S_{wi}	0.76	0.60	0.67	–
S	0.157	0.157	0.157	–
T	26.7	26.7	26.7	^{o}C
	80	80	80	^{o}F
C_R	2.02	139.96	42.14	std m^3/d/bar^2
	3.39E-4	2.35E-2	7.07E-3	scf/d/psi^2

direction, and one horizontal cell-layer per reservoir layer.

The wells negative skin, s, is implemented in the model according to Hawkins [6].

$$s = \left(\frac{k}{k_a} - 1\right) \ln \frac{r_a}{r_w} \tag{3.14}$$

The extent of the stimulated region, r_a, was selected to be 21.8 m (corresponding to the outer boundary of radial cell 58 in the model). This gives permeabilities in the stimulated region of 17, 1537, and 564 md for the three layers respectively.

A comparison of the tubinghead pressures from the numerical model and the BPE is shown in Fig. 3.10. The reservoir layer pressures are presented in Fig. 3.11, and the individual layer gas rates are shown in Fig. 3.12. As can be seen from these figures, the predictions of the BPE are at all times within symbol thickness of the numerical model results.

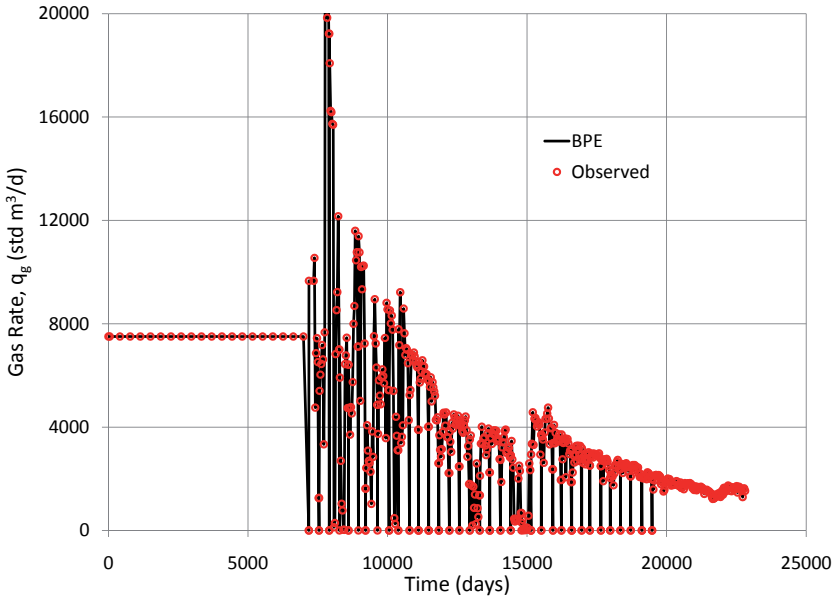

Fig. 3.6 – Production gas rates for the Buf #3 well in the Guymon-Hugoton field. Production rate prior to 1967 is assumed constant.

3.2.8 Backpressure Analysis for Monitoring Well Performance

Backpressure analysis may be used as a tool to detect deterioration in well performance for wells producing from layered gas reservoirs. Fig. 3.13 shows the backpressure plot for a well with different shut-in durations. Each set of shut-ins corresponding to a specific shut-in duration fall on a straight line on a log-log plot. Thrasher [10], as well as Golan and Whitson [5], illustrates this behavior for a single-layer system. As seen from Fig. 3.13, this also applies for a multi-layer system. The model used to generate the data in Fig. 3.13 is a two layer model with layer thicknesses of 6.1 and 61 m, layer permeabilities of 0.1 and 0.01 md, and a stimulated region with permeability of 100 md extending 22.9 m into the reservoir. The initial reservoir pressure is138 bara. All other properties are equal to the two layer model previously described.

When using layered backpressure analysis to monitor a wells performance, it is important to be consistent from test to test. Each shut-in period should be of $\sim$ equal length, and the shut-in pressure, $\overline{p}_c$, should be recorded at the end of the shut-in. The gas rate, q_g, and associated flowing pressure, p_t, to be used in backpressure analysis together with $\overline{p}_c$ should be

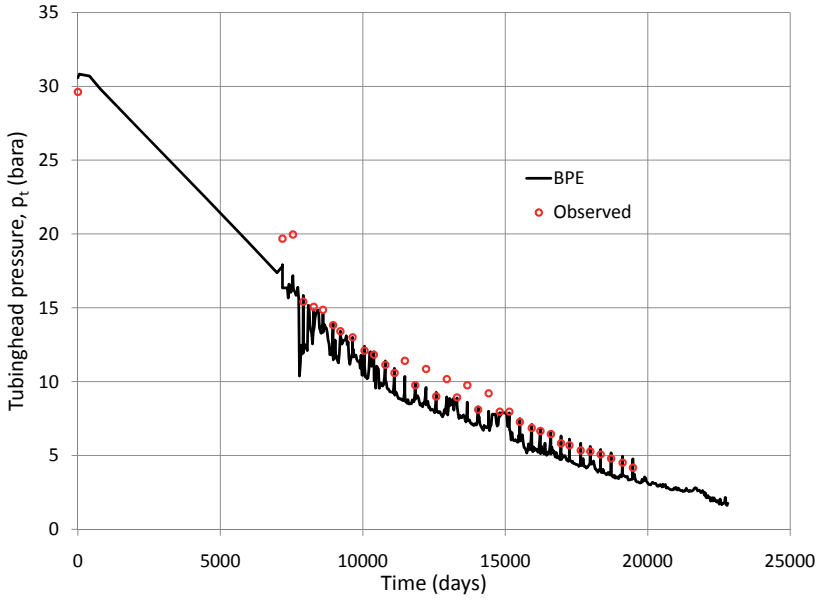

Fig. 3.7 – Tubinghead pressures calculated by the BPE vs. measured pressures for the Buf #3 well in the Guymon-Hugoton field.

recorded following the shut-in. We recommend a post shut-in flow period equal to the shut-in time, e.g. if the shut-in lasted 48 hours, the well should flow for 48 hours prior to recording the gas rate and flowing pressure.

The BPE presented in this paper is a reservoir-only equation. Fetkovich 1975 shows that the reservoir BPE (Eq. 3.9) and the tubing equation (Eq. 3.11) can be combined to yield the wellhead BPE:

$$B_{wh}q_g^2 + A_{wh}q_g = \overline{p}_c^2 - p_t^2 \tag{3.15}$$

or,

$$q_g \approx C_{wh}\left(\overline{p}_c^2 - p_t^2\right)^{n_{wh}} \tag{3.16}$$

In our work using the Darcy equation for reservoir flow $B_{wh} = 1/C_t^2$, and $A_{wh} = 1/C_R$.

Any deviation from the established wellhead backpressure curve signifies a change in either reservoir or tubing performance. If the deviating point lies above the established line, the performance of the well has deteriorated. If the point lies below the line, the performance has improved. Fig. 3.14 shows a well where a large positive skin (+20) was introduced after 10 years. A clear shift in the wellhead backpressure curve is seen after this

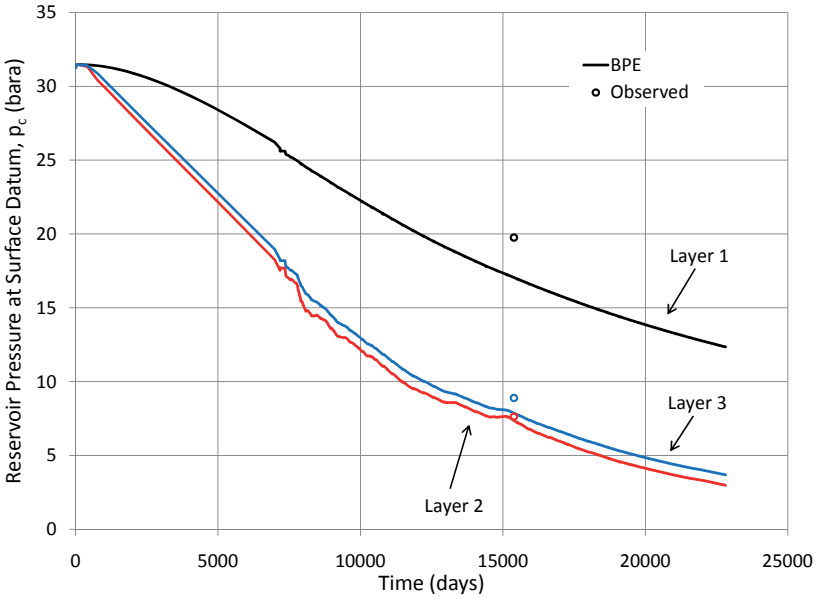

Fig. 3.8 – Layer pressures calculated by the BPE for the Buf #3 well in the Guymon-Hugoton field. The observed data represents a layer pressure test conducted on the well in 1989.

point. When a deviation from the backpressure curve is detected, actions should be considered to restore the wells productivity.

Test conditions during the flow period often differ from the normal flowing conditions of the well. This may affect backpressure analysis, because rate contributions from the different layers can vary greatly with small changes to the flowing pressure. Fig. 3.15 shows the wellhead backpressure curve for a well that was flowed with a tubinghead pressure of 3.5 bara during tests, and 1 bara otherwise. As seen from the figure, all the tests still fall on a straight line, and the backpressure analysis is valid.

The numerical model was altered to allow varying degrees of communication between the two layers throughout the reservoir. This was achieved by increasing the z-direction transmissibility multiplier (TZ) from 0 to 0.01 to 1 between the two layers. The reservoir is still experiencing differential depletion for the TZ = 0.01 case, and the layer reservoir pressures are 122 and 131 bara after 20 years (layer pressures are 105 and 133 bara for the corresponding no-crossflow model after 20 years). As seen from Fig. 3.16, backpressure analysis is still applicable.

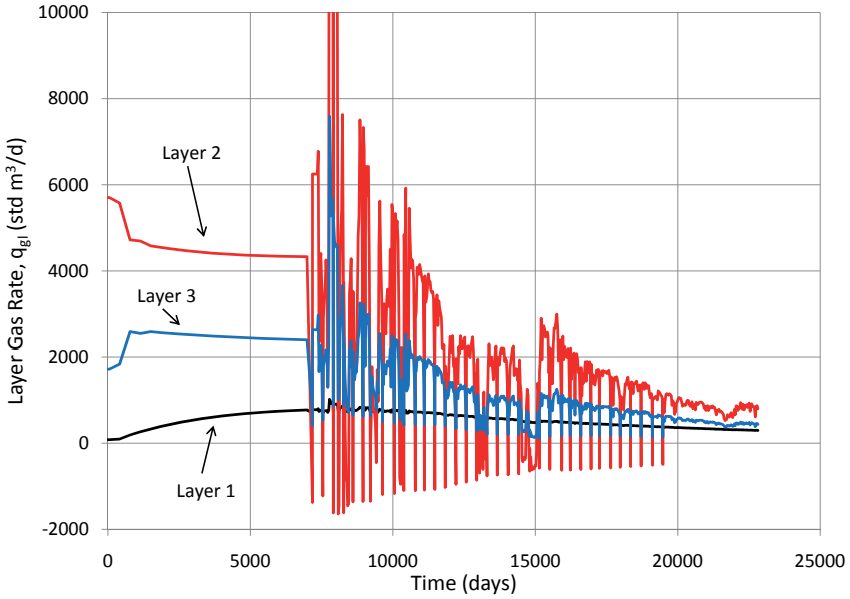

Fig. 3.9 – Layer gas rates calculated by the BPE for the Buf #3 well in the Guymore-Hugoton field. No observed data is available.

3.2.9 Model Limitations

When layer permeabilities are low enough, the well performance may be dominated by transient effects, and the BPE looses accuracy, mainly because the steady-state assumption is violated.

The layer permeabilities of the two-layer numerical model based on Fetkovich et al. [3] were reduced by 1 – 2 orders of magnitude to test when the BPE no longer is able to reproduce the performance of the simulator. Both layer permeabilities were scaled by the same multiplier.

Fig. 3.17 shows the bottomhole pressure behavior for the BPE applied to a model with permeabilities one order of magnitude lower than the original example (10 and 0.1 md for the high- and low-permeability layers, respectively). As can be seen from the figure, the predicted bottomhole pressure is mismatched because of transients, but the model still replicates the general pressure behavior fairly well. When lowering the permeabilities another order of magnitude (1 and 0.01 md), the BPE is no longer able to calculate the bottomhole pressure with any certainty, as shown in Fig. 3.18. This is due to the BPEs inability to reproduce the transient behavior of the numerical model gas rates, as seen in Fig. 3.19.

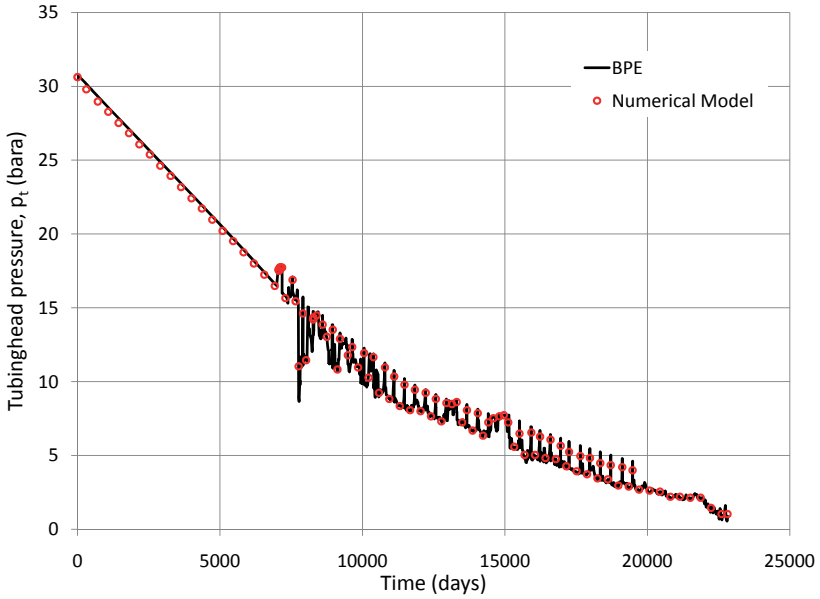

Fig. 3.10 – Tubinghead pressure for the numerical model based on the Buf #3 well, and the BPE predictions.

3.2.10 Discussion

Layered backpressure analysis as proposed in this paper should be valid:

- For reservoirs with permeability greater than ~ 0.01 md.
- When using surface pressures, p_c and p_t, as long as the well hydraulics are accurately described by the gas tubing equation (e.g. Eq. 3.11).
- When the reservoir pressure squared assumption is applicable. Higher pressure reservoirs require the use of the pseudopressure rate equation.
- Wells not significantly affected by rate dependent skin. We were not successful in developing a layered (Forchheimer) quadratic rate equation using average rate constants (A_R and B_R) and $\overline{p}_c^2$, though we suspect an extension of our work using the quadratic rate equation, even if approximate, should exist and deserves further study.

3.2.11 Conclusions

1. The presented backpressure equation (BPE) for layered gas reservoirs accurately predicts pressure and rate data from field examples and

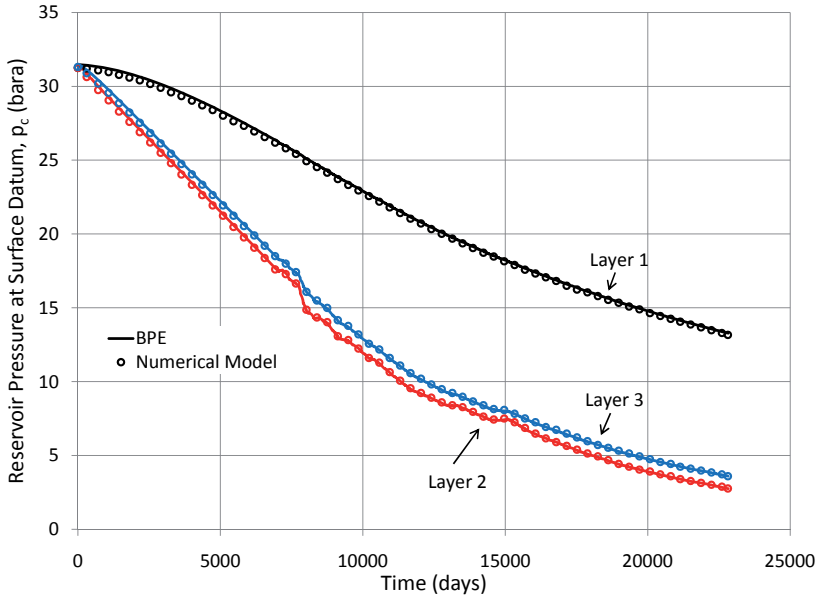

Fig. 3.11 – Layer pressures for the numerical model based on the Buf #3 well, and the pressures predicted by the BPE.

numerical simulation models. The form of the BPE is identical with the single layer equation.

2. Backpressure analysis with the layered (wellhead) BPE can be used as a monitoring tool to detect deterioration in tubing and/or reservoir performance. Any deviation from the established wellhead backpressure curve indicates a change in the wells performance.

3. The layered BPE can be used to forecast depletion performance for layered no-crossflow gas reservoirs when coupled with layer material balances.

Nomenclature

C	Backpressure constant (std $m^3/d/bar^2$)
D	Depth (m)
F_r	Friction factor
F_{SSQ}	Sum of squares

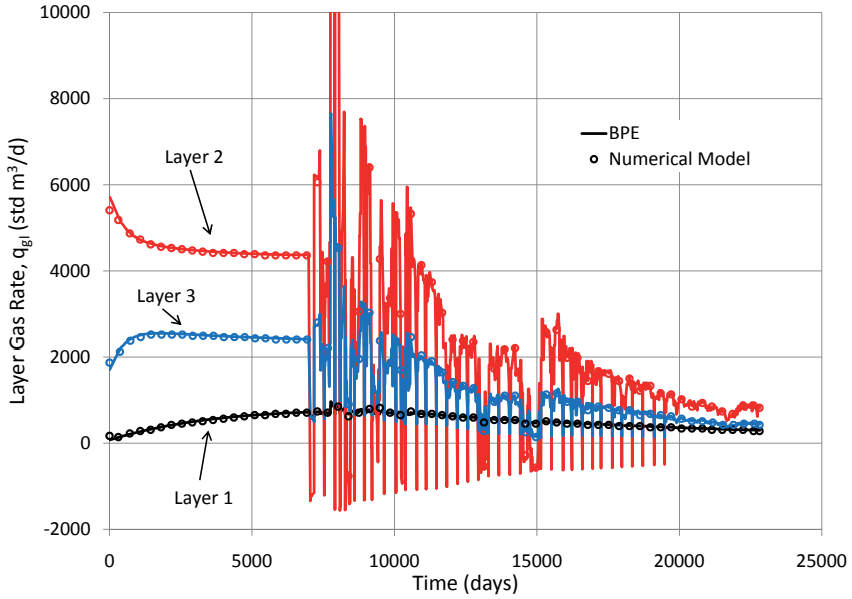

Fig. 3.12 – Individual layer gas rates for the numerical model based on the Buf #3 well, and the BPE predicted rates.

G	Gas in place (std m^3)
G_p	Cumulative gas produced (std m^3)
h	Layer thickness (m)
k	Permeability (md)
p	Pressure (bara)
q	Flow rate (m^3/d)
r_e	Drainage radius (m)
r_w	Wellbore radius (m)
s	Skin factor
S	Gravity term
S_{wi}	Irreducible water saturation
T	Temperature (K)
z	Z-factor

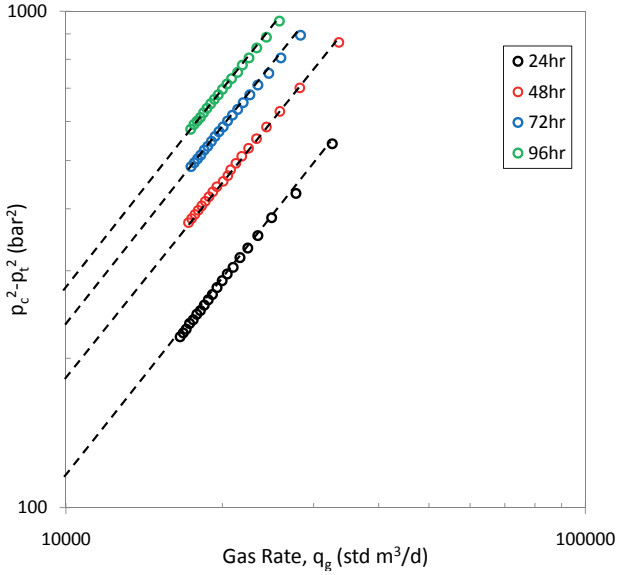

Fig. 3.13 – Backpressure plot using different shut-in periods. The tests corresponding to a specific shut-in duration all fall on a straight line on the log-log plot.

Greek Symbols

μ	Viscosity (cp)
γ	Specific gravity

Subscripts

a	Altered region (stimulated)
c	Reservoir property at surface datum
g	Gas
i	Initial
l	Layer number
R	Reservoir
t	Tubing

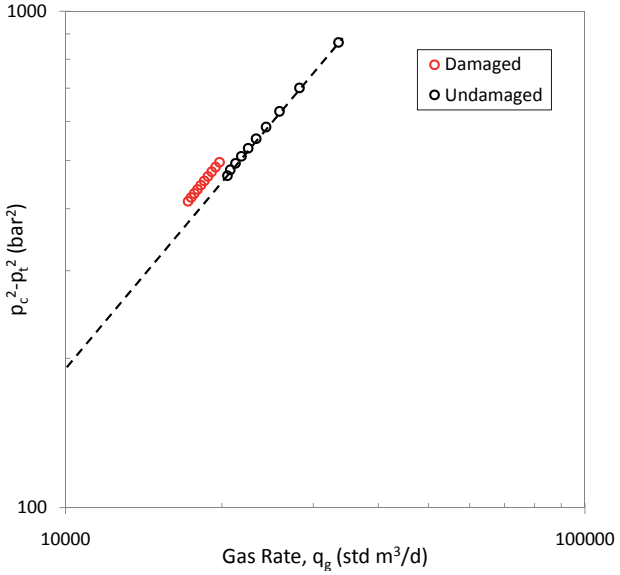

Fig. 3.14 – A large positive skin factor (+20) was introduced in the model after 10 years, to show how the performance of the well deviates from the established backpressure curve when the formation is damaged.

w Bottomhole property at surface datum

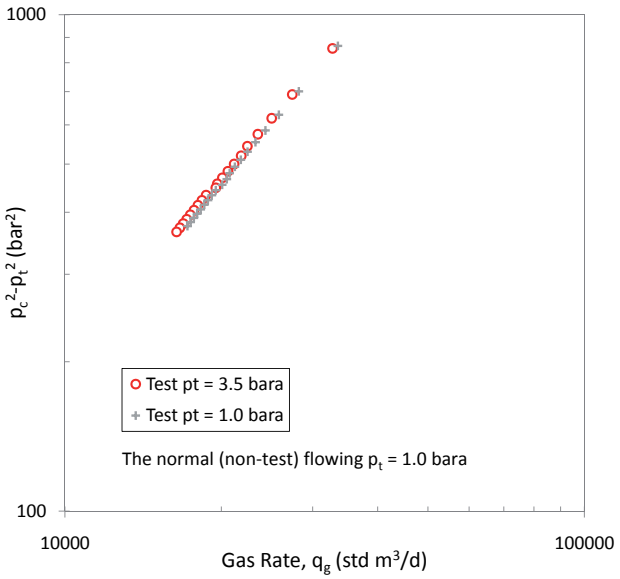

Fig. 3.15 – Backpressure plot of a two layer model where the wellhead pressure during the post shut-in flow period was higher than the normal flowing pressure.

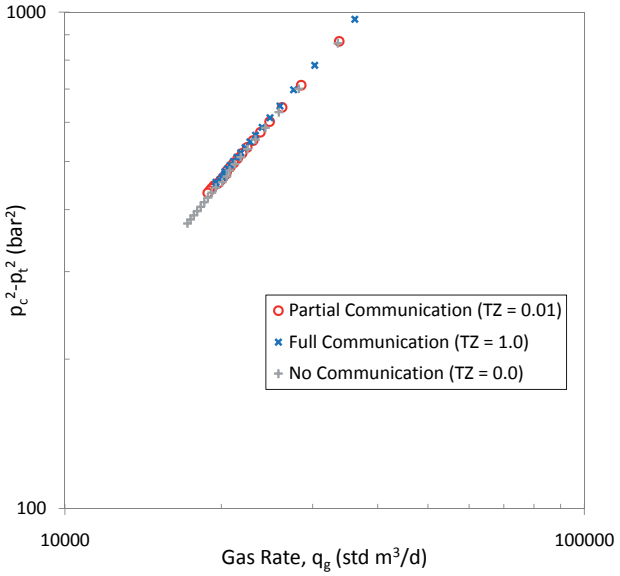

Fig. 3.16 – Backpressure plot of a two layer model where the two layers are communicating with varying degrees throughout the reservoir.

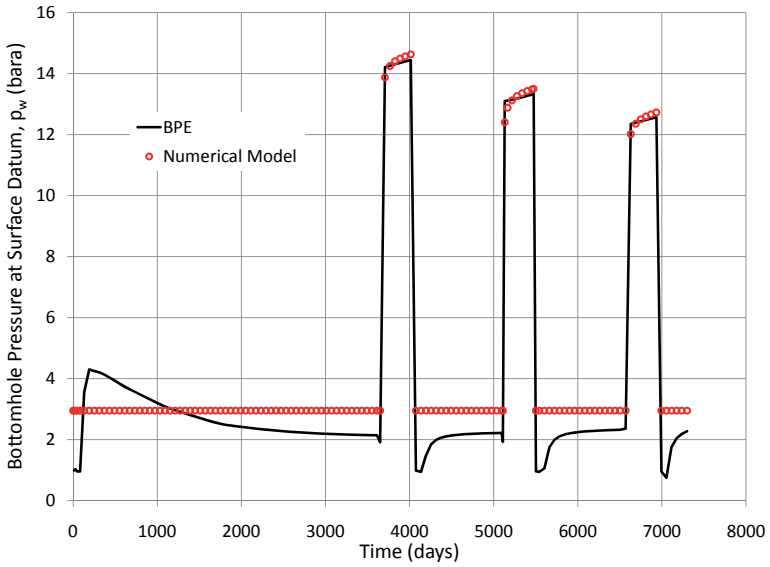

Fig. 3.17 – Bottomhole pressure prediction for the two-layer model based on Fetkovich et al. [3] with permeabilities of 10 and 0.1 md for the high- and low-perm layers respectively.

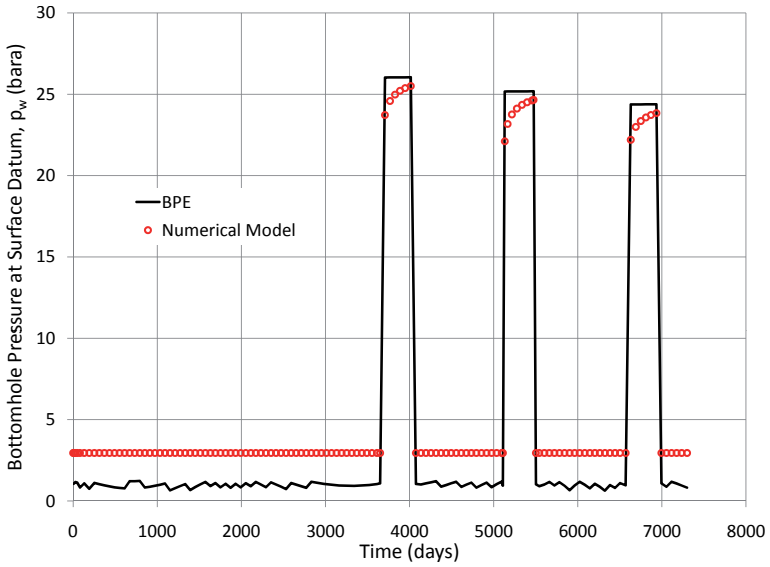

Fig. 3.18 – Bottomhole pressure prediction for the two-layer model based on Fetkovich et al. [3] with permeabilities of 1 and 0.01 md for the high- and low-perm layers respectively.

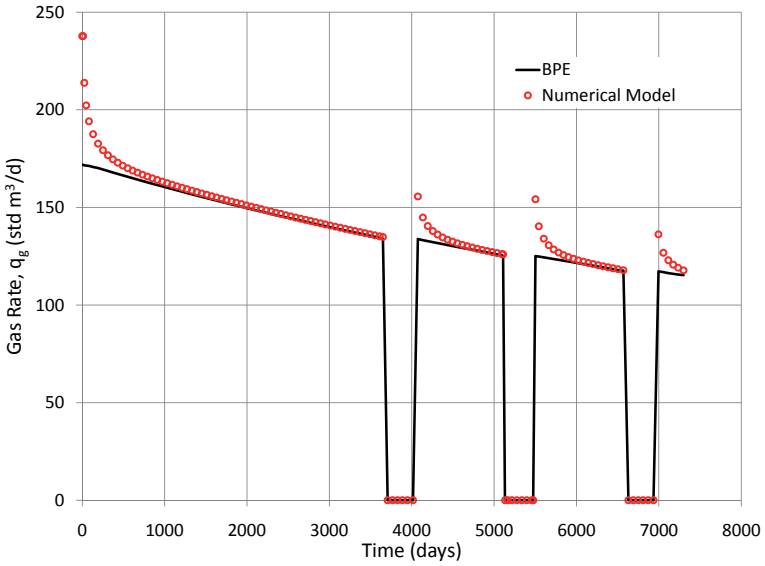

Fig. 3.19 – Gas rates for the two-layer model based on Fetkovich et al. [3] with permeabilities of 1 and 0.01 md for the high- and low-perm layers respectively. The BPE is no longer able to predict the transients in the gas rate.

Bibliography

[1] A El-Banbi and R Wattenbarger. Analysis of commingled tight gas reservoirs. In *SPE Annual Technical Conference and Exhibition*, 1996.

[2] M.J Fetkovich. Multipoint testing of gas wells. Presented at the SPE Mid-Continent Section, Continuing Education Course in Tulsa, Oklahoma, March 1975.

[3] M.J Fetkovich, M Bradley, A Works, and T.S Thrasher. Depletion performance of layered reservoirs without crossflow. *SPE Formation Evaluation*, 5(3):310–318, 1990.

[4] M.J Fetkovich, D.J Ebbs Jr., and J.J Voelker. Multiwell, multilayer model to evaluate infill-drilling potential in the oklahoma hugoton field. *SPE Reservoir Engineering*, 9(3):162–168, 1994.

[5] M Golan and C.H Whitson. *Well Performance*, volume 2. Tapir Akademiske Forlag, Trondheim, Norway, 2003.

[6] M Hawkins Jr. A note on the skin effect. *Journal of Petroleum Technology*, 8(12):65–66, 1956.

[7] A Juell and C.H Whitson. Backpressure equation for layered gas reservoirs. In *SPE Annual Technical Conference and Exhibition*, 2011.

[8] F. Kuppe, S. Chugh, and P. Connell. Material balance for multi-layered, commingled, tight gas reservoirs. In *SPE/CERI Gas Technology Symposium*, 2000.

[9] H.C Lefkovits, P Hazebroek, E.E Allen, and C.S Matthews. A study of the behavior of bounded reservoirs composed of stratified layers. *SPE Journal*, 1(1):43–58, 1961.

[10] T.S Thrasher. Gas-well deliverability monitoring: Case histories. *SPE Production and Facilities*, 10(3):177–183, 1995.

Chapter 4

Integrated Modeling

4.1 Contributions

All major work in completing this paper [3] was performed by the author. M. Hoda helped setting up an integration framework that was used as a starting point for the work presented in the paper. C.H. Whitson had important input during the course of the work on solving coupling problems between the different parts of the integration project.

4.2 Model-Based Integration and Optimization — Gas-Cycling Benchmark

The following section is a reprint of Juell et al. [3].

4.2.1 Abstract

A benchmark for computational integration of petroleum operations has been constructed. The benchmark consists of two gas-condensate reservoirs producing to a common process facility. A fraction of the processed gas is distributed between the two reservoirs for gas injection. Total project economics are calculated from the produced streams and process related costs. This benchmark may be used to compare different computational integration frameworks, and optimization strategies. Even though this benchmark aims to integrate all parts of a petroleum operation, from up-stream to down-stream, certain simplifications are made. For example pipe flow from reservoir to process facility is not included in the integrated model. The methods of model integration and optimization discussed in this paper are applicable to complex petroleum operations where it is difficult to quantify

cause-and-effect without comprehensive model-based integration. A framework for integration of models describing petroleum operations has been developed. An example test problem is described and studied in detail. Substantial gains in full-field development may be achieved by optimizing over the entire production system.

All models and data in the benchmark problem are made available so that different software platforms can study the effects of alternative integration methods and optimization solver strategy. The project itself can, and probably should, be extended by others to add more complexity (realism) to the reservoir, process, and economics modeling.

4.2.2 Introduction

The petroleum industry has developed advanced modeling tools and applications for describing the key segments of upstream-to-downstream projects reservoir simulators, network pipeline simulators, compressor models, surface product process simulators, and economic applications. The custodians of these models are specialists and often know little about the complexities of models used by other disciplines. Historically, educational institutions and most industry discipline structures (Reservoir, Production, Drilling, Transportation, Process, Financial) lead to segregation of people. In recent years, integrated operations has led to improved localization and communication amongst discipline groups in large petroleum projects. Control room technology, high-speed communication, and some physical changes in localization into project vs discipline housing has moved the industry towards better integration.

Despite the improved integration of people and communication, less progress has been seen with integration of the models themselves. Todays practice involves using models independently, often with clumsy and time-consuming hand-shaking interfaces that are adhoc file transfers from one modeling group to another. More automated integration software solutions tend to work smoothly with applications from a particular vendor, but dont provide an ecumenical interfacing capability for any application.

With a truly integrated model, one can optimize (for example) project net present value by changing controllable variables such as gas injection rate and composition, process unit conditions, pipeline size, etc., subject to constraints such as number of wells, sales gas heating value and CO_2 content, etc. Optimization can involve rigorous multi-variable maximization, or it can simply provide quantitative cause-and-effect assessment. Several interesting papers have dealt with model-based integration and optimization (Bailey et al. [1]; Cullick et al. [2]). These authors discuss complex

petroleum projects with emphasis on uncertainty analysis within an optimized and integrated modeling environment. Unfortunately those papers, and similar ones by the same authors, are not amenable to creating an open benchmark, as is our intention here. Also, these authors do not deal with compositional issues and surface processing as done in the project presented here.

This paper provides a benchmark for an integrated petroleum project that uses several models to integrate streams from reservoir to market value. This project provides a starting point for discussion and comparative solutions to a simple-yet-realistic integrated petroleum project. Hopefully the benchmark will provide a platform for comparison of model integration software and optimization methods developed by academia and industry.

4.2.3 Overview

An integrated model of a petroleum operation has been created. The model consists of two gas condensate reservoir models, coupled with process and economics models. A fraction of the produced gas is distributed between the two reservoirs for gas injection. Fig. 4.1 shows an overview of the integrated project.

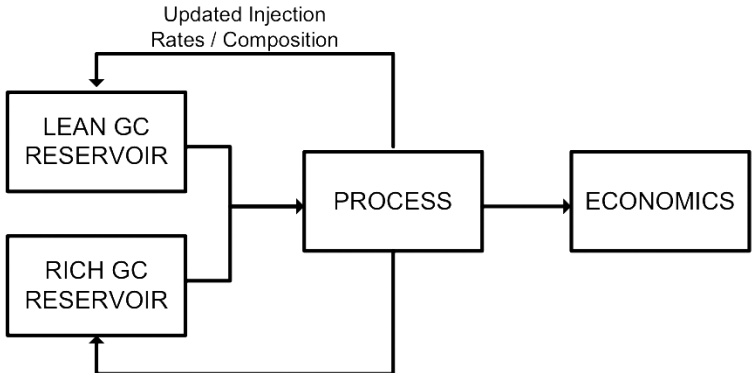

Fig. 4.1 – Integrated project overview.

4.2.4 Reservoir Description

The two gas-condensate reservoir models used in this benchmark are based on the reservoir model given in Kenyon and Behie [4], the third comparative solution project (SPE3). The two reservoirs differ from the original SPE3 study, and each other, only in permeability distribution and initial fluid

composition, as given in Table 4.1 and Table 4.2. Vertical permeabilities are input as a tenth of the horizontal permeabilities. The sector model has one production well, and one injection well. The wells are perforated in opposite corners of the grid. The producer is given a rate constraint of 1.756E5 m^3/d, and a bottomhole pressure constraint of 34.5 *bara*. A maximum bottomhole pressure constraint of 275.8 *bara* is given for the injector. The wells are constrained by bottomhole conditions, so wellbore hydraulics are not considered. Both reservoirs have an initial pressure of 245 *bara*, and a reservoir temperature of 93 ^oC. The reservoir grids consist of 9 by 9 equal-size grid blocks in the horizontal plane, each measuring 89.4 m by 89.4 m. The Arco equation of state (EOS) model from the SPE3 is used in this project, both by the reservoir simulator and the process simulator. Details on the EOS are given in Tables 4.3 and 4.4.

TABLE 4.1 – Horizontal permeability distributions used in the two reservoir models.

Horizontal Permeabilities				
Layer	Original	Heterogeneous	Homogeneous	Thickness
	md	*md*	*md*	*m*
1	130	350	85	9.1
2	40	45	85	9.1
3	20	25	85	15.2
4	150	10	85	15.2

4.2.5 Process Description

The process model consists of four oil-gas separators. The oil product stream temperature and pressure is taken to standard conditions (STC) at the last stage of separation (Table 4.5).

Gas from the first separation stage is fed to a dew point controller (DPC) which cools the gas to condense out natural gas liquids (NGL). This unit operation is modeled as a single separator that brings the gas from the first stage separator down to a pressure of 13.8 *bara* and a temperature that can be varied between $T_{max} = 27\,^oC$ (no cooling) and $T_{min} = -57\,^oC$ (maximum cooling). This is a rather simplistic way to model a DPC unit.

Gas from the DPC is split into a sales gas stream and an injection gas

stream. The injection gas is again split in two streams, for distribution between the two reservoir models.

A fraction of the DPC produced gas is used to run the DPC unit. This fraction increases when the DPC temperature is decreased:

$$f_{DPC} = 0.1\sqrt{\frac{T_{DPC} - T_{max}}{T_{min} + \frac{160}{9}}} \tag{4.1}$$

The sales gas rate is calculated as follows:

$$q_{gs} = (1 - f_{DPC})\,(1 - f_{gi})\,q_g \tag{4.2}$$

where f_{gi} is the fraction of DPC produced gas being reinjected.

The total injection gas rate is:

$$q_{gi} = (1 - f_{DPC})\,f_{gi} q_g \tag{4.3}$$

The injection gas rate for the lean gas condensate reservoir is:

$$q_{gi,l} = f_{gl} q_{gi} \tag{4.4}$$

The injection gas rate for the rich gas condensate reservoir is:

$$q_{gi,r} = (1 - f_{gl})\,q_{gi} \tag{4.5}$$

The main control parameters in the process are: DPC temperature, T_{DPC}; fraction of DPC gas reinjected, f_{gi}; and fraction of reinjected gas delivered to the lean gas condensate reservoir, f_{gl}. An overview of the process is shown in Fig. 4.2.

4.2.6 Economics Description

If the CO_2 content in the sales gas exceeds a limit, L_{CO_2}, for a period of time, the price of gas is halved for that period.

After the well streams are processed into final products, the project economics are calculated. The annual cash flow is calculated from:

$$R_t = \int_{t-1}^{t} (q_{gs} P_g + q_{NGL} P_{NGL} + q_o P_o)\,\mathrm{d}t \tag{4.6}$$

The cooling required by the DPC is considered a major cost item in the project. The capital cost of the DPC unit is calculated from:

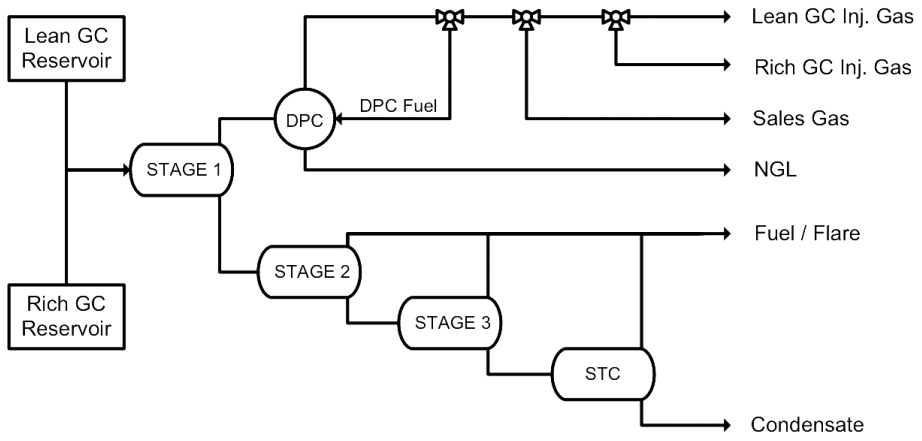

Fig. 4.2 – Process overview.

$$C_{DPC} = 50 \times 10^6 \sqrt{\frac{T_{DPC} - T_{max}}{T_{min} + \frac{160}{9}}} \tag{4.7}$$

The total project economics is evaluated by the net present value (NPV).

$$V_p = \sum_{t=1}^{N} \left[\frac{R_t}{(1+i)^t} \right] - C_{DPC} \tag{4.8}$$

4.2.7 Software Solutions

Petrostreamz Pipe-It is the integration and optimization (IO) application used to build the project presented here. This IO application features a Runner that facilitates execution of all models in a project in the order needed as defined by a graphical layout, consisting of three primitive elements: Resources (file references), Processes (any application that can be launched from an available operating system), and Connectors (lines which link, sequentially and in parallel, interconnected Resources and Processes making up a Project). The IO application allows the Project to be executed repeatedly as a function call to the Optimizer a graphically-controlled suite of vendor-provided optimizer solvers (Nelder-Mead bounded Simplex, Random, Experimental Design) and solver plug-ins built with a C/C++ API for 3rd-party solvers (e.g. IBM open-source IPOPT). The IO application provides a graphical utility to build required links to tokens (numbers and

text values) found in Project Resources (files) for defining the Optimizer target objective, control variables, and constraints. The reservoir models are simulated with SENSOR from Coats Engineering, and the process is simulated with Streamz from Petrostreamz.

4.2.8 Reservoir Interaction

Because the injection gas for both reservoirs is a product of the combined produced well stream, there is a certain degree of interaction between the two models. The gas injection rates and composition changes with time, and this must be updated in the reservoir models. Restart commands are used to facilitate the reservoir model updating. Each model is run for a predefined time interval, called the project time step, Δt_P. The model states are saved at the end of the project time step. Then the well streams are processed to yield sales products, and gas injection rates and composition. The injection gas information is updated in the project, and the models are run for another project time step. Smaller time steps give more accurate reservoir performance, but increase run time of the project. With 9 project time steps, each requiring a reservoir simulator restart, the project run time is ∼30 seconds on a 2.33 GHz dual core computer with 3GB of RAM. The two reservoir simulation models run within the project each take ∼1 second to run; without restarts, the same reservoir simulator models each take ∼0.5 seconds to run. The remaining 28 seconds (30 - 2×1) includes: launching multiple applications (process, economics), run times for those applications, translating streams for inter-application handshaking, and overhead for coordinating the entire project.

4.2.9 Coupling Errors

When a project time step finishes, the injection rates and composition are updated for use in the next step. These values are modeled as invariant in the next step, while in reality they continuously change. Because the two reservoir models have different simulation time steps, Δt_R, both models must be put on a common time step basis to combine the streams for processing. Each project time step is divided into a number of equal-sized divisions, Δt_S. The streams from the two reservoir models are summed and averaged over each division. The calculated average injection rates and composition for the last division in the project time step is used to update the models for the next project time step. If a small number of divisions is used, and there is a variation in the produced streams over the project time step, the next step might get a wrong starting point. This is shown

in Fig. 4.3a - 4.3b. The injection rates and composition are assumed to be constant over one project time step. If the project time steps are large, this leads to errors, as shown in Fig. 4.3c. Reducing the project time step size will decrease this effect. The effects of these two types of coupling error can be seen from Fig. 4.4. The coupling error will approach zero when $\Delta t_P \rightarrow 0$. Increasing the number of divisions per step decreases the coupling error significantly for large project time step sizes. It is also important to consider the run time of the project when choosing a value for the project step size, and the number of divisions per step. The project run time increases inversely proportional to the project time step size, as shown in Fig. 4.5.The number of divisions per step has little effect on run time. Choosing a project time step size of 1000 days, and 100 divisions per step, gives a reasonable run time while keeping the total coupling error less than $\sim$0.5% for this project.

4.2.10 Base Case and Sensitivities Definition

A base case for the variables and all model sensitivities is defined in Table 4.6 6, case 1. If nothing else is specified, this is the model definition used in this paper. The molar rates from the two reservoirs for the base case are presented in Fig. 4.6 and 4.6. The base case sales product rates are presented in Fig. 4.8, and the injection gas rate and composition are presented in Fig. 4.9. The key sensitivities are:

- Composition. The initial compositon in a gas-condensate reservoir has a significant effect on condensate reserves by depletion and, accordingly, target condensate reserve for gas cycling. More importantly, interaction of the condensate recoveries with heterogeneities is paramount for gas cycling projects.

- Permeability distribution. Volumetric sweep efficiency in gas-condensate cycling projects is dominated by vertical permeability distribution. Standing et al. [8] and Muskat [6] discuss this effect in detail.

- CO_2 limit. Sales gas quality constraints on heating value and inerts have a strong impact on gas price. Exceeding CO_2 limits may even result in field production being curtailed.

- Price escalation and discount factor. The time-value of money has a particularly large impact on gas cycling project because of delayed gas sales, and an increasing international market for natural gas. Large

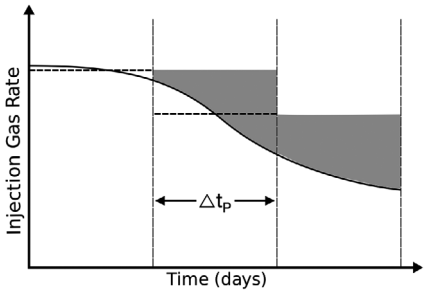

(a) If only an average gas injection rate and composition for the previous time step is used to initiate the next time step, and the step size is large, siginificant coupling errors may result

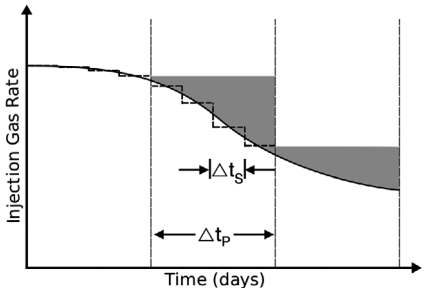

(b) Dividing each time step into smaller divisions gives a better approximation of the gas injection rate and composition at the end of each time step, and coupling errors are reduced.

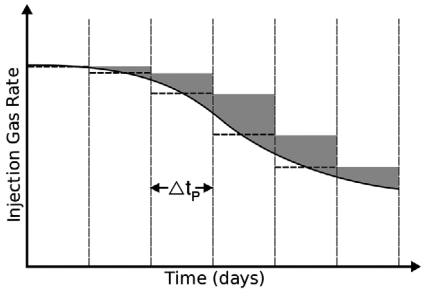

(c) Reducing the time step size between each update of injection rate and composition leads to smaller coupling errors.

Fig. 4.3 – Coupling errors in the integrated model. Shaded area indicates error in injected gas volume due to coupling.

and unpredictable fluctuations in oil and gas prices introduce considerable uncertainties in economic evaluation of petroleum projects.

An initial gas price of 0.177 USD/m^3 (5 USD/Mcf), and an initial condensate and NGL price of 314.5 USD/m^3 (50 USD/bbl) are used in the project. The base case gives a NPV of 188.4E6 USD.

4.2.11 Parameter Analysis

The four main optimization variables in the benchmark model are the total gas injection fraction, split of the injection gas between the two reservoirs, injection time, and the DPC temperature. This creates a four-dimensional optimization problem. The objective surface (NPV) in an integrated project

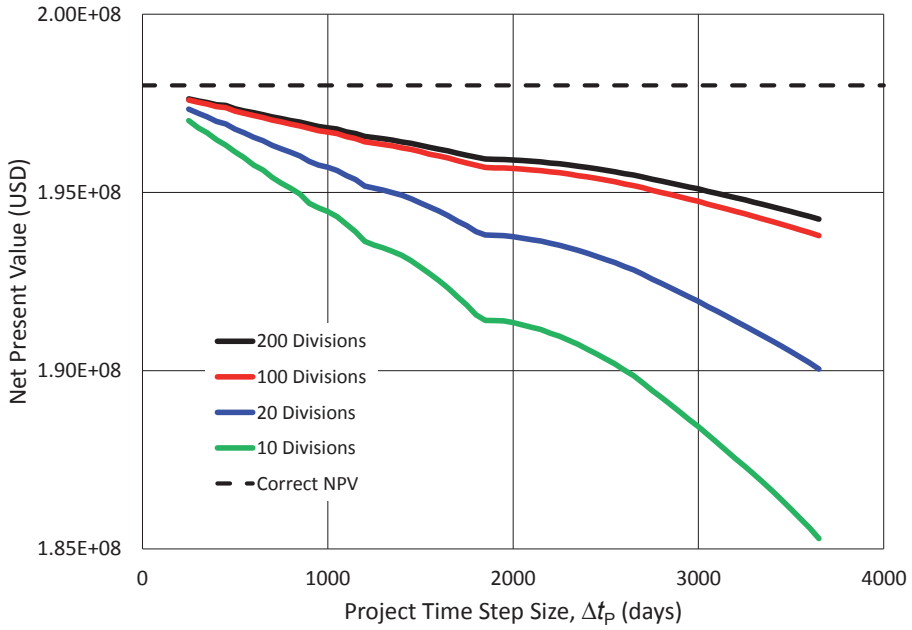

Fig. 4.4 – Coupling errors as a function of project time step size, and number of divisions per step. Zero coupling error is assumed when $\Delta t_P \to 0$.

like this may have several local maxima. Fully automated optimization might get stuck at one of these local solutions, and not reach the global maximum. To understand how each optimization variable affects the objective, it is useful to do parameter analysis of each variable. This is done by running cases with changing values of one variable at the time, while keeping all other variables constant. With a parametric analysis it is possible to identify non-convex behavior. Fig. 4.10 - 4.13 shows the results of the parametric analysis for the optimization variables. As seen from Fig. 4.10, the NPV as a function of DPC temperature has two maxima. When performing optimization on this variable, it is necessary to initiate the optimization algorithm near both maxima. It is important to remember that the parameter analysis only gives information about the objective function at certain points in the solution space i.e. along a line. To get a clearer understanding of how the objective function behaves, it is possible to create surface plots of the objective versus two optimization variables, to yield a 2D parameter analysis. A surface plot of NPV versus total injection fraction and injection time is shown in Fig. 4.14, and a surface plot of NPV versus total injection fraction and lean injection fraction is shown in Fig. 4.15. It is clear from

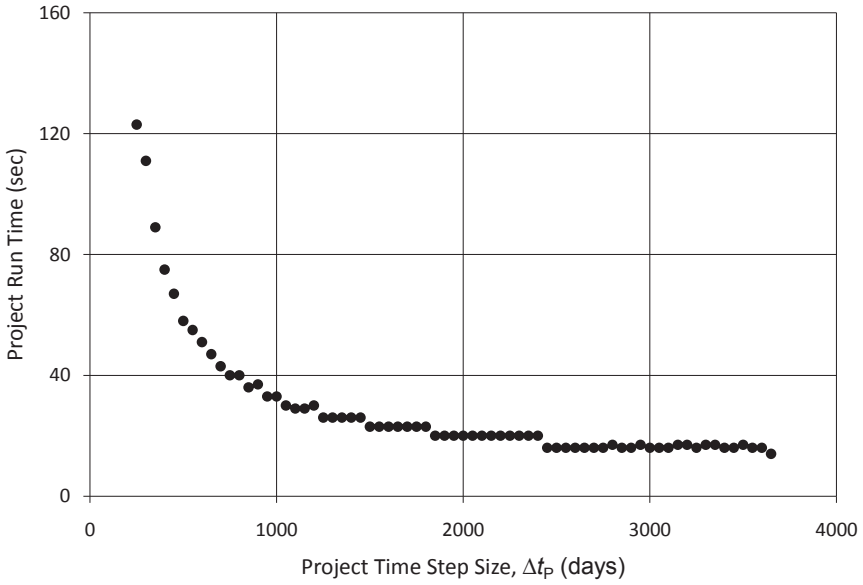

Fig. 4.5 – Project run time versus project time step size on a 2.33 GHz dual core computer with 3 GB of RAM. Run time increases inversely proportional to the project time step size.

Fig. 4.15 that several combinations of f_{gi} and f_{gl} give approximately the same optimum value of NPV. This information was not possible to obtain from the single-variable parameter analysis. Even if 2D parameter analysis gives additional information on the objective function, they require a large number of project runs, and may be impractical for long-running projects.

4.2.12 Optimization

The Nelder and Mead [7] reflection simplex algorithm is used to perform all optimization in this paper. This algorithm does not required derivatives and is very robust. Lagarias et al. [5] studies the convergience properties of the Nelder-Mead reflection simplex, and concludes that they are at best linear. Selection of starting point for the optimizations is often important. Choosing a poor starting point may lead to slow convergence, or convergence to a local instead of a global maximum. Two optimizations of the base case with different starting points were performed to illustrate this: One with starting point at the base case values ($t_i = 3650$ days, $f_{gi} = 0.6$, $f_{gl} = 0.5$, $T_{DPC} = 27\ ^oC$), and the other with starting point from the optimum of the 1D parameter analyses ($t_i = 730$ days, $f_{gi} = 0$, $f_{gl} = 0$, $T_{DPC} = 27\ ^oC$).

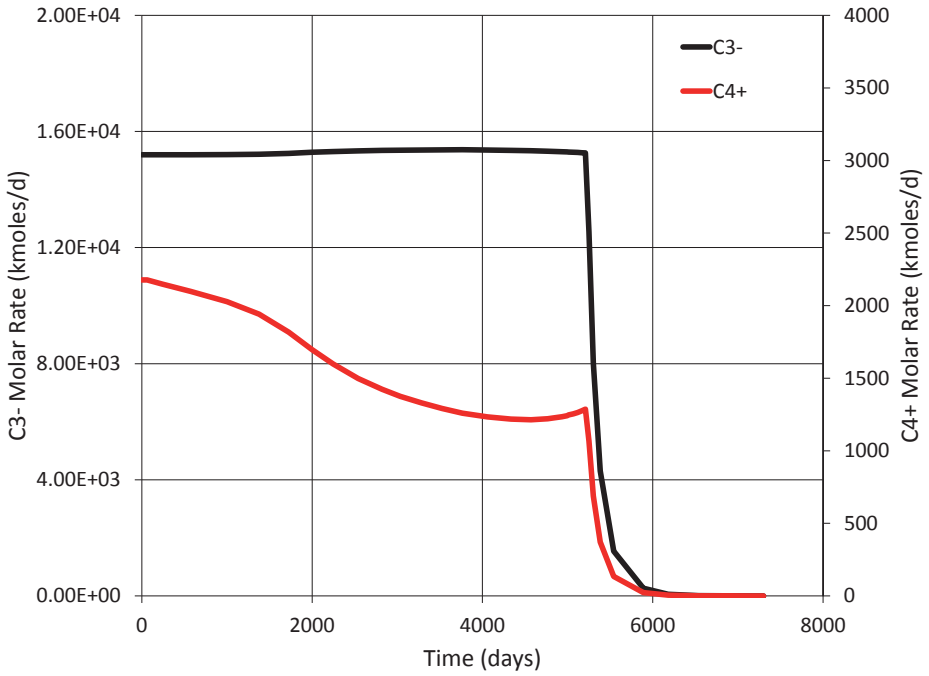

Fig. 4.6 – Lean gas-condensate reservoir molar rates for the base case.

Both optimizations converge to the same solution, but the latter converges ∼40 iterations faster. The convergence behavior of the optimizations is presented in Fig. 4.16. The values of the variables during the optimization of the base case are presented in Fig. 4.17. A suite of cases have been optimized. The results of these optimizations are presented in Table 4.7. Each case has different values for the sensitivities defined in Table 4.6, or is optimized with respect to different sets of variables. Two sets of optimized total injection fractions and lean injection fractions for the base case (A1) give the same NPV as seen in Table 4.7, rows three and four. The same behavior is seen for case B2, in row seven and eight. This behavior is predicted from the parameter analysis in Fig. 4.15. Several combinations of the optimization variables may result in the same NPV. When non-unique solutions like this exist, it is best to choose the one that gives the most desirable operational conditions.

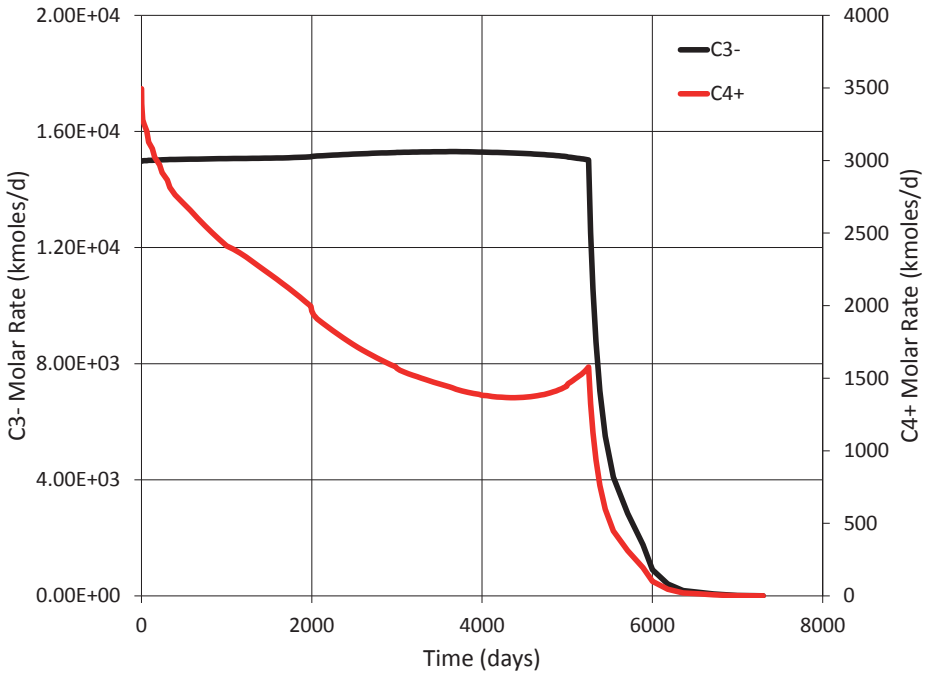

Fig. 4.7 – Rich gas-condensate reservoir molar rates for the base case.

4.2.13 Conclusions

1. Having an integrated model allows quantification of cause and effect in complex petroleum projects.

2. Loose coupling of models may lead to coupling errors. It is important to quantify and minimize these errors.

3. The magnitude of the total coupling error in this project is believed to be ∼0.5% in terms of NPV.

4. Single parameter analysis of key variables is highly recommended, because it provides a graphical and quantitative orientation on the objective function smoothness, magnitude, and direction.

5. Optimization of key variables in the integrated model may lead to significant increase in NPV for the project. In this project the improvement in NPV is ∼10%

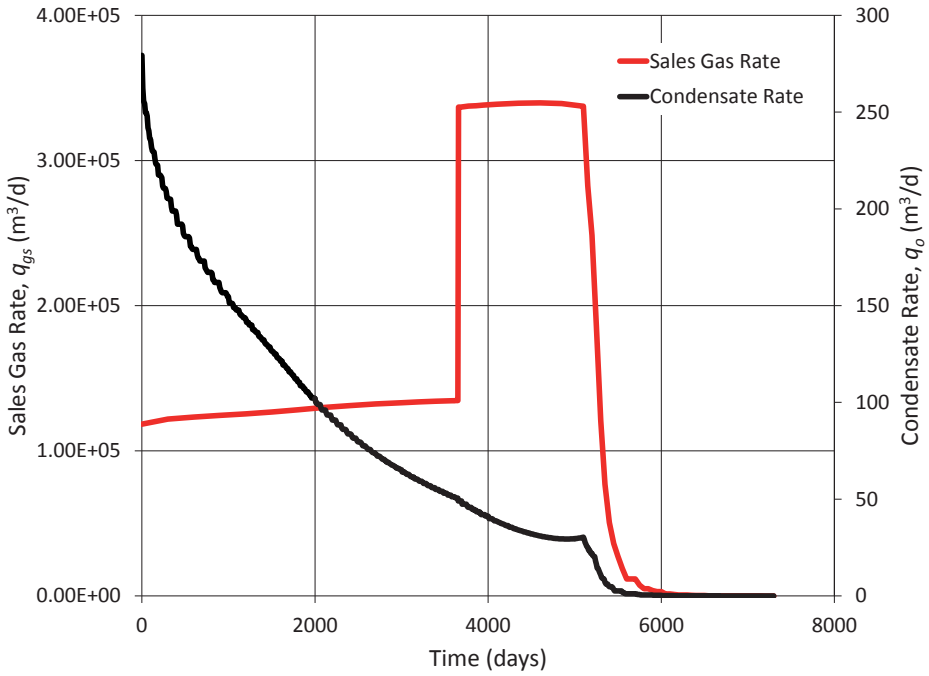

Fig. 4.8 – Sales product rates for the base case.

4.2.14 Recommendations for Further Work

The model for the DPC unit used in this project is most likely a poor approximation. This unit should be modeled in more detail, at least as a two stage process: the first stage should reduce the temperature down to the desired outlet temperature, and the second stage should reduce the pressure down to the outlet pressure.

Only one optimization algorithm is used in this paper. The algorithm is very robust, but does not have fast convergence properties. Efforts should be made to find an optimization algorithm with better convergence properties, while still maintaining robustness.

Pipeflow modeling is not considered in the integrated model presented in this paper, but should be included in the future. Both pressure drops in the tubing, from bottomhole to wellhead, and pressure drops from wellhead to process facilities should be considered. Other extentions of the benchmark problem may include:

- Improved surface process modeling and related cost.

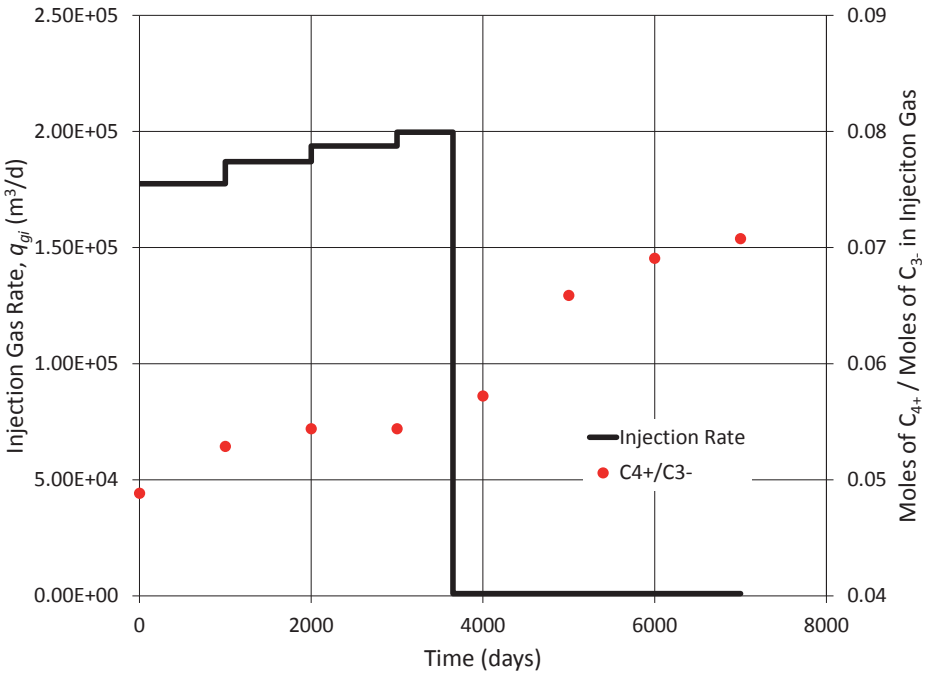

Fig. 4.9 – Injection gas rate and composition for the base case.

- Injection gas compression modeling and related cost.
- Scaling up to full-field modeling.
- Impact of late life tie-ins from undeveloped fields, particularly in regard to selecting gas processing solution.
- Optimization on well count and location, and well target rates.
- Uncertainty analysis: geology, price forecasting, and market demand.

Nomenclature

C_{DPC}	Capital cost of dew point controller unit (USD)
f_{DPC}	Fraction of DPC product gas used as fuel for the DPC
f_{gi}	Fraction of available DPC product gas injected

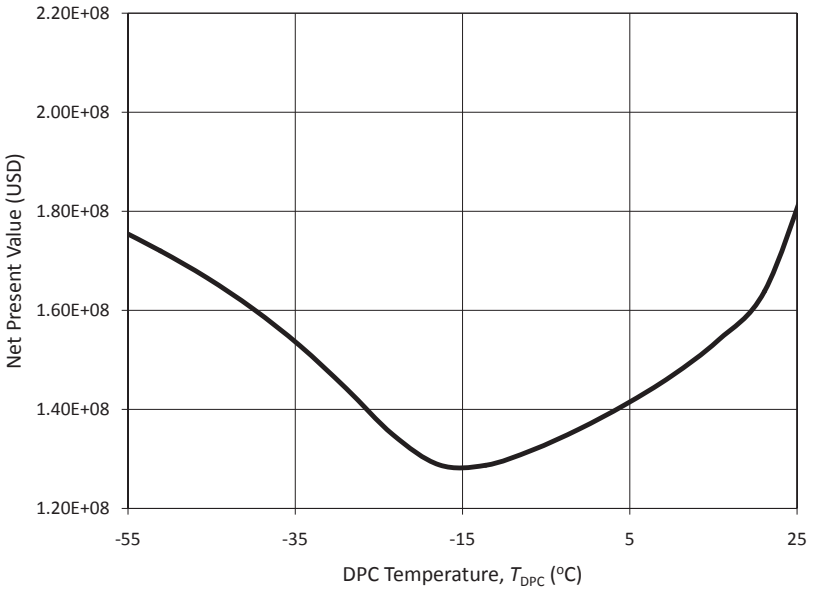

Fig. 4.10 – Parameter analysis of DPC temperature. The NPV as a function of DPC temperature has two maxima, at the upper and lower bound. Special care must be taken when optimizing with respect to this variable.

f_{gl}	Fraction of injection gas distributed to the lean gas-condensate reservoir
i	Discount factor
L_{CO2}	CO_2 limit in the sales gas (mol-%)
M	Molecular weight
N_S	Number of divisions the product streams are divided into per project time step
p	Pressure (bara)
P_g	Price of gas (USD/m^3)
P_{NGL}	Price of natural gas liquids (USD/m^3)
P_o	Price of condensate (USD/m^3)
q_g	Total gas rate from the DPC (m^3/d)
q_{gs}	Sales gas rate (m^3/d)

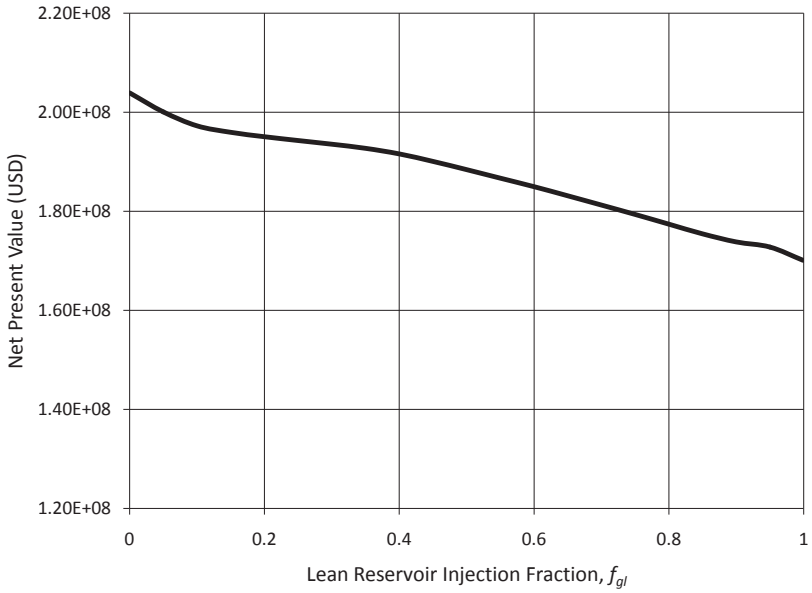

Fig. 4.11 – Parameter analysis of lean injection fraction. NPV is monotonically increasing with decreasing f_{gl}.

q_{gi}	Gas injection rate (m^3/d)
q_{NGL}	Natural gas liquids rate (m^3/d)
q_o	Condensate rate (m^3/d)
R_t	Annual cash flow (USD/year)
s	Volume shift factor
t	Time (days)
t_i	Injection end time (days)
T	Temperature (^{o}C)
T_{DPC}	Dew point controller temperature (^{o}C)
V_p	Net present value (USD)
Z	Z-factor

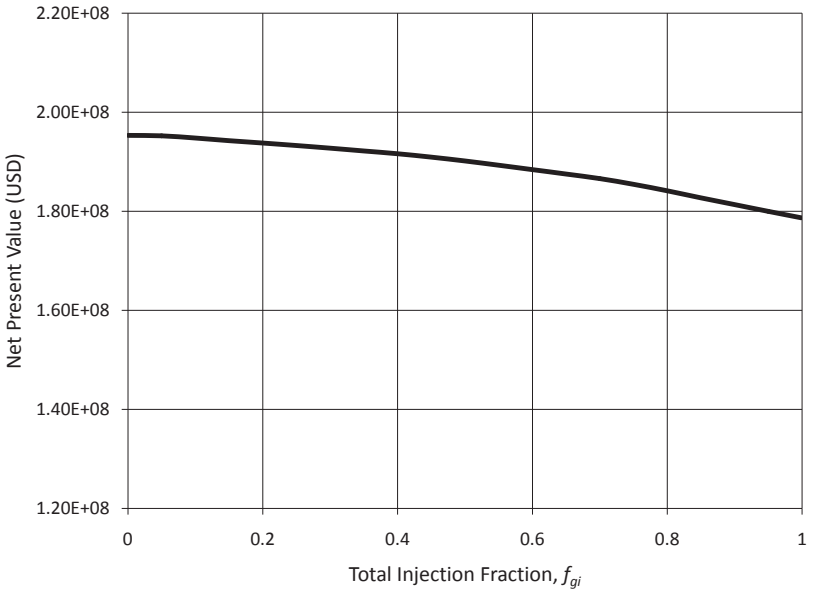

Fig. 4.12 – Parameter analysis of total injection fraction. NPV is monotonically increasing with decreasing f_{gi}.

Greek Symbols

Δt_P	Project time step size (days)
Δt_R	Reservoir model simulation time step (days)
Δt_S	Division time step size, $\Delta t_P / N_S$ (days)
μ	Viscosity (cp)
ρ	Density (kg/m^3)

Subscripts

c	Critical
l	Lean gas-condensate reservoir
max	Maximum value
min	Minimum value
r	Rich gas-condensate reservoir

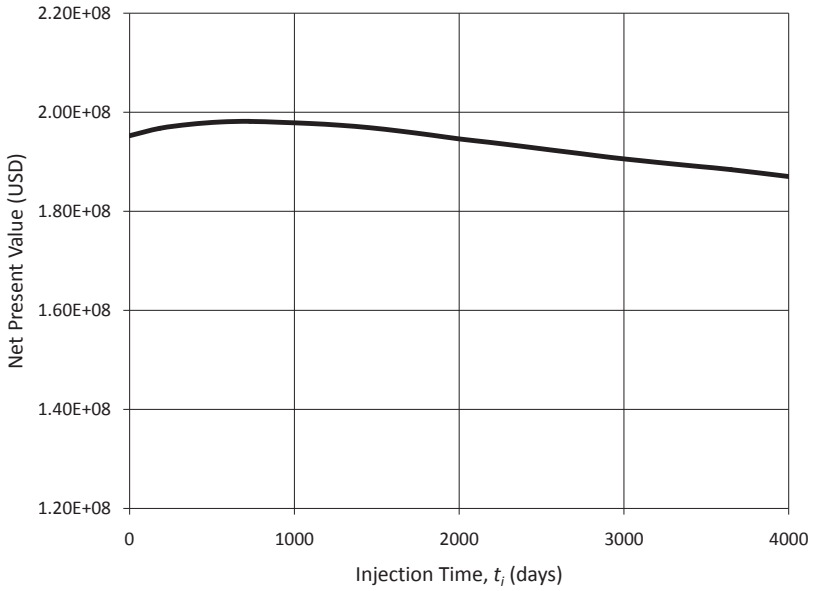

Fig. 4.13 – Parameter analysis of injection time. The NPV reaches maximum when $t_i = 730$ days.

s Saturation

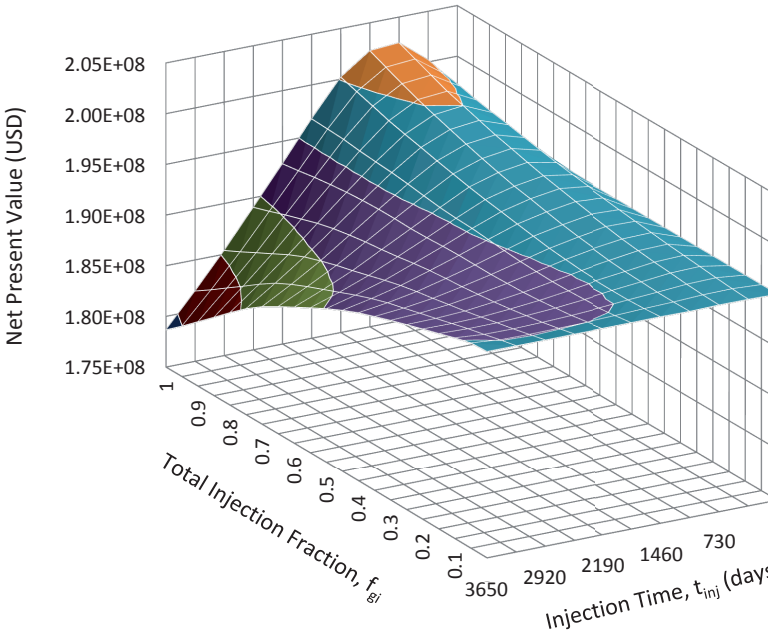

Fig. 4.14 – Surface plot of NPV versus total injection fraction and injection time. The NPV reaches maximum when $t_i = 730$ days and $f_{gi} = 1$.

TABLE 4.2 – Composition and EOS calculated properties for the different reservoir fluid models.

Initial Fluid Properties							
Component	Original	Lean	Rich	Rich	Rich	Rich	
			Layer 1	Layer 2	Layer 3	Layer 4	
CO_2	0.01210	0.011950	0.057940	0.057890	0.057770	0.057130	
N_2	0.01940	0.019947	0.018520	0.018290	0.017890	0.016550	
C_1	0.65990	0.669358	0.628580	0.623980	0.615730	0.586840	
C_2	0.08690	0.108675	0.082880	0.083100	0.083470	0.084420	
C_3	0.05910	0.064739	0.056400	0.056910	0.057780	0.060480	
C_{4-6}	0.09670	0.079760	0.092510	0.093820	0.096110	0.103590	
C_{7+1}	0.04720	0.032719	0.045210	0.046900	0.049950	0.060780	
C_{7+2}	0.01530	0.010517	0.014680	0.015430	0.016800	0.021750	
C_{7+3}	0.00340	0.002335	0.003270	0.003670	0.004490	0.008450	
p_s $(bara)$	240.0	239.9	236.2	237.4	239.4	243.0	
GOR (m^3/m^3)	1596	2422	1677	1591	1451	1073	
ρ_{gs} (kg/m^3)	306.4	275.6	311.6	317.8	329.2	367.6	
μ_{gs} (cp)	0.0372	0.0328	0.0373	0.0384	0.0403	0.0483	
ρ_{os} (kg/m^3)	425.8	484.1	437.9	431.5	420.0	381.7	
μ_{os} (cp)	0.0723	0.1480	0.0757	0.0718	0.0660	0.0520	

TABLE 4.3 – Properties for the Arco EOS.

EOS Properties						
Component	M	T_c	p_c	Z_c	s	ω
		K	$bara$			
CO_2	44.01	304.21	73.82	0.27400	-0.00089	0.225
N_2	28.02	126.27	33.90	0.29000	-0.16453	0.040
C_1	16.04	186.61	46.20	0.28800	-0.17817	0.013
C_2	30.07	305.33	48.80	0.28500	-0.06456	0.098
C_3	44.10	369.85	42.50	0.28100	-0.06439	0.152
C_{4-6}	67.28	396.22	34.35	0.27228	-0.18129	0.234
C_{7+1}	110.90	572.50	25.94	0.26444	0.12080	0.332
C_{7+2}	170.90	630.22	16.92	0.25140	0.23442	0.495
C_{7+3}	282.10	862.61	8.61	0.22436	0.54479	0.833

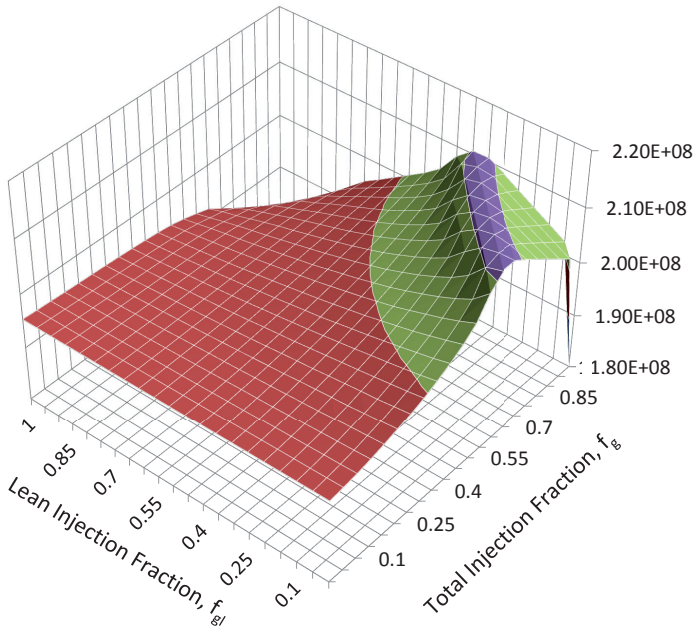

Fig. 4.15 – Surface plot of NPV versus total injection fraction and lean injection fraction. The NPV shows a constant maximum value along a line/path in the f_{gi} - f_{gl} space.

TABLE 4.4 – Binary interaction parameters for the Arco EOS.

	Binary Interaction Parameters								
	CO_2	N_2	C_1	C_2	C_3	C_{4-6}	C_{7+1}	C_{7+2}	C_{7+3}
CO_2	0								
N_2	0	0							
C_1	0.13	0.036	0						
C_2	0.135	0.05	0	0					
C_3	0.1277	0.08	0	0	0				
C_{4-6}	0.1	0.1002	0.09281	0	0	0			
C_{7+1}	0.1	0.1	0	0.00385	0.00385	0	0		
C_{7+2}	0.1	0.1	0	0.00630	0.00630	0	0	0	
C_{7+3}	0.1	0.1	0.1 392	0.00600	0.00600	0	0	0	0

TABLE 4.5 – Separator conditions for the four oil-gas separators modeled.

Separator Conditions		
Stage	Temperature	Pressure
	^oC	$bara$
1	27	56.2
2	27	21.7
3	27	4.5
4	15.6	1.01

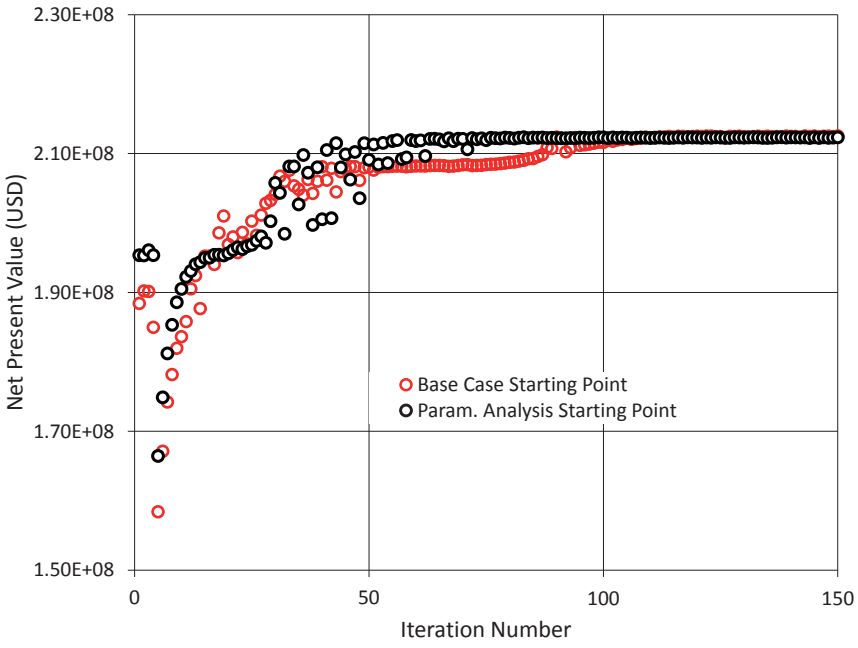

Fig. 4.16 – Choosing the right starting point may be important for fast convergance to the global optimum.

TABLE 4.6 – Case matrix.

Case Matrix				
ID	Description	Case		
		0	1	2
A	Composition		Lean / Rich	Orig / Orig
B	Permeability		Orig / Orig	Orig / Hetro
C	Discount Factor		10 %	0 %
D	DPC Temperature (^oC)	Opt.	27	-57
E	Price Escalation (% / year)		0	5
F	Divisions/Timestep, N_S		100	
G	CO_2 Limit (mol-%)		none	3
H	Injection Time, t_i (days)	Opt.	3650	
I	Total Injection Fraction, f_{gi}	Opt.	0.6	
J	Lean Injection Fraction, f_{gl}	Opt.	0.5	
K	Project Time Step Size, Δt_P (days)		1000	
L	Simulation End Time (days)		7300	

TABLE 4.7 – Optimization results. Variables in parenthesis are set to fixed values.

Optimization Results					
Case	NPV	f_{gi}	f_{gl}	t_{inj}	T_{DPC}
	$1E6\,USD$			$days$	^oC
A1	195	0	(0.5)	(3650)	(27)
A1	203	1	(0.5)	871	(27)
A1	213	0.637	0	1180	(27)
A1	213	0.733	0.134	1194	27
B2	194	0	(0.5)	(3650)	(27)
B2	197	1	(0.5)	437	(27)
B2	198	0.626	0	440	(27)
B2	198	0.781	0.220	445	27
E2	262	0.943	0.334	1594	27
G2	198	0.741	0.454	502	27
C2	399	1	0.247	3625	-54.5

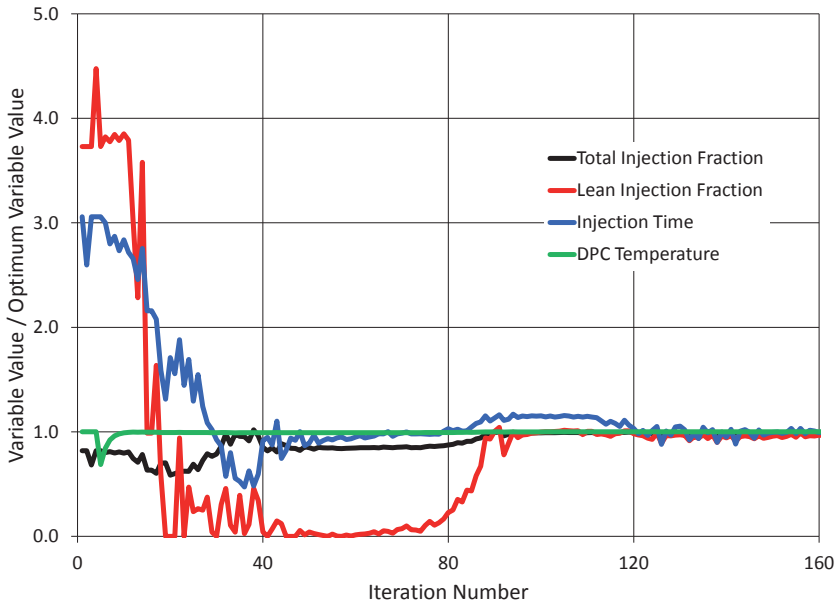

Fig. 4.17 – Normalized variable values for the optimization of the base case. A variable is converged when the normalized variable value stabilizes at 1.

Bibliography

[1] W.J Bailey, B Couet, and D Wilkinson. Framework for field optimization to maximize asset value. *SPE Reservoir Evaluation and Engineering*, 8(1):7–21, 2005.

[2] A.S Cullick, H David, N Keshav, A Jay, and K James. Optimizing multiple-field scheduling and production strategy with reduced risk. In *SPE Annual Technical Conference and Exhibition*, 2003.

[3] A Juell, C.H Whitson, and M Hoda. Model-based integration and optimization–gas-cycling benchmark. *SPE Journal*, 15(2):646–657, 2010.

[4] D.E Kenyon and A Behie. Third spe comparative solution project: gas cycling of retrograde condensate reservoirs. *Journal of petroleum technology*, 39(8):981–997, 1987.

[5] J.C Lagarias, J.A Reeds, M.H Wright, and P.E Wright. Convergence properties of the nelder-mead simplex method in low dimensions. *SIAM Journal on Optimization*, 9(1):112–147, 1999.

[6] M Muskat. Effect of permeability stratification in cycling operations. *Trans. AIME*, 179:313–328, 1949.

[7] J.A Nelder and R Mead. A simplex method for function minimization. *The computer journal*, 7(4):308, 1965.

[8] M.B Standing, E.N Lindblad, and R.L Parsons. Calculated recoveries by cycling from a retrograde reservoir of variable permeability. *Trans. AIME*, 174(1):165–190, 1948.

Appendices

Appendix A

Evolutionary Strategy Algorithm

A.1 Intorduction

Evolutionary strategy algorithms are stochastic search methods trying to mimic natural biological evolution. Evolutionary strategy algorithms operate on a population of potential solutions applying the principal of survival of the fittest to produce better and better approximations to a solution. At each generation, a new set of approximations is created by the process of selecting individuals according to their level of fitness in the problem domain and breeding them together using operators borrowed from natural genetics. This process leads to the evolution of populations of individuals that are better suited to their environment than the individuals that they were created from, just as in natural adaptation.

A.2 Problem Statement

A general optimization problem is given in the form:

$$\min [f(\mathbf{x})], \quad \mathbf{x} \in \mathbb{R}^n \tag{A.1}$$

such that,

$$x_{i,min} \leq x_i \leq x_{i,max}, \quad i \in \{1, ..., n\} \tag{A.2}$$

and,

$$c_{i,min} \leq c_i(\mathbf{x}) \leq c_{i,max}, \quad i \in \{1, ..., m\} \tag{A.3}$$

A.3 Initialization

At the beginning of computation, a number of individuals are randomly initialized to form the population of the first generation. The objective function is evaluated for these individuals.

If the optimization criteria are not met for the first generation, the creation of a new generation starts. This generation is created by recombining the parents (individuals in the previous generation). All offspring is mutated with a certain probability. The fitness of the offspring is then calculated, and the offspring is inserted into the population, replacing the parents.

A.4 Selection

Selection determines which individuals are chosen for recombination. The fitness of the individuals in the population is determined by a combination of the objective function, $f(\mathbf{x})$, and violations of constraints:

$$G_i(\mathbf{x}) = \begin{cases} 0 & \text{if } c_{i,min} \leq c_i(\mathbf{x}) \leq c_{i,max} \\ f(\mathbf{x})(c_{i,min} - c_i(\mathbf{x}))^2 & \text{if } c_i(\mathbf{x}) \leq c_{i,min} \\ f(\mathbf{x})(c_i(\mathbf{x}) - c_{i,max})^2 & \text{if } c_i(\mathbf{x}) \geq c_{i,max} \end{cases}$$

$$F(x) = f(\mathbf{x}) + \sum_{i=1}^{m} [G_i(\mathbf{x})] \tag{A.4}$$

Eq. A.4 gives the fitness function for the individuals in the population. The individuals with the smallest fitness function value are used as parents in the next generation.

A.5 Recombination

Recombination produces new individuals by combining the parents from the previous generation. The new individuals are called children of the parents in the previous generation.

Each variable value, x_i, in a child is a combination of the values of that variable in the parents:

$$x_i^c = \sum_{p=1}^{k} \left(a_i^p x_i^p\right), \quad i \in \{1, ..., n\} \tag{A.5}$$

where a_i^p are random numbers between 0 and 1, and:

$$\sum_{p=1}^{k} \left(a_i^p\right) = 1 \tag{A.6}$$

and, k is the number of parents selected from the previous generation.

The recombination technique used is called intermediate recombination, and produces children that may span the entire variable space occupied by the parents.

A.6 Mutation

The optimal solution to the problem may lay outside the variable space occupied by the parents. Since recombination only produces children inside this space, this is insufficient to find the optimal solution. Mutation is used to expand this search area. After the recombination is performed, the variable values of the children are mutated as follows:

$$x_i^{mut} = x_i^c + s_i r_i b_i \tag{A.7}$$

where,

$$s_i \in \{-1, 1\}, \text{uniformly distributed} \tag{A.8}$$

and,

$$r_i = r\left(x_{i,max} - x_{i,min}\right) \tag{A.9}$$

where r is the mutation range, and

$$b_i = 2^{-uk}, \;\; u \in \{0, 1\} \tag{A.10}$$

where k is the mutation precision.

The mutation algorithm is able to produce most points in the hypercube defined by the variable space of the individuals and the range of the

mutation, r. Most mutated individuals will end up close to the pre-mutated starting point. Only some individuals will be far away from the starting point.

The mutation precision, k, defines the minimal step-size possible, and the distribution of the mutation steps inside the mutation range. The smallest relative mutation step-size is 2^{-k}, and the largest is $2^0 = 1$. This means that the mutation steps are created inside the area $\left[r, r2^{-k}\right]$

Typical values of the mutation parameters are:

$$k \in \{4, 5, ..., 20\} \tag{A.11}$$

$$r \in \{0.1, 10^{-6}\} \tag{A.12}$$

A.7 Destabilization

After several generations, the algorithm might get stuck at a local minima. To avoid this, and expand the search area, a destabilization process is applied.

Destabilization is applied when there has not been a change in the parent population for a generation. This means that no children has substituted any of the parents, and the parents continue to be the best fit individuals.

When destabilization is applied, the mutation range, r, is set equal to 1. This causes the mutated children to be able to span the entire hyper-cube defined by the variable upper and lower bounds. If there is a better solution to the problem than within the converged area, there is a chance that one of the destabilized children might end up there.

A.8 Strategies

Evolutionary strategy is not a single optimization algorithm, but a collection of algorithms. Two of these algorithms are discussed in the sections below.

A.8.1 Plus Strategy

The plus strategy selects the fittest individuals both from the parents and the children to yield parents for the next generation, and is denoted $k + j$, where k is the number of parents, and j is the number of children.

This strategy ensures that the best known solution so far is kept in memory. This makes the algorithm converge faster than other strategies,

but it might also narrow the search area, and end up at a local minima instead of the global.

A.8.2 Comma Strategy

The comma strategy only selects the fittest individuals among the children when selecting parents for the next generation, and is denoted k, j, where k is the number of parents, and j is the number of children. The parents of the current generation are discarded, and thus the fittest individuals might be lost.

This strategy tends to get less stuck at local minima than the plus strategy, but might take longer to converge to a solution.

Appendix B

Numerical Model Input File

B.1 Intorduction

This is an example of the input files used for the numerical modeling of liquid-loading gas wells described in Section 2.7.

B.2 File

```
GRID  50 1 118
RUN
IMPLICIT

MAPSPRINT 1  P SO DEPTH
PRINTKR

C     Bwi   cw        denw    visw    cr        pref
MISC  1     3.0E-6    62.4    0.8     4.0E-6    1000

C Radial grid with geometric spacing
C 640 acre spacing ; tubing ID/OD(avg) = 2.16" ; casing ID = 4.1"

RADIAL
  3
0.0     2979.0
0.000   0.09   0.17   0.208   0.255   0.313   0.384   0.470
0.577   0.707  0.866  1.062   1.30    1.60    1.96    2.40
2.94    3.60   4.42   5.41    6.63    8.13    10.0    12.2
15.0    18.4   22.5   27.6    33.8    41.4    50.8    62.3
76.3    93.6   114.7  140.6   172.3   211.2   258.9   317.4
389.0   476.9  584.5  716.5   878.2   1076.5  1319.6  1617.5
```

```
1982.7  2430.3

   360.

C -------------------------------------------------------------
C Vertical Equilibrium
C -------------------------------------------------------------

THVE CON
0

MOD
 2  2  1  1   1 100 = 35.05
 2  2  1  1 100 108 = 4
 2  2  1  1 108 118 = 4




C -------------------------------------------------------------
C Rock Types: 1 = tubing , annulus , casing ; 2 = reservoir
C -------------------------------------------------------------
ROCKTYPE CON
 1
MOD
 23 50  1  1  1 118 = 2
 3  22  1  1  1 118 = 3

C -------------------------------------------------------------
C Tubing "relative permeability" (near-straight lines).
C -------------------------------------------------------------
KRANALYTICAL 1
 0.0  0.0  0.0  0.0     ! Swc  Sorw  Sorg  Sgc
 1.0  1.0  1.0          ! krw(Sorw)  krg(Swc)  kro(Swc)
 1.1  1.1  1.1  1.1     ! nw now ng nog ; slight curv. for stability.

C -------------------------------------------------------------
C Rock
C -------------------------------------------------------------
KRANALYTICAL 2
 0.0  0.0  0.0  0.00    ! Swc  Sorw  Sorg  Sgc
 1.0  1.0  1.0          ! krw(Sorw)  krg(Swc)  kro(Swc)
 3.0  3.0  3.0  3.0     ! nw now ng nog
```

```
C ------------------------------------------------------------
C Skin Zone
C ------------------------------------------------------------
KRANALYTICAL 3
 0.0  0.0  0.0  0.00    ! Swc  Sorw  Sorg  Sgc
 0.1  1.0  0.0012         ! krw(Sorw)  krg(Swc)  kro(Swc)
 3.0  3.0  3.0  3.0     ! nw now ng nog


C ------------------------------------------------------------
C Regions: 1 = Tubing ; 2 = Annulus ; 3 = Skin zone; 4 = Reservoir
C ------------------------------------------------------------
REGION CON
 1
MOD
   1   1  1 1   1  118 = 1   ! Tubing
   2   2  1 1   1  118 = 2   ! Annulus
   3  22  1 1 100  107 = 3   ! Skin zone
  23  50  1 1 100  107 = 4   ! Reservoir

REGNAME
 1  TUBING
 2  ANNULUS
 3  SKIN
 4  RESERVOIR


C ------------------------------------------------------------
C Permeability.
C ------------------------------------------------------------
KX CON
 1.0E9    ! Controls tubing pressure loss
MOD
   3 22 1 1 100 107 = 15.0  ! Skin zone perm
  23 50 1 1 100 107 = 10.0  ! Reservoir perm

KY EQUALS KX

KZ EQUALS KX

C ------------------------------------------------------------
C Porosity.
C ------------------------------------------------------------
POROS CON
 1.0
```

```
MOD
  3 50  1 1  1   100 = 0.0    ! deactivate above reservoir
  3 50  1 1  100 107 = 0.1    ! reservoir
  1  1  1 1  1   118 = 0.0    ! deactivate tubing
  3 50  1 1  108 118 = 0.0    ! deactivate below reservoir
 45 50  1 1  100 107 = 0.0    ! decrease to 55 acre spacing

C -------------------------------------------------------------
C Depth.
C -------------------------------------------------------------
DEPTH CON
 0.001                        ! can't be zero.

C -------------------------------------------------------------
C Gross thicknesses.
C -------------------------------------------------------------
THICKNESS ZVAR
99*35.05 ! above reservoir
 8*4     ! reservoir
11*4     ! rathole

PVTBO   !       T=100 F ; Tsp=20 F ; Psp=50 psia
DENSITY 1       0.55    3.00E-06        1.00E-07

PRESSURES       44      44
15.0    25.0    50.0    75.0    100.0   125.0   150.0   175.0
200.0   225.0   250.0   300.0   350.0   400.0   450.0   500.0
550.0   600.0   650.0   700.0   750.0   800.0   850.0   900.0
950.0   1000.0  1500.0  2000.0  2500.0  3000.0  3500.0  4000.0
4500.0  5000.0  5500.0  6000.0  6500.0  7000.0  7500.0  8000.0
8500.0  9000.0  9500.0  10000.0

PSAT    BG              SRS     VISG    BO      VISO    RS

15.0    1.995E-01       1.0   0.01142 1.0176  1.0232  0.00006
25.0    1.166E-01       1.0   0.01148 1.0176  1.0233  0.00013
50.0    5.702E-02       1.0   0.01153 1.0176  1.0236  0.00028
75.0    3.767E-02       1.0   0.01156 1.0175  1.0239  0.00043
100.0   2.808E-02       1.0   0.01158 1.0175  1.0242  0.00057
125.0   2.236E-02       1.0   0.01160 1.0175  1.0245  0.00072
150.0   1.855E-02       1.0   0.01162 1.0174  1.0248  0.00086
175.0   1.584E-02       1.0   0.01164 1.0174  1.0251  0.00101
200.0   1.381E-02       1.0   0.01166 1.0174  1.0254  0.00115
225.0   1.223E-02       1.0   0.01168 1.0173  1.0257  0.00129
250.0   1.097E-02       1.0   0.01170 1.0173  1.0260  0.00143
```

```
300.0   9.086E-03       1.0   0.01175 1.0173  1.0266  0.00170
350.0   7.740E-03       1.0   0.01179 1.0172  1.0272  0.00196
400.0   6.732E-03       1.0   0.01184 1.0171  1.0277  0.00222
450.0   5.950E-03       1.0   0.01190 1.0171  1.0283  0.00247
500.0   5.324E-03       1.0   0.01195 1.0170  1.0289  0.00272
550.0   4.814E-03       1.0   0.01201 1.0170  1.0295  0.00296
600.0   4.389E-03       1.0   0.01207 1.0169  1.0301  0.00320
650.0   4.030E-03       1.0   0.01214 1.0169  1.0307  0.00343
700.0   3.723E-03       1.0   0.01221 1.0168  1.0313  0.00366
750.0   3.457E-03       1.0   0.01228 1.0167  1.0318  0.00388
800.0   3.225E-03       1.0   0.01236 1.0167  1.0324  0.00409
850.0   3.021E-03       1.0   0.01244 1.0166  1.0330  0.00430
900.0   2.840E-03       1.0   0.01252 1.0166  1.0336  0.00451
950.0   2.678E-03       1.0   0.01261 1.0165  1.0342  0.00471
1000.0  2.533E-03       1.0   0.01270 1.0165  1.0348  0.00491
1500.0  1.632E-03       1.0   0.01385 1.0159  1.0406  0.00667
2000.0  1.204E-03       1.0   0.01541 1.0153  1.0464  0.00810
2500.0  9.649E-04       1.0   0.01728 1.0148  1.0522  0.00930
3000.0  8.170E-04       1.0   0.01929 1.0142  1.0580  0.01031
3500.0  7.187E-04       1.0   0.02133 1.0137  1.0638  0.01120
4000.0  6.497E-04       1.0   0.02329 1.0132  1.0695  0.01199
4500.0  5.989E-04       1.0   0.02516 1.0126  1.0753  0.01270
5000.0  5.600E-04       1.0   0.02693 1.0121  1.0810  0.01335
5500.0  5.294E-04       1.0   0.02859 1.0116  1.0867  0.01394
6000.0  5.045E-04       1.0   0.03017 1.0111  1.0924  0.01450
6500.0  4.840E-04       1.0   0.03168 1.0106  1.0981  0.01501
7000.0  4.668E-04       1.0   0.03312 1.0100  1.1038  0.01550
7500.0  4.520E-04       1.0   0.03453 1.0095  1.1095  0.01595
8000.0  4.393E-04       1.0   0.03589 1.0090  1.1151  0.01638
8500.0  4.281E-04       1.0   0.03723 1.0085  1.1208  0.01679
9000.0  4.183E-04       1.0   0.03854 1.0081  1.1264  0.01717
9500.0  4.095E-04       1.0   0.03984 1.0076  1.1320  0.01754
10000.0 4.017E-04       1.0   0.04112 1.0071  1.1376  0.01789
```

```
C -------------------------------------------------------------
C Initialization Regions; 1 = pipe ; 2 = reservoir
C -------------------------------------------------------------
INITREG CON
 1
MOD
 3  50  1 1 100 107 = 2   ! reservoir
```

```
C ------------------------------------------------------------
C Initialize.
C ------------------------------------------------------------
INITIAL 1
  DEPTH PSATDP
  3500   450
  PINIT  400
  GOC   3500

INITIAL 2
  DEPTH PSATDP
  3600   450
  PINIT  400    ! initial reservoir pressure
  ZINIT  3470



DATE 1 1 1991

ENDINIT

MODIFY TX 1.0
 1   1  1 1   1  118 * 0.0 ! tubing-annulus barrier


PSM

C ------------------------------------------------------------
C Define wells.
C ------------------------------------------------------------
WELL
            I  J   K1   K2   PI
   PROD     2  1    1    1   100
   OBS      2  1  117  117   100
   PUMP     2  1  118  118   100
   WINJ     2  1  115  115   100
   ACID     2  1  116  116   100

WELLTYPE
  PROD  MCF
  OBS   MCF
  PUMP  STBLIQ
  WINJ  RBGASINJ
  ACID  RBGASINJ
```

```
WELLPLAT
 PROD 1
 WINJ 1

BHP
  PROD   15
  OBS    15
  PUMP   50
  WINJ   500
  ACID   500

RATE
PROD 0.001
OBS 0.001
PUMP 0
ACID 50    !50 bbl water to simulate acid injection.
WINJ 0


YPLAT 1
 1.0 0.0

PTARG  1 MCF  500  NOREDUCEQ
ITARG  1 G 0.00221  1

INJGAS
WINJ
1
ACID
1


DT 0.001

TIME 1

RATE
PROD 1.7
WINJ 1
ACID 0

INCLUDE
  schedule.inc

END
```